ANALYSIS AND QUANTIFICATION OF INOSITOL POLY- AND PYROPHOSPHATES BY NMR SPECTROSCOPY AND MASS SPECTROMETRY

Dissertation zur Erlangung des akademischen Grades
doctor rerum naturalium (Dr. rer. nat.)

im Fach: Chemie
Spezialisierung: Organische und Bioorganische Chemie

Eingereicht an der
Mathematisch-Naturwissenschaftlichen Fakultät der Humboldt-Universität zu Berlin

von
M. Sc. Robert Puschmann

Präsidentin der Humboldt-Universität zu Berlin
Prof. Dr.-Ing. Dr. Sabine Kunst
Dekan der Mathematisch-Naturwissenschaftlichen Fakultät
Prof. Dr. Elmar Kulke

1. Gutachterin: Prof. Dr. Dorothea Fiedler
2. Gutachter: Prof. Dr. Christian P.R. Hackenberger
3. Gutachter: Prof. Dr. Michael Hothorn

Tag der mündlichen Prüfung: 08.01.2020

For my parents

Erklärung des Autors

Diese Arbeit wurde vom 01.05.2015 bis zum 31.07.2019 unter der Aufsicht von Prof. Dorothea Fiedler am Institut für Chemie der Humboldt-Universität zu Berlin und am Leibniz-Forschungsinstitut für Molekulare Pharmakologie angefertigt.

Deklaration

Ich erkläre, dass ich die Dissertation selbständig und nur unter Verwendung der von mir gemäß § 7 Abs. 3 der Promotionsordnung der Mathematisch-Naturwissenschaftlichen Fakultät, veröffentlicht im Amtlichen Mitteilungsblatt der Humboldt-Universität zu Berlin Nr. 42/2018 am 11.07.2018 angegebenen Hilfsmittel angefertigt habe.

Robert Puschmann
Berlin, 21.07.2019

Hereby, I declare that I have authored the present dissertation independently and only by means of the stated resources in accordance to § 7 Abs. 3 der PromotionsordnungderMathematischNaturwissenschaftlichen Fakultät, published in the Amtlichen Mitteilungsblatt der HumboldtUniversität zu Berlin Nr. 42/2018 am 11.07.2018. All citations are marked as such. This thesis was not submitted to other examination boards in the same or similar form before.

Robert Puschmann
Berlin, 21.07.2019

Acknowledgments

First, I want to thank my parents and my brother. I could fill this whole page with things you did for me and with anecdotes of how you fueled my scientific curiosity. However, I will simply say: I love you and thank you for everything!

Next, I want to thank Dorothea. You provided a fantastic environment and a congenial group of colleagues and I enjoyed every day I worked for you. Your enthusiasm for my research and the constructive feedback, whenever it was needed, enabled me to become a better, more complete scientist (I think, eventually even my writing got better).

I want to thank Ferike for being a fantastic friend and for providing a strong shoulder every time I needed support. The time with you has been a blast. Should you ever put your mind to conquering the world, count on me; I'll be your minion.

Berti, you were not only a brilliant colleague but also an awesome friend and we were a great team. There is a reason why most of the FMP knowns us simply as the Roberties. It is sad that our careers will divert here and I hope that, sooner rather than later, we will be Co-group leaders.

Katy, you are now the group veteran. Make sure all PhD students know how to work properly. It was fun having you as my desk neighbor.

I want to thank all Fiedler group members, past and present. You guys made the days brighter each time an experiment failed, as well as every other moment. Thanks to all who took the time to edit my thesis. Every single person who ever brought ice cream to the office: You are heroes. Everyone else: There is still hope for you.

Lastly, I want to thank the Jungsozialist*innen. You helped make Berlin my home.

Table of Contents

Abstract

Inositol pyrophosphates (PP-InsPs) are a well conserved group of second messengers that are involved in a plethora of cellular processes including phosphate homeostasis, insulin signaling, and apoptosis. Despite much effort, it is still mostly unknown how PP-InsPs exert their diverse functions. In order to decipher the mechanisms, researchers have relied either on metabolic labeling with radioactive inositol or on electrophoretic separation on polyacrylamide gels but these methods either lack ease of use or sensitivity. Therefore, two new analytical tools, based on nuclear magnetic resonance (NMR) spectroscopy, and liquid chromatography coupled mass spectrometry (LCMS), were developed.

To overcome the limited sensitivity provided by NMR spectroscopy, a high yielding synthesis of NMR-active ^{13}C-labeled inositol was designed and optimized. Furthermore, a chemoenzymatic synthesis of all mammalian PP-InsPs isomers was developed that relied on a scalable purification strategy utilizing precipitation with Mg^{2+} ions. Human cells were metabolically labeled with ^{13}C-inositol and the prepared PP-InsPs were used as standards to identify fingerprint peaks in the NMR-spectra of the labeled cells. These fingerprint signals enabled the quantification of the corresponding molecules.

The LCMS-based method was envisioned to be based on the derivatization of the highly charged inositol pyrophosphates to their corresponding methyl esters by trimethylsilyldiazomethane. The uncharged, permethylated InsPs and PP-InsPs were suitable for LC separation and MS measurement, and provide a sensitivity unmatched by NMR spectroscopy. The method was established using inositol hexakisphosphate ($InsP_6$), a simpler analog of PP-InsPs, and methylated $InsP_6$ could be detected at quantities as low as 10 femtomole, emphasizing the validity of the approach. However, the adaptation of the derivatization for PP-InsPs proved challenging as the reaction caused degradation of the analyte but strategies to circumvent the decay by changing the derivatization agent to diazomethane were promising.

In summary, both the NMR spectroscopy based method and the derivatization-LCMS approach, once fully developed, provide great versatility and will be indispensable for

the research of inositol poly- and pyrophosphates. NMR spectroscopy will provide information on PP-InsPs in complex mixtures while the high sensitivity of mass spectrometry will enable the quantification of low-abundant PP-InsPs, thereby reciprocally complementing the other method.

Zusammenfassung

Inositolpyrophosphate (PP-InsP) sind eine Gruppe sekundärer Signalmoleküle, die in einer Vielzahl zellulärer Prozesse, von Phosphathomeostase über Insulinsignalisierung bis Apoptose eine Rolle spielen. Trotz großem Aufwand ist die Art und Weise, wie PP-InsPs ihre Funktion ausführen, noch weitgehend unbekannt. Um den zugrundeliegenden Mechanismus zu entschlüsseln, nutzen Forscher bisher hauptsächlich Isotopenmarkierung mit radioaktivem Inositol oder elektrophoretische Auftrennungen auf Polyacrylamidgelen, doch diese Methoden sind entweder schwierig anzuwenden oder nicht sensitiv genug. Deshalb wurden zwei neue analytische Methoden basierend auf Kernspinresonanzspektroskopie und Flüssigchromatographie mit Massenspektrometrie-Kopplung (LCMS) entwickelt.

Um die limitierende Sensitivität der Kernresonanzspektroskopie zu umgehen, wurde die Synthese von kernspinresonanzaktivem, ^{13}C-markiertem Inositol optimiert. Des Weiteren wurde eine chemoenzymatische Synthese für alle Säugetier-PP-InsP-Isomere entwickelt, die auf der skalierbaren Ausfällung mittels Mg^{2+} Ionen basiert. Menschliche Zellen wurden mit ^{13}C-Inositol isotopenmarkiert und in den Spektren der Zellextrakte wurde, basierend auf den PP-InsP-Standards, Fingerabdrucksignale identifiziert mit denen die Konzentrationen der dazugehörigen Moleküle bestimmt werden konnte.

Die LCMS basierte Methode wurde auf dem Prinzip der Umsetzung von hochgeladenen Inositolpyrophosphaten zu ihren korrespondieren Methylestern mittels Trimethylsilyldiazomethan geplant. Die ungeladenen, permethylierten PP-InsPs wären geeignet für LC-Auftrennungen und MS-Messungen und sollten eine von Kernspinresonanzspektroskopie nicht erreichbare Sensitivität ermöglichen. Die Methode wurde mittels Inositolhexakisphosphat ($InsP_6$), einem einfacheren PP-InsP-Analog, etabliert und methyliertes $InsP_6$ konnte in Mengen von 10 femtomol detektiert werden. Die Adaption der Methode für die PP-InsPs gestaltete sich jedoch herausfordernd, da der Analyt während der Reaktion zersetzt wurde. Ein Wechsel zu Diazomethan als Methylierungsagens zeigte vielversprechende Resultate.

Zusammenfassend zeigten sowohl die kernspinresonanzspektroskopiebasierte Methode als auch die Herangehensweise mittels Derivatisierung gefolgt von LCMS,

sobald sie vollständig entwickelt sein wird, vielversprechende Ergebnisse und sie werden unverzichtbare Werkzeuge für die Erforschung von Inositolpyrophosphaten sein.

List of Figures

List of Tables

List of Abbreviations

1,5(PP)$_2$-InsP$_4$	1,5-bisdiphosphoinositol tetrakisphosphate
[^{13}C$_6$]5PP-InsP$_5$	[^{13}C$_6$]5-diphosphoinositol pentakisphosphate
[^{13}C$_6$]InsP$_6$	[^{13}C$_6$]inositol hexakisphosphate
5PP-InsP$_5$	5-diphosphoinositol pentakisphosphate
ADP	adenosine diphosphate
ATP	adenosine triphosphate
BIRD	bilinear rotation decoupling
BIRD-HMQC	HMQC experiment with BIRD-pulse
CH_2N_2	Diazimethane
CSA	Camphorsulfonic acid
CV	column volume
DAPI	4',6-diamidin-2-phenylindol
DCM	dichloromethane
DIPP1	diphosphoinositol phosphate phosphohydrolase 1
DNP	dynamic nuclear polarization
DMEM	Dulbecco's Modified Eagle Medium
DMF	*N,N*-dimethylformamide
DMSO	dimethylsulfoxide
DTT	dithiothreitol
EDTA	ethylenediaminetetraacetic acid
HDAC	histone deacetylase
FID	free induction decay
FPLC	fast protein liquid chromatography
HEPES	2-[4-(2-hydroxyethyl)piperazin-1-yl]ethanesulfonic acid
HMQC	Heteronuclear Multiple-Quantum Correlation
Ins(1,4,5)P$_3$	*myo*-inositol 1,4,5-trisphosphate
InsP	inositol polyphosphate
InsP$_6$	inositol hexakisphosphate
IP6K1	(human) inositol hexakisphosphate kinase 1 (Genbank: AC099668)
IP6KA	inositol hexakisphosphate kinase A from Entamoeba histolytica (Genbank: XP_648490.2)
IPK1	inositol pentakisphosphate kinase 1
IPS	inositol-3-phosphate synthase (WP_010879290.1)
ITPK1	inositol tetrakisphosphate kinase 1
k_{cat}	turnover number
K_M	Michaelis-Menten constant
LCMS	liquid chromatography coupled mass spectrometry
LOD	limit of detection
LOQ	limit of quantification
*m*CPBA	*meta*-chloroperoxybenzoic acid

MES	2-(*N*-morpholino)ethanesulfonic acid
MOPS	3-morpholinopropane-1-sulfonic acid
NADH	nicotinamide adenine dinucleotide (reduced form)
NAD^+	nicotinamide adenine dinucleotide
MeCN	acetonitrile
NMR	nuclear magnetic resonance (spectroscopy)
NTA	nitriloacetic acid
PAGE	polyacrylamide gel electrophoresis
PBS	phosphate buffered saline
pH*	the measured pH of a deuterated solution
PP-InsP	inositol pyrophosphate
PPIP5K	diphosphoinositol pentakisphosphate kinase
PtdInsP	phosphatidyinolsitol phosphate
PLC	phospholipase C
PTM	posttranslational modification
rt	room temperature
SPX domain	SYG1/Pho81/XPR1domain
TEA	triethylamine or triethylammonium
TEAB	triethylammonium hydrogen carbonate
TFA	trifluoroacetic acid
THF	tetrahydrofuran
TMS-CHN_2	Trimethylsylyldiazomethane
TRIS	tris(hydroxymethyl)-aminomethan
V_0	initial specific velocity
V_{max}	maximum specific velocity
VIH1/2	Inositol hexakisphosphate and diphosphoinositol-pentakisphosphate kinase 1/2

Publications and Posters

Robert Puschmann[‡], Robert K. Harmel[‡], Dorothea Fiedler. "Scalable Chemoenzymatic Synthesis of Inositol Pyrophosphates" *Biochemistry* **2019**, *submitted*

Robert Puschmann[‡], Robert K. Harmel[‡], Minh Nguyen Trung, Adolfo Saiardi, Peter Schmieder, Dorothea Fiedler. „Harnessing ^{13}C-labeled myo-inositol to interrogate inositol phosphate messengers by NMR", *Chem. Sci*. **2019**, *10 (20), 5267–5274.* doi: 10.1039/c9sc00151d.

Jinsheng Zhu, Kelvin Lau, Robert Harmel, Robert Puschmann, Larissa Broger, Ludwig A. Hothorn, Dorothea Fiedler, Michael Hothorn. "Two bifunctional inositol pyrophosphate kinases/phosphatases control plant phosphate homeostasis.", *bioRxiv* **2018**, doi: https://doi.org/10.1101/467076, *eLife* **2019**, *under revision*

([‡] contributed equally)

Robert Puschmann and Dorothea Fiedler. An analog sensitive approach to investigate ATP-grasp enzymes, Poster presentation to be delivered at the ECBS & ICBS joint meeting **2015**, Berlin, Germany

Robert Puschmann and Dorothea Fiedler. An analog sensitive approach to investigate ATP-grasp enzymes, Poster presentation to be delivered at the EMBO conference Chemical Biology **2016**, Heidelberg, Germany

Chapter 1: Inositol pyrophosphates are important signaling molecules[a]

1.1 Inositol phosphates are cellular messengers

Small molecule messengers are key components in cellular decision-making processes.[1] Among those, inositol-based signaling molecules occupy a privileged node and include both water-soluble, diffusible inositol phosphates (InsPs), as well as the lipid-anchored phosphatidylinositol phosphates (PtdInsPs).[2,3] The InsPs are derived from the head group of PtdIns(4,5)P_2 that is cleaved from its diacyl glycerol lipid tail by phospholipase C (PLC) (Figure 1.1). The resulting Ins(1,4,5)P_3 is a Ca^{2+} releasing factor and an excellent example for a second messenger.[4] Ins(1,4,5)P_3 is subsequently phosphorylated via various inositol tetrakisphosphate ($InsP_4$) isoforms to yield Ins(1,3,4,5,6)P_5 ($InsP_5$). The responsible kinases are inositol polyphosphate multikinase (IPMK) and inositol tetrakisphosphate 1-kinase (ITPK1). $InsP_5$ is then phosphorylated by inositol pentakisphosphate 2-kinase (IPK1) to provide the fully phosphorylated inositol hexakisphosphate ($InsP_6$) (Figure 1.1).

Remarkably, eukaryotic cells comprise a subgroup of inositol polyphosphates termed inositol pyrophosphates (PP-InsPs) which contain, in addition to the six phosphate esters present in $InsP_6$, up to two additional phosphoryl groups in the form of di- or pyrophosphates. These high energy bonds are formed by two families of conserved kinases, the inositol hexakisphosphate kinases (IP6Ks) and diphosphoinositol pentakisphosphate kinases (PPIP5Ks). Removal of the pyrophosphate groups is catalyzed by diphosphoinositol polyphosphate phosphohydrolase 1 (DIPP1). In yeast, another pyrophosphatase is known, called Siw14.[5,6] In all, the involved enzymes form a complicated network that is still not fully annotated e.g. no Siw14 homolog is known yet in mammals. This is noteworthy as the majority of the enzymes are conserved in all eukaryotes.

[a] Part of this chapter was taken from "Puschmann, R.‡; Harmel, R. K.‡; Nguyen Trung, M.; Saiardi, A.; Schmieder, P.; Fiedler, D. Harnessing ^{13}C-Labeled *Myo*-Inositol to Interrogate Inositol Phosphate Messengers by NMR. *Chem. Sci.* **2019**, *10* (20), 5267–5274." (‡ contributed equally)

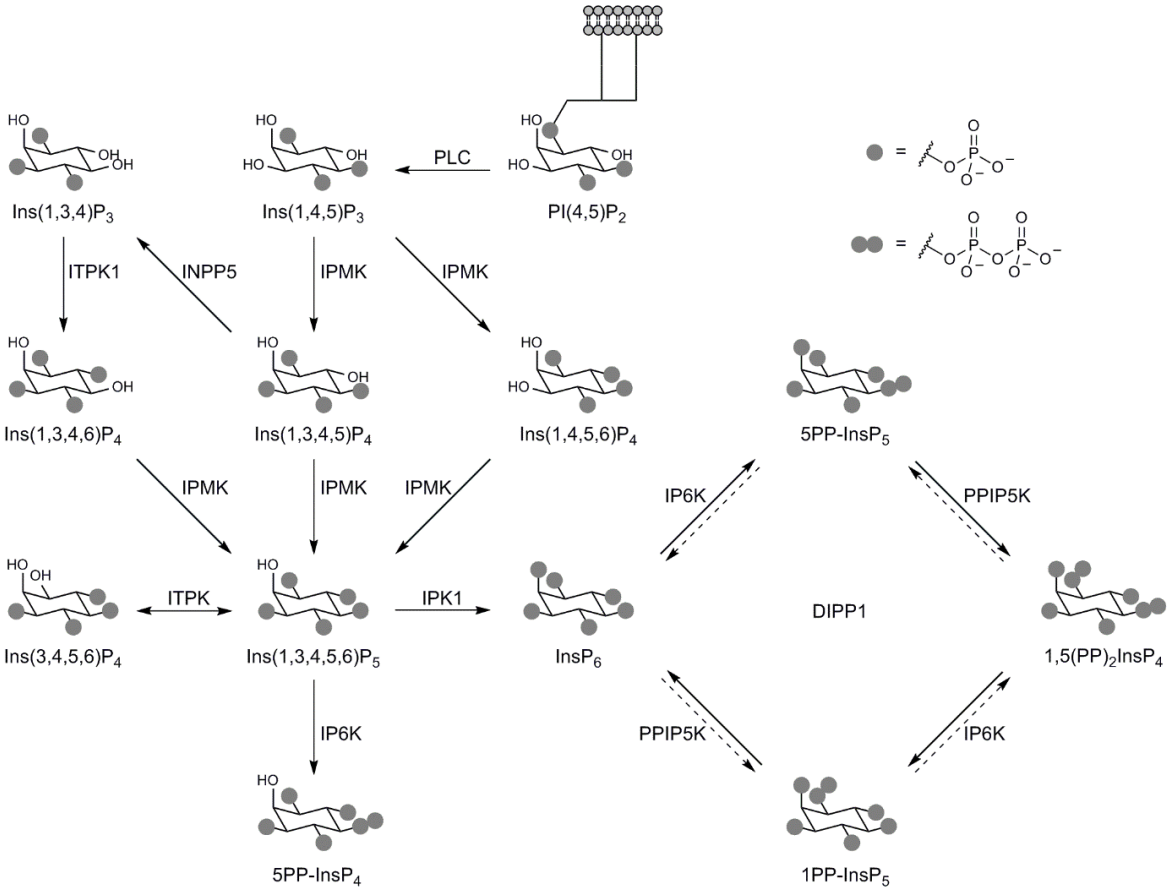

Figure 1.1. Biosynthetic pathway of inositol pyrophosphates. PLC: phospholipase C, IPMK: inositol phosphate multikinase, INPP5: Inositol Polyphosphate-5-Phosphatase, ITPK1: inositol tetrakisphosphate 1-kinase, IPK1: inositol pentakisphosphate 2-kinase, IP6K: inositol hexakisphosphate kinase, PPIP5K: diphosphoinositol pentakisphosphate kinase, DIPP1: diphosphoinositol polyphosphate phosphohydrolase 1.

1.2 Functions of inositol poly- and pyrophosphates

$InsP_3$ is a well-known second messenger involved in Ca^{2+} release and insulin signaling and has been extensively reviewed.[4,7] IPMK then attaches phosphoryl groups to $InsP_3$ and forms different $InsP_4$ isomers that have a wide variety of activities, ranging from protein membrane recruitment, and regulation of protein-protein interactions ($Ins(1,3,4,5)P_4$) over Ca^{2+} mobilization ($Ins(1,3,4,5)P_4$), and the regulation of ClC-3 chloride channels ($Ins(3,4,5,6)P_4$) to the maturation of B and T cells ($Ins(1,3,4,5)P_4$).[8–15] Of special interest is the modulation of histone deacetylases (HDAC), here $InsP_4$ binds to a pocket formed by HDAC and a corepressor protein, leading to activation of the enzyme. The resulting upregulation of deacetylation leads to a downregulation of transcription.[16]

IPMK attaches another phosphoryl group to $InsP_4$ to generate $InsP_5$, a compound that is involved PI3K/Akt activity regulation, angiogenesis and knockouts of its biosynthetic enzyme IPMK are embryonically lethal.[17–19] The question remains if the lethality arises due to a lack of $InsP_4$ and $InsP_5$, the direct products of IPMK or whether the deprivation of all downstream metabolites is the main cause.

Inositol hexakisphosphate possesses function in the context of mRNA export and necroptosis.[20–23] A unanticipated role of $InsP_6$ is as an integral structural component of several large protein complexes, including TIR1, the receptor of the plant hormone auxin, and in the maturation and release of HIV capsids.[24–26] This role is reminiscent of the InsP4-HDAC complex and might point towards a general function of InsPs in the mediation of protein-protein complexes.

PP-InsPs are involved in a wide variety of cellular processes and seem to connect different aspects of cellular homeostasis, like hormone signaling and nutrient homeostasis that are not usually thought of as directly linked (Table 1.1). Most of these phenotypes were discovered by knocking out one or more of the IP6Ks and PPIP5Ks responsible for PP-InsP synthesis. This approach led to a good understanding of the processes PP-InsPs are involved in but the mechanistic targets remain mostly elusive.

5-Diphosphoinositol pentakisphosphate (5PP-$InsP_5$) possesses a pyrophosphoryl group in the 5-position and is the best studied inositol pyrophosphate. 5PP-$InsP_5$ is the major component of the cellular $InsP_7$ pool. It is involved in a wide variety of cellular processes, some of which seem to rely only on 5PP-$InsP_5$ and are independent of the IP6K isoform that synthesized the PP-InsP (i.e. phosphate homeostasis). However, some effects are dependent on the specific IP6K isoform (e.g. insulin sensitivity for IP6K1 or lifespan regulation in mice for IP6K3) (Table 1.1).[27–30] This connection could be important in the context of specific inhibitors to treat, for example, diabetes, while having as little off-target effects as possible.

1PP-$InsP_5$ and $InsP_8$ are synthesized by PPIP5Ks and not much is known about their cellular functions of 1PP-$InsP_5$ (Table 1.1). An exciting exception is a link between $InsP_8$ and phosphate sensing in mammals. Shears an coworkers found that free phosphate upregulates the kinase domain and downregulates the phosphatase domain of PPIP5K2, greatly increasing the rate of $InsP_8$ production.[31]

Table 1.1. Cellular processes associated with IP6Ks and PPIP5Ks.

Enzyme	Organism	Effect	Reference
IP6K1	Mouse	Regulation of exocytosis	32–34
	Mouse	Chromatin remodeling	35,36
	Mouse	DNA damage and repair	37,38
	Mouse	Hemostasis	39
	Mouse	Impaired spermatogenesis	30,40,41
	Mouse, human	Reduced migration and invasion	42,43
	Mouse	Neutrophil regulation	44–47
	Mouse	Insulin signaling and sensitivity	30,48–50
	Human	Phosphate homeostasis	27
IP6K2	Mouse, human	Promoting apoptosis	51–59
	Mouse	Cancer metastasis and cell migration	43,60
	Human	Phosphate homeostasis	27
IP6K3	Mouse	Morphology defects in synapse formation	61
	Human	Susceptibility to Alzheimer's disease	62
	Mouse	Lifespan	29
	Human	Phosphate homeostasis	28
Kcs1	Yeast	Regulation of rRNA transcription	63
	Yeast	Regulation of inositol biosynthesis	64
	Yeast	Cell cycle progression	65
	Yeast	Phosphate homeostasis	66
	Yeast	Telomere maintenance	67,68
PPIP5K1	Human	Bioenergetics homeostasis	69
	Human	Downregulation of apoptosis	70
	Human	Cell migration	71
	Human	Hyperosmotic stress	72
PPIP5K2	human	Phosphate homeostasis	31
	Mouse, human	Hearing loss	73
	Human	Survival in colorectal cancer	74
	Human	Type-I interferon response	75
Vip1	Yeast	Regulation of dimorphic shift	76,77

1.3 Inositol pyrophosphates act *via* two distinct mechanisms

Inositol pyrophosphates are thought to act via two distinct mechanisms (Figure 1.2). First, the binding of PP-InsPs to a protein to trigger an effect. This type of interaction requires PP-InsP binding domains that can interact with different forms of PP-InsPs. To date, the only known PP-InsP-specific binding domain is the SPX domain (named after SYG1/Pho81/XPR1 proteins).[27,78–80] These domains are usually found on the N-terminus of proteins involved in phosphate metabolism.[81–83] Recently, it was shown that SPX domains specifically interact with PP-InsP *via* a positively charged surface binding site.[80] While plants and yeast contain several SPX-containing proteins, mammals only possess one, XPR1 (Xenotropic and Polytropic

Retrovirus Receptor 1), which is a phosphate exporter, expressed predominantly in kidneys. It is therefore impossible to account for all characterized effects of PP-InsPs with just this one protein-PP-InsP interaction. Therefore, additional protein binding partners or domains other than SPX must exist.

Apart from proteins that specifically interact with PP-InsPs as their endogenous ligand, it was shown that inositol poly- and pyrophosphates can bind to PH-domains and compete with their canonical PtdInsPs ligands. PtdInsP - PH-domain interactions localize the protein to the plasma membrane, an important regulatory element e.g., in Akt signaling. Increased levels of PP-InsPs have been shown to sequester Akt from the membrane, downregulating its activity.[49,84] Another example is the downregulation of synaptotagmin dependent exocytosis by interaction of 5PP-$InsP_5$ with synaptotagmin's C2B domain.[85,86] In conclusion, two varieties of PP-InsP protein binding are proposed: interaction with PP-Ins-specific domains like SPX, and competitive binding to domains with distinct selectivity.

The second mechanism of action of PP-InsPs was proposed soon after their initial identification. The high energy phosphoanhydride was suggested to participate in phosphoryl transfer chemistry. Indeed, Snyder and coworkers demonstrated that the radioactively labeled beta-phosphate of 5PP-$InsP_5$ could be transferred to various proteins in a cell lysate.[87] Unexpectedly, this process required only Mg^{2+} as a cofactor and no enzyme was involved. Subsequent work showed that the beta-phosphate was transferred onto a pre-phosphorylated sidechain of the substrate protein.[88] Hence, this non-enzymatic post translational modification (PTM) was termed protein pyrophosphorylation. *In vitro*, several targets of pyrophosphorylation have been described but an *in vivo* verification of this modification remains a much sought after question in the field.[63,87] However, should this PTM be confirmed *in vivo*,

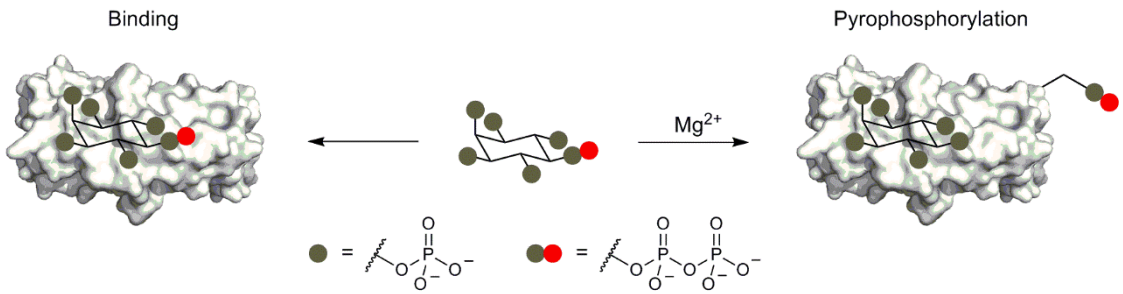

Figure 1.2. PP-InsPs act via two distinct modes of action.

it would supplement the model of how PP-InsPs exert their diverse functions with additional information and could better explain the multifaceted phenotypes of PP-InsPs.

1.4 Methods for the detection of inositol pyrophosphates

In order to dissect the molecular mechanisms that guide the diverse cellular effects of PP-InsP, it is essential to reliably and sensitively quantify PP-InsPs. Depending on the context this can mean quantifying either cellular PP-InsP pools or reaction products in biochemical reaction. This analysis, however, has proven to be the major bottleneck for the advancement of the field. Although the structure of InsPs appears simple, the detection of these compounds poses a challenge due to their lack of an analytical handle, high charge density, and propensity to precipitate with divalent metal cations.[89,90] For the analysis of cellular inositol pyrophosphates, researchers traditionally have relied heavily on a radiolabeling approach where cells are supplied with tritiated *myo*-inositol (Figure 1.3a).[91] The growing cells incorporate the [^{3}H]*myo*-inositol into their PtdInsPs and, eventually, the pool of soluble PP-InsPs is labeled as well. While this method has enabled many seminal finding in the field, it is limited by several factors. [^{3}H]*myo*-Inositol is only incorporated by growing cells and at least six doublings are required to achieve steady state labeling. The labeling can take from one night in the case of yeast up to several days for mammalian cells, that is, if the mammalian cells survive the constant exposure to ionizing radiation. A further limitation is the dependence on dedicated HPLC equipment for radioactive compounds, limiting this method to a few research groups worldwide. A parallel approach circumvented the use of radioactivity by analyzing HPLC fractions in the presence of a metal-dependent dye, but has remained sparsely used (Figure 1.3b).[92] More recently, a method based on gel electrophoresis was reported.[93] Here, the extracted InsPs and PP-InsPs have to be enriched over TiO_2 beads, and are then resolved on a high-percentage polyacrylamide gel (PAGE) (Figure 1.3c).[94] Although the independence from radioactive tracers has allowed more laboratories to employ this approach, the lack of an InsP-specific analytical handle requires a more elaborate sample preparation and is limited to the detection of only the most highly phosphorylated InsPs ($InsP_6$ and higher for cell extracts).

Liquid chromatography coupled mass spectrometry (LCMS), as an application for the analysis of small analyte amounts, is well established. This method has been mostly used for the analysis of inositol hexakisphosphate in food samples but was recently adapted for cellular PP-InsP pools (Figure 1.3d).[95–98] All reported LCMS methods for the analysis of InsPs and PP-InsPs rely on ion exchange liquid

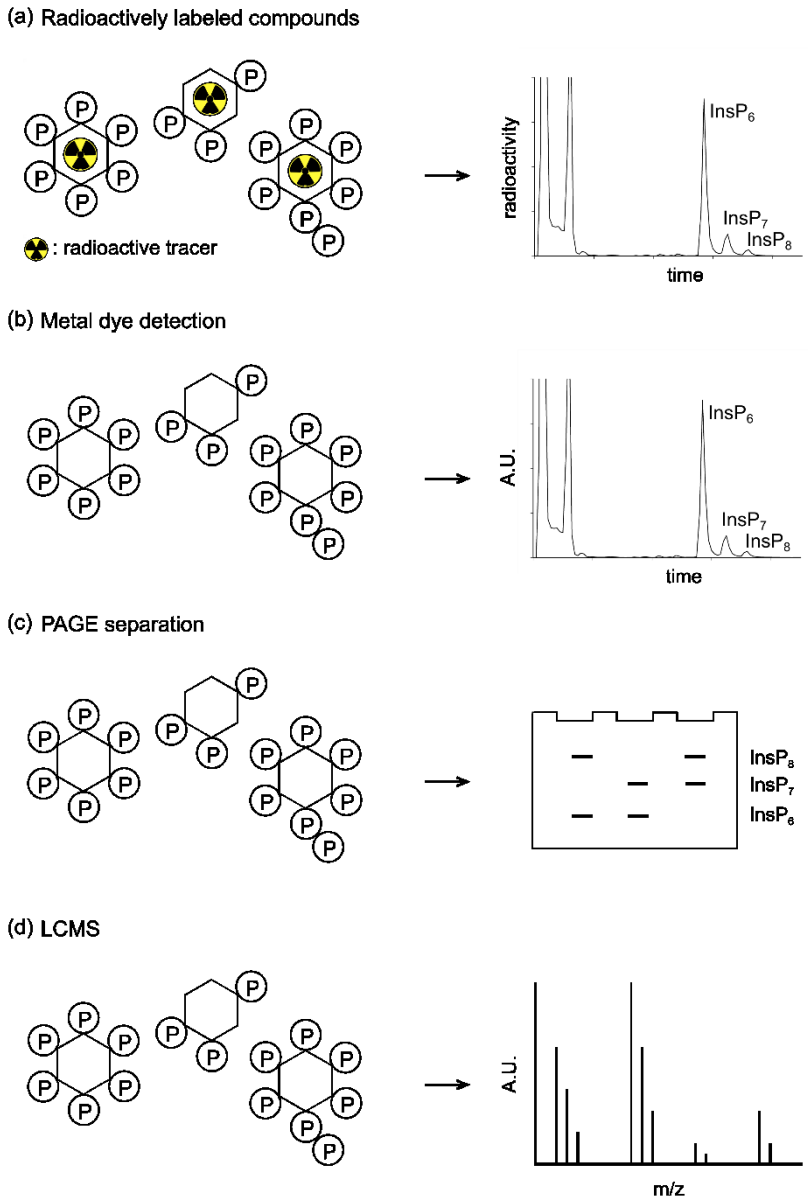

Figure 1.3. Established methods for the analysis of inositol pyrophosphates. (a) Cells are grown with [^{3}H]*myo*-inositol and labeled PP-InsPs are extracted. The PP-InsPs are resolved *via* SAX-HPLC and the radioactivity in each sample is detected *via* scintillation counting. (b) Unlabeled cells are extracted and the PP-InsPs are resolved on a SAX-HPLC and the PP-InsPs are detected *via* a metal dependent dye. (c) PP-InsPs are extracted from cells and enriched on TiO_2 beads before resolution *via* PAGE and staining. (d) PP-InsPs are resolved on a SAX-HPLC and directly injected into mass spectrometer. The analytes are ionizes in negative ion mode.

chromatography, introducing large amounts of salt into the instrument (up to 570 mM) and use negative ionization mode. The highly charged InsPs are difficult to ionize and the methods have a limit of detection of > 1 pmol, rendering the method more sensitive than PAGE analysis but less sensitive than radiolabeling. Taken together, LCMS has not reached its potential yet and therefore seen no adoption in the field as of now.

Similar to the analysis of cellular PP-InsPs, the quantification of inositol pyrophosphates in biochemical reactions has relied on the same basic methods and only the differences are discussed here.

In addition to the use of [^{3}H]*myo*-inositol hexakisphosphate as a radioactive tracer, [^{32}P] was used in the form of ATPγ^{32}P to monitor kinase reactions as well.[99,100] When analyzing *in vitro* reactions by PAGE, a TiO_2 enrichment is usually not required as the samples contain less contaminants then cell extracts.[101]

The methods mentioned above have been used to varying degrees, but cannot provide structural information about the InsPs and PP-InsPs, such as the clear distinction of the structural isomers of PP-InsPs. Furthermore, radiotracers are so far the only valid approach to quantify low-abundant PP-InsPs. The methods also lack the ability to monitor conversion of InsP species in real time *in vitro*, thereby forfeiting informative kinetic insight contained within biochemical experiments. In addition, because of the various separation and resolution steps, direct measurements in complex samples, such as cell extracts, have not been possible so far. These drawbacks have limited the advancement of the field and new analytical tools are urgently needed.

1.5 Goal

The aim of this thesis is the development of analytical tools based on NMR spectroscopy and mass spectrometry to measure and quantify inositol poly- and pyrophosphates both *in vitro* and *ex vivo*. These methods are necessary to better correlate cellular concentrations with phenotypes to ultimately facilitate a better understanding of InsP and PP-InsP functions.

NMR spectroscopy provides not only quantification of analytes, but also information on structure and conformation, enabling the differentiation of inositol pyrophosphate isomers, a feature no current analytical method is able to deliver. To take full advantage of NMR, however, ^{13}C-labeled compounds are necessary. Therefore, scalable, high-yielding synthetic approaches for ^{13}C-labeled *myo*-inositol and PP-InsPs have to be developed.

The most significant limitation of NMR spectroscopy is its low sensitivity, restricting the applicability to medium analyte concentrations. For this reason, mass spectrometry's superb sensitivity complements the analytical tool box well in that regard. To unlock the full potential of LCMS for the analysis of inositol poly- and pyrophosphates, the charge of the compounds has to be mitigated *via* a derivatization approach to allow for reverse phase separation and to facilitate analyte ionization.

1.6 References

(1) Alberts, Johnson, Lewis, Raff, Roberts, Walter Lefers, M. F.-F. T. *"Molecular Biology of the Cell.";* Garland Science, 2009.

(2) Balla, T. Phosphoinositides: Tiny Lipids With Giant Impact on Cell Regulation. *Physiol. Rev.* **2013**, *93* (3), 1019–1137. https://doi.org/10.1152/physrev.00028.2012.

(3) Irvine, R. F.; Schell, M. J. Back in the Water: The Return of the Inositol Phosphates. *Nat. Rev. Mol. Cell Biol.* **2001**, *2* (5), 327–338. https://doi.org/10.1038/35073015.

(4) Berridge, M. J. The Inositol Trisphosphate/Calcium Signaling Pathway in Health and Disease. *Physiol. Rev.* **2016**, *96* (4), 1261–1296. https://doi.org/10.1152/physrev.00006.2016.

(5) Steidle, E. A.; Chong, L. S.; Wu, M.; Crooke, E.; Fiedler, D.; Resnick, A. C.; Rolfes, R. J. A Novel Inositol Pyrophosphate Phosphatase in Saccharomyces Cerevisiae: Siw14 Protein Selectively Cleaves the β-Phosphate from 5-Diphosphoinositol Pentakisphosphate (5PP-IP5). *J. Biol. Chem.* **2016**, *291* (13), 6772–6783. https://doi.org/10.1074/jbc.M116.714907.

(6) Wang, H.; Gu, C.; Rolfes, R. J.; Jessen, H. J.; Shears, S. B. Structural and Biochemical Characterization of Siw14: A Protein-Tyrosine Phosphatase Fold That Metabolizes Inositol Pyrophosphates. *J. Biol. Chem.* **2018**, *293* (18), 6905–6914. https://doi.org/10.1074/jbc.RA117.001670.

(7) Hagar, R. E.; Ehrlich, B. E. Regulation of the Type III InsP3 Receptor and Its Role in β Cell Function. *Cellular and Molecular Life Sciences*. Birkhäuser Verlag December 2000, pp 1938–1949. https://doi.org/10.1007/PL00000674.

(8) Mitchell, J.; Wang, X.; Zhang, G.; Gentzsch, M.; Nelson, D. J.; Shears, S. B. An Expanded Biological Repertoire for Ins(3,4,5,6)P4 through Its Modulation of ClC-3 Function. *Curr. Biol.* **2008**, *18* (20), 1600–1605. https://doi.org/10.1016/j.cub.2008.08.073.

(9) Marechal, Y.; Pesesse, X.; Jia, Y.; Pouillon, V.; Perez-Morga, D.; Daniel, J.; Izui, S.; Cullen, P. J.; Leo, O.; Luo, H. R.; et al. Inositol 1,3,4,5-Tetrakisphosphate Controls Proapoptotic Bim Gene Expression and Survival in B Cells. *Proc. Natl. Acad. Sci.* **2007**, *104* (35), 13978–13983. https://doi.org/10.1073/pnas.0704312104.

(10) Wen, B. G.; Pletcher, M. T.; Warashina, M.; Choe, S. H.; Ziaee, N.; Wiltshire, T.; Sauer, K.; Cooke, M. P. Inositol (1,4,5) Trisphosphate 3 Kinase B Controls Positive Selection of T Cells and Modulates Erk Activity. *Proc. Natl. Acad. Sci.* **2004**, *101* (15), 5604–5609. https://doi.org/10.1073/pnas.0306907101.

(11) Huang, Y. H.; Grasis, J. A.; Miller, A. T.; Xu, R.; Soonthornvacharin, S.; Andreotti, A. H.; Tsoukas, C. D.; Cooke, M. P.; Sauer, K. Positive Regulation of Itk PH Domain Function by Soluble IP 4. *Science* **2007**, *316* (5826), 886–889. https://doi.org/10.1126/science.1138684.

(12) Larsson, O.; Barker, C. J.; Sjöholm, A.; Carlqvist, H.; Michell, R. H.; Bertorello, A.; Nilsson, T.; Honkanen, R. E.; Mayr, G. W.; Zwiller, J.; et al. Inhibition of Phosphatases and Increased Ca2+ Channel Activity by Inositol Hexakisphosphate. *Science* **1997**, *278* (5337), 471–474.

(13) Yang, S.-N.; Yu, J.; Mayr, G. W.; Hofmann, F.; Larsson, O.; Berggren, P.-O. Inositol Hexakisphosphate Increases L-Type Ca 2+ Channel Activity by Stimulation of Adenylyl Cyclase. *FASEB J.* **2002**, *15* (10), 1753–1763. https://doi.org/10.1096/fj.00-0799com.

(14) Stricker, R.; Chow, K. M.; Walther, D.; Hanck, T.; Hersh, L. B.; Reiser, G. Interaction of the Brain-Specific Protein P42IP4/Centaurin- A1 with the Peptidase Nardilysin Is Regulated by the Cognate Ligands of P42IP4, PtdIns(3,4,5)P3 and Ins(1,3,4,5)P4, with Stereospecificity. *J. Neurochem.* **2006**, *98* (2), 343–354. https://doi.org/10.1111/j.1471-4159.2006.03869.x.

(15) Sauer, K.; Cooke, M. P. Regulation of Immune Cell Development through Soluble Inositol-1,3,4,5- Tetrakisphosphate. *Nature Reviews Immunology*. April 2010, pp 257–271. https://doi.org/10.1038/nri2745.

(16) Watson, P. J.; Millard, C. J.; Riley, A. M.; Robertson, N. S.; Wright, L. C.; Godage, H. Y.; Cowley, S. M.; Jamieson, A. G.; Potter, B. V. L.; Schwabe, J. W. R. Insights into the Activation Mechanism of Class i HDAC Complexes by Inositol Phosphates. *Nat. Commun.* **2016**, *7*, 11262. https://doi.org/10.1038/ncomms11262.

(17) Frederick, J. P.; Mattiske, D.; Wofford, J. A.; Megosh, L. C.; Drake, L. Y.; Chiou, S.-T.; Hogan,

B. L. M.; York, J. D. An Essential Role for an Inositol Polyphosphate Multikinase, Ipk2, in Mouse Embryogenesis and Second Messenger Production. *Proc. Natl. Acad. Sci.* **2005**, *102* (24), 8454–8459. https://doi.org/10.1073/pnas.0503706102.

(18) Fu, C.; Tyagi, R.; Chin, A. C.; Rojas, T.; Li, R. J.; Guha, P.; Bernstein, I. A.; Rao, F.; Xu, R.; Cha, J. Y.; et al. Inositol Polyphosphate Multikinase Inhibits Angiogenesis via Inositol Pentakisphosphate-Induced HIF-1α Degradation. *Circ. Res.* **2018**, *122* (3), 457–472. https://doi.org/10.1161/CIRCRESAHA.117.311983.

(19) Piccolo, E.; Vignati, S.; Maffucci, T.; Innominato, P. F.; Riley, A. M.; Potter, B. V.; Pandolfi, P. P.; Broggini, M.; Iacobelli, S.; Innocenti, P.; et al. Inositol Pentakisphosphate Promotes Apoptosis through the PI 3-K/Akt Pathway. *Oncogene* **2004**, *23* (9), 1754–1765. https://doi.org/10.1038/sj.onc.1207296.

(20) Montpetit, B.; Thomsen, N. D.; Helmke, K. J.; Seeliger, M. A.; Berger, J. M.; Weis, K. A Conserved Mechanism of DEAD-Box ATPase Activation by Nucleoporins and InsP6 in MRNA Export. *Nature* **2011**, *472* (7342), 238–242. https://doi.org/10.1038/nature09862.

(21) Weirich, C. S.; Erzberger, J. P.; Flick, J. S.; Berger, J. M.; Thorner, J.; Weis, K. Activation of the DExD/H-Box Protein Dbp5 by the Nuclear-Pore Protein Gle1 and Its Coactivator InsP6 Is Required for MRNA Export. *Nat. Cell Biol.* **2006**, *8* (7), 668–676. https://doi.org/10.1038/ncb1424.

(22) McNamara, D. E.; Dovey, C. M.; Hale, A. T.; Quarato, G.; Grace, C. R.; Guibao, C. D.; Diep, J.; Nourse, A.; Cai, C. R.; Wu, H.; et al. Direct Activation of Human MLKL by a Select Repertoire of Inositol Phosphate Metabolites. *Cell Chem. Biol.* **2019**, *26* (6), 863-877.e7. https://doi.org/10.1016/j.chembiol.2019.03.010.

(23) Dovey, C. M.; Diep, J.; Clarke, B. P.; Hale, A. T.; McNamara, D. E.; Guo, H.; Brown, N. W.; Cao, J. Y.; Grace, C. R.; Gough, P. J.; et al. MLKL Requires the Inositol Phosphate Code to Execute Necroptosis. *Mol. Cell* **2018**, *70* (5), 936-948.e7. https://doi.org/10.1016/j.molcel.2018.05.010.

(24) Mallery, D. L.; Márquez, C. L.; McEwan, W. A.; Dickson, C. F.; Jacques, D. A.; Anandapadamanaban, M.; Bichel, K.; Towers, G. J.; Saiardi, A.; Böcking, T.; et al. IP6 Is an HIV Pocket Factor That Prevents Capsid Collapse and Promotes DNA Synthesis. *Elife* **2018**, *7*. https://doi.org/10.7554/eLife.35335.

(25) Dick, R. A.; Zadrozny, K. K.; Xu, C.; Schur, F. K. M.; Lyddon, T. D.; Ricana, C. L.; Wagner, J. M.; Perilla, J. R.; Ganser-Pornillos, B. K.; Johnson, M. C.; et al. Inositol Phosphates Are Assembly Co-Factors for HIV-1. *Nature*. August 1, 2018, pp 509–512. https://doi.org/10.1038/s41586-018-0396-4.

(26) Tan, X.; Calderon-Villalobos, L. I. A.; Sharon, M.; Zheng, C.; Robinson, C. V.; Estelle, M.; Zheng, N. Mechanism of Auxin Perception by the TIR1 Ubiquitin Ligase. *Nature* **2007**, *446* (7136), 640–645. https://doi.org/10.1038/nature05731.

(27) Wilson, M. S.; Jessen, H. J.; Saiardi, A. The Inositol Hexakisphosphate Kinases IP6K1 and -2 Regulate Human Cellular Phosphate Homeostasis, Including XPR1-Mediated Phosphate Export. *J. Biol. Chem.* **2019**, jbc.RA119.007848. https://doi.org/10.1074/jbc.RA119.007848.

(28) Kestenbaum, B.; Glazer, N. L.; Köttgen, A.; Felix, J. F.; Hwang, S.-J.; Liu, Y.; Lohman, K.; Kritchevsky, S. B.; Hausman, D. B.; Petersen, A.-K.; et al. Common Genetic Variants Associate with Serum Phosphorus Concentration. *J. Am. Soc. Nephrol.* **2010**, *21* (7), 1223–1232. https://doi.org/10.1681/asn.2009111104.

(29) Moritoh, Y.; Oka, M.; Yasuhara, Y.; Hozumi, H.; Iwachidow, K.; Fuse, H.; Tozawa, R. Inositol Hexakisphosphate Kinase 3 Regulates Metabolism and Lifespan in Mice. *Sci. Rep.* **2016**, *6*, 32072. https://doi.org/10.1038/srep32072.

(30) Bhandari, R.; Juluri, K. R.; Resnick, A. C.; Snyder, S. H. Gene Deletion of Inositol Hexakisphosphate Kinase 1 Reveals Inositol Pyrophosphate Regulation of Insulin Secretion, Growth, and Spermiogenesis. *Proc. Natl. Acad. Sci. U. S. A.* **2008**, *105* (7), 2349–2353. https://doi.org/10.1073/pnas.0712227105.

(31) Gu, C.; Nguyen, H. N.; Hofer, A.; Jessen, H. J.; Dai, X.; Wang, H.; Shears, S. B. The Significance of the Bifunctional Kinase/Phosphatase Activities of Diphosphoinositol

Pentakisphosphate Kinases (PPIP5Ks) for Coupling Inositol Pyrophosphate Cell Signaling to Cellular Phosphate Homeostasis. *J. Biol. Chem.* **2017**, *292* (11), 4544–4555. https://doi.org/10.1074/jbc.M116.765743.

(32) Illies, C.; Gromada, J.; Fiume, R.; Leibiger, B.; Yu, J.; Juhl, K.; Yang, S.-N.; Barma, D. K.; Falck, J. R.; Saiardi, A.; et al. Requirement of Inositol Pyrophosphates for Full Exocytotic Capacity in Pancreatic Beta Cells. *Science* **2007**, *318* (5854), 1299–1302. https://doi.org/10.1126/science.1146824.

(33) Lee, T.-S.; Lee, J.-Y.; Kyung, J. W.; Yang, Y.; Park, S. J.; Lee, S.; Pavlovic, I.; Kong, B.; Jho, Y. S.; Jessen, H. J.; et al. Inositol Pyrophosphates Inhibit Synaptotagmin-Dependent Exocytosis. *Proc. Natl. Acad. Sci.* **2016**, *113* (29), 8314–8319. https://doi.org/10.1073/pnas.1521600113.

(34) Azevedo, C.; Burton, A.; Ruiz-Mateos, E.; Marsh, M.; Saiardi, A. Inositol Pyrophosphate Mediated Pyrophosphorylation of AP3B1 Regulates HIV-1 Gag Release. *Proc. Natl. Acad. Sci. U. S. A.* **2009**, *106* (50), 21161–21166. https://doi.org/10.1073/pnas.0909176106.

(35) Yu, W.; Ye, C.; Greenberg, M. L. Inositol Hexakisphosphate Kinase 1 (IP6K1) Regulates Inositol Synthesis in Mammalian Cells. *J. Biol. Chem.* **2016**, *291* (20), 10437–10444. https://doi.org/10.1074/jbc.M116.714816.

(36) Burton, A.; Azevedo, C.; Andreassi, C.; Riccio, A.; Saiardi, A. Inositol Pyrophosphates Regulate JMJD2C-Dependent Histone Demethylation. *Proc. Natl. Acad. Sci. U. S. A.* **2013**, *110* (47), 18970–18975. https://doi.org/10.1073/pnas.1309699110.

(37) Jadav, R. S.; Chanduri, M. V. L.; Sengupta, S.; Bhandari, R. Inositol Pyrophosphate Synthesis by Inositol Hexakisphosphate Kinase 1 Is Required for Homologous Recombination Repair. *J. Biol. Chem.* **2013**, *288* (5), 3312–3321. https://doi.org/10.1074/jbc.M112.396556.

(38) Rao, F.; Xu, J.; Khan, A. B.; Gadalla, M. M.; Cha, J. Y.; Xu, R.; Tyagi, R.; Dang, Y.; Chakraborty, A.; Snyder, S. H. Inositol Hexakisphosphate Kinase-1 Mediates Assembly/Disassembly of the CRL4–Signalosome Complex to Regulate DNA Repair and Cell Death. *Proc. Natl. Acad. Sci.* **2014**, *111* (45). https://doi.org/10.1073/pnas.1417900111.

(39) Ghosh, S.; Shukla, D.; Suman, K.; Jyothi Lakshmi, B.; Manorama, R.; Kumar, S.; Bhandari, R. Inositol Hexakisphosphate Kinase 1 Maintains Hemostasis in Mice by Regulating Platelet Polyphosphate Levels. *Blood* **2013**, *122* (8), 1478–1486. https://doi.org/10.1182/blood-2013-01-481549.

(40) Malla, A. B.; Bhandari, R. IP6K1 Is Essential for Chromatoid Body Formation and Temporal Regulation of Tnp2 and Prm2 Expression in Mouse Spermatids. *J. Cell Sci.* **2017**, *130* (17), 2854–2866. https://doi.org/10.1242/jcs.204966.

(41) Fu, C.; Rojas, T.; Chin, A. C.; Cheng, W.; Bernstein, I. A.; Albacarys, L. K.; Wright, W. W.; Snyder, S. H. Multiple Aspects of Male Germ Cell Development and Interactions with Sertoli Cells Require Inositol Hexakisphosphate Kinase-1. *Sci. Rep.* **2018**, *8* (1), 7039. https://doi.org/10.1038/s41598-018-25468-8.

(42) Jadav, R. S.; Kumar, D.; Buwa, N.; Ganguli, S.; Thampatty, S. R.; Balasubramanian, N.; Bhandari, R. Deletion of Inositol Hexakisphosphate Kinase 1 (IP6K1) Reduces Cell Migration and Invasion, Conferring Protection from Aerodigestive Tract Carcinoma in Mice. *Cell. Signal.* **2016**, *28* (8), 1124–1136. https://doi.org/10.1016/j.cellsig.2016.04.011.

(43) Fu, C.; Xu, J.; Cheng, W.; Rojas, T.; Chin, A. C.; Snowman, A. M.; Harraz, M. M.; Snyder, S. H. Neuronal Migration Is Mediated by Inositol Hexakisphosphate Kinase 1 via α-Actinin and Focal Adhesion Kinase. *Proc. Natl. Acad. Sci.* **2017**. https://doi.org/10.1073/pnas.1700165114.

(44) Chanduri, M.; Rai, A.; Malla, A. B.; Wu, M.; Fiedler, D.; Mallik, R.; Bhandari, R. Inositol Hexakisphosphate Kinase 1 (IP6K1) Activity Is Required for Cytoplasmic Dynein-Driven Transport. *Biochem. J.* **2016**, *473* (19). https://doi.org/10.1042/BCJ20160610.

(45) Xu, Y.; Li, H.; Bajrami, B.; Kwak, H.; Cao, S.; Liu, P.; Zhou, J.; Zhou, Y.; Zhu, H.; Ye, K.; et al. Cigarette Smoke (CS) and Nicotine Delay Neutrophil Spontaneous Death via Suppressing Production of Diphosphoinositol Pentakisphosphate. *Proc. Natl. Acad. Sci.* **2013**, *110* (19), 7726–7731. https://doi.org/10.1073/pnas.1302906110.

(46) Luo, H. R.; Mondal, S. Molecular Control of PtdIns(3,4,5)P3 Signaling in Neutrophils. *EMBO*

Rep. **2015**, *16* (2), 149–163. https://doi.org/10.15252/embr.201439466.

(47) Hou, Q.; Liu, F.; Chakraborty, A.; Jia, Y.; Prasad, A.; Yu, H.; Zhao, L.; Ye, K.; Snyder, S. H.; Xu, Y.; et al. Inhibition of IP6K1 Suppresses Neutrophil-Mediated Pulmonary Damage in Bacterial Pneumonia. *Sci. Transl. Med.* **2018**, *10* (435), eaal4045. https://doi.org/10.1126/scitranslmed.aal4045.

(48) Chakraborty, A.; Kim, S.; Snyder, S. H. Inositol Pyrophosphates as Mammalian Cell Signals. *Sci. Signal.* **2011**, *4* (188), re1. https://doi.org/10.1126/scisignal.2001958.

(49) Chakraborty, A.; Koldobskiy, M. A.; Bello, N. T.; Maxwell, M.; Potter, J. J.; Juluri, K. R.; Maag, D.; Kim, S.; Huang, A. S.; Dailey, M. J.; et al. Inositol Pyrophosphates Inhibit Akt Signaling, Thereby Regulating Insulin Sensitivity and Weight Gain. *Cell* **2010**, *143* (6), 897–910. https://doi.org/10.1016/j.cell.2010.11.032.

(50) Zhu, Q.; Ghoshal, S.; Rodrigues, A.; Gao, S.; Asterian, A.; Kamenecka, T. M.; Barrow, J. C.; Chakraborty, A. Adipocyte-Specific Deletion of Ip6k1 Reduces Diet-Induced Obesity by Enhancing AMPK-Mediated Thermogenesis. *J. Clin. Invest.* **2016**, *126* (11), 4273–4288. https://doi.org/10.1172/JCI85510.

(51) Nagata, E.; Saiardi, A.; Tsukamoto, H.; Okada, Y.; Itoh, Y.; Satoh, T.; Itoh, J.; Margolis, R. L.; Takizawa, S.; Sawa, A.; et al. Inositol Hexakisphosphate Kinases Induce Cell Death in Huntington Disease. *J. Biol. Chem.* **2011**, *286* (30), 26680–26686. https://doi.org/10.1074/jbc.M111.220749.

(52) Nagata, E.; Luo, H. R.; Saiardi, A.; Bae, B.-I.; Suzuki, N.; Snyder, S. H. Inositol Hexakisphosphate Kinase-2, a Physiologic Mediator of Cell Death. *J. Biol. Chem.* **2005**, *280* (2), 1634–1640. https://doi.org/10.1074/jbc.M409416200.

(53) Nagata, E.; Nonaka, T.; Moriya, Y.; Fujii, N.; Okada, Y.; Tsukamoto, H.; Itoh, J.; Okada, C.; Satoh, T.; Arai, T.; et al. Inositol Hexakisphosphate Kinase 2 Promotes Cell Death in Cells with Cytoplasmic TDP-43 Aggregation. *Mol. Neurobiol.* **2016**, *53* (8), 5377–5383. https://doi.org/10.1007/s12035-015-9470-1.

(54) Koldobskiy, M. A.; Chakraborty, A.; Werner, J. K.; Snowman, A. M.; Juluri, K. R.; Vandiver, M. S.; Kim, S.; Heletz, S.; Snyder, S. H. P53-Mediated Apoptosis Requires Inositol Hexakisphosphate Kinase-2. *Proc. Natl. Acad. Sci.* **2010**, *107* (49), 20947–20951. https://doi.org/10.1073/pnas.1015671107.

(55) Morrison, B. H.; Bauer, J. A.; Kalvakolanu, D. V.; Lindner, D. J. Inositol Hexakisphosphate Kinase 2 Mediates Growth Suppressive and Apoptotic Effects of Interferon-β in Ovarian Carcinoma Cells. *J. Biol. Chem.* **2001**, *276* (27), 24965–24970. https://doi.org/10.1074/jbc.M101161200.

(56) Morrison, B. H.; Tang, Z.; Jacobs, B. S.; Bauer, J. A.; Lindner, D. J. Apo2L/TRAIL Induction and Nuclear Translocation of Inositol Hexakisphosphate Kinase 2 during IFN-β-Induced Apoptosis in Ovarian Carcinoma. *Biochem. J.* **2005**, *385* (2), 595–603. https://doi.org/10.1042/bj20040971.

(57) Morrison, B. H.; Haney, R.; Lamarre, E.; Drazba, J.; Prestwich, G. D.; Lindner, D. J. Gene Deletion of Inositol Hexakisphosphate Kinase 2 Predisposes to Aerodigestive Tract Carcinoma. *Oncogene* **2009**, *28* (25), 2383–2392. https://doi.org/10.1038/onc.2009.113.

(58) Morrison, B. H.; Bauer, J. A.; Hu, J.; Grane, R. W.; Ozdemir, A. M.; Chawla-Sarkar, M.; Gong, B.; Almasan, A.; Kalvakolanu, D. V; Lindner, D. J. Inositol Hexakisphosphate Kinase 2 Sensitizes Ovarian Carcinoma Cells to Multiple Cancer Therapeutics. *Oncogene* **2002**, *21* (12), 1882–1889. https://doi.org/10.1038/sj/onc/1205265.

(59) Moriya, Y.; Nagata, E.; Fujii, N.; Satoh, T.; Ogawa, H.; Hadano, S.; Takizawa, S. Inositol Hexakisphosphate Kinase 2 Is a Presymptomatic Biomarker for Amyotrophic Lateral Sclerosis. *Tokai J. Exp. Clin. Med.* **2017**, *42* (1), 13–18.

(60) Rao, F.; Xu, J.; Fu, C.; Cha, J. Y.; Gadalla, M. M.; Xu, R.; Barrow, J. C.; Snyder, S. H. Inositol Pyrophosphates Promote Tumor Growth and Metastasis by Antagonizing Liver Kinase B1. *Proc. Natl. Acad. Sci.* **2015**, *112* (6), 1773–1778. https://doi.org/10.1073/pnas.1424642112.

(61) Fu, C.; Xu, J.; Li, R.-J.; Crawford, J. A.; Khan, A. B.; Ma, T. M.; Cha, J. Y.; Snowman, A. M.; Pletnikov, M. V.; Snyder, S. H. Inositol Hexakisphosphate Kinase-3 Regulates the Morphology

and Synapse Formation of Cerebellar Purkinje Cells via Spectrin/Adducin. *J. Neurosci.* **2015**, *35* (31), 11056–11067. https://doi.org/10.1523/JNEUROSCI.1069-15.2015.

(62) Crocco, P.; Saiardi, A.; Wilson, M. S.; Maletta, R.; Bruni, A. C.; Passarino, G.; Rose, G. Contribution of Polymorphic Variation of Inositol Hexakisphosphate Kinase 3 (IP6K3) Gene Promoter to the Susceptibility to Late Onset Alzheimer's Disease. *Biochim. Biophys. Acta - Mol. Basis Dis.* **2016**, *1862* (9), 1766–1773. https://doi.org/10.1016/j.bbadis.2016.06.014.

(63) Thota, S. G.; Unnikannan, C. P.; Thampatty, S. R.; Manorama, R.; Bhandari, R. Inositol Pyrophosphates Regulate RNA Polymerase I-Mediated RRNA Transcription in Saccharomyces Cerevisiae. *Biochem. J.* **2014**, *466* (1), 105–114. https://doi.org/10.1042/bj20140798.

(64) Ye, C.; Bandara, W. M. M. S.; Greenberg, M. L. Regulation of Inositol Metabolism Is Fine-Tuned by Inositol Pyrophosphates in Saccharomyces Cerevisiae. *J. Biol. Chem.* **2013**, *288* (34), 24898–24908. https://doi.org/10.1074/jbc.M113.493353.

(65) Banfic, H.; Bedalov, A.; York, J. D.; Visnjic, D. Inositol Pyrophosphates Modulate S Phase Progression after Pheromone-Induced Arrest in Saccharomyces Cerevisiae. *J. Biol. Chem.* **2013**, *288* (3), 1717–1725. https://doi.org/10.1074/jbc.M112.412288.

(66) Auesukaree, C.; Tochio, H.; Shirakawa, M.; Kaneko, Y.; Harashima, S. Plc1p, Arg82p, and Kcs1p, Enzymes Involved in Inositol Pyrophosphate Synthesis, Are Essential for Phosphate Regulation and Polyphosphate Accumulation in Saccharomyces Cerevisiae. *J. Biol. Chem.* **2005**, *280* (26), 25127–25133. https://doi.org/10.1074/jbc.M414579200.

(67) Banfic, H.; Crljen, V.; Lukinovic-Skudar, V.; Dembitz, V.; Lalic, H.; Bedalov, A.; Visnjic, D. Inositol Pyrophosphates Modulate Cell Cycle Independently of Alteration in Telomere Length. *Adv. Biol. Regul.* **2016**, *60*, 22–28. https://doi.org/10.1016/j.jbior.2015.09.003.

(68) Saiardi, A.; Resnick, A. C.; Snowman, A. M.; Wendland, B.; Snyder, S. H. Inositol Pyrophosphates Regulate Cell Death and Telomere Length through Phosphoinositide 3-Kinase-Related Protein Kinases. *Proc. Natl. Acad. Sci.* **2005**, *102* (6), 1911–1914. https://doi.org/10.1073/pnas.0409322102.

(69) Gu, C.; Nguyen, H.-N.; Ganini, D.; Chen, Z.; Jessen, H. J.; Gu, Z.; Wang, H.; Shears, S. B. KO of 5-InsP 7 Kinase Activity Transforms the HCT116 Colon Cancer Cell Line into a Hypermetabolic, Growth-Inhibited Phenotype. *Proc. Natl. Acad. Sci. U. S. A.* **2017**, *114* (45), 11968–11973. https://doi.org/10.1073/pnas.1702370114.

(70) Machkalyan, G.; Hèbert, T. E.; Miller, G. J. PPIP5K1 Suppresses Etoposide-Triggered Apoptosis. *J. Mol. Signal.* **2016**, *11*, 4. https://doi.org/10.5334/1750-2187-11-4.

(71) Machkalyan, G.; Trieu, P.; Pétrin, D.; Hébert, T. E.; Miller, G. J. PPIP5K1 Interacts with the Exocyst Complex through a C-Terminal Intrinsically Disordered Domain and Regulates Cell Motility. *Cell. Signal.* **2016**, *28* (5), 401–411. https://doi.org/10.1016/j.cellsig.2016.02.002.

(72) Choi, J. H.; Williams, J.; Cho, J.; Falck, J. R.; Shears, S. B. Purification, Sequencing, and Molecular Identification of a Mammalian PP-InsP 5 Kinase That Is Activated When Cells Are Exposed to Hyperosmotic Stress. *J. Biol. Chem.* **2007**, *282* (42), 30763–30775. https://doi.org/10.1074/jbc.M704655200.

(73) Yousaf, R.; Gu, C.; Ahmed, Z. M.; Khan, S. N.; Friedman, T. B.; Riazuddin, S.; Shears, S. B.; Riazuddin, S. Mutations in Diphosphoinositol-Pentakisphosphate Kinase PPIP5K2 Are Associated with Hearing Loss in Human and Mouse. *PLOS Genet.* **2018**, *14* (3), e1007297. https://doi.org/10.1371/journal.pgen.1007297.

(74) Chen, H.; Sun, X.; Ge, W.; Qian, Y.; Bai, R.; Zheng, S. A Seven-Gene Signature Predicts Overall Survival of Patients with Colorectal Cancer. *Oncotarget* **2017**, *8* (56), 95054–95065. https://doi.org/10.18632/oncotarget.10982.

(75) Pulloor, N. K.; Nair, S.; Kostic, A. D.; Bist, P.; Weaver, J. D.; Riley, A. M.; Tyagi, R.; Uchil, P. D.; York, J. D.; Snyder, S. H.; et al. Human Genome-Wide RNAi Screen Identifies an Essential Role for Inositol Pyrophosphates in Type-I Interferon Response. *PLoS Pathog.* **2014**, *10* (2), e1003981. https://doi.org/10.1371/journal.ppat.1003981.

(76) Pohlmann, J.; Fleig, U. Asp1, a Conserved 1/3 Inositol Polyphosphate Kinase, Regulates the Dimorphic Switch in Schizosaccharomyces Pombe. *Mol. Cell. Biol.* **2010**, *30* (18), 4535–4547. https://doi.org/10.1128/mcb.00472-10.

(77) Pöhlmann, J.; Risse, C.; Seidel, C.; Pohlmann, T.; Jakopec, V.; Walla, E.; Ramrath, P.; Takeshita, N.; Baumann, S.; Feldbrügge, M.; et al. The Vip1 Inositol Polyphosphate Kinase Family Regulates Polarized Growth and Modulates the Microtubule Cytoskeleton in Fungi. *PLoS Genet.* **2014**, *10* (9), e1004586. https://doi.org/10.1371/journal.pgen.1004586.

(78) Jung, J. Y.; Ried, M. K.; Hothorn, M.; Poirier, Y. Control of Plant Phosphate Homeostasis by Inositol Pyrophosphates and the SPX Domain. *Current Opinion in Biotechnology*. February 2018, pp 156–162. https://doi.org/10.1016/j.copbio.2017.08.012.

(79) Gerasimaite, R.; Pavlovic, I.; Capolicchio, S.; Hofer, A.; Schmidt, A.; Jessen, H. J.; Mayer, A. Inositol Pyrophosphate Specificity of the SPX-Dependent Polyphosphate Polymerase VTC. *ACS Chem. Biol.* **2017**, *12* (3), 648–653. https://doi.org/10.1021/acschembio.7b00026.

(80) Wild, R.; Gerasimaite, R.; Jung, J. Y.; Truffault, V.; Pavlovic, I.; Schmidt, A.; Saiardi, A.; Jacob Jessen, H.; Poirier, Y.; Hothorn, M.; et al. Control of Eukaryotic Phosphate Homeostasis by Inositol Polyphosphate Sensor Domains. *Science* **2016**, *352* (6288), 986–990. https://doi.org/10.1126/science.aad9858.

(81) Hamburger, D.; Rezzonico, E.; MacDonald-Comber Petétot, J.; Somerville, C.; Poirier, Y. Identification and Characterization of the Arabidopsis PHO1 Gene Involved in Phosphate Loading to the Xylem. *Plant Cell* **2002**, *14* (4), 889–902. https://doi.org/10.1105/tpc.000745.

(82) Giovannini, D.; Touhami, J.; Charnet, P.; Sitbon, M.; Battini, J. L. Inorganic Phosphate Export by the Retrovirus Receptor XPR1 in Metazoans. *Cell Rep.* **2013**, *3* (6), 1866–1873. https://doi.org/10.1016/j.celrep.2013.05.035.

(83) Hürlimann, H. C.; Pinson, B.; Stadler-Waibel, M.; Zeeman, S. C.; Freimoser, F. M. The SPX Domain of the Yeast Low-Affinity Phosphate Transporter Pho90 Regulates Transport Activity. *EMBO Rep.* **2009**, *10* (9), 1003–1008. https://doi.org/10.1038/embor.2009.105.

(84) Pavlovic, I.; Thakor, D. T.; Vargas, J. R.; McKinlay, C. J.; Hauke, S.; Anstaett, P.; Camunã, R. C.; Bigler, L.; Gasser, G.; Schultz, C.; et al. Cellular Delivery and Photochemical Release of a Caged Inositol-Pyrophosphate Induces PH-Domain Translocation in Cellulo. *Nat. Commun.* **2016**, *7* (1), 10622. https://doi.org/10.1038/ncomms10622.

(85) Joung, M. J.; Mohan, S. K.; Yu, C. Molecular Level Interaction of Inositol Hexaphosphate with the C2B Domain of Human Synaptotagmin I. *Biochemistry* **2012**, *51* (17), 3675–3683. https://doi.org/10.1021/bi300005w.

(86) Lee, T.-S.; Lee, J.-Y.; Kyung, J. W.; Yang, Y.; Park, S. J.; Lee, S.; Pavlovic, I.; Kong, B.; Jho, Y. S.; Jessen, H. J.; et al. Inositol Pyrophosphates Inhibit Synaptotagmin-Dependent Exocytosis. *Proc. Natl. Acad. Sci.* **2016**, *113* (29), 8314–8319. https://doi.org/10.1073/pnas.1521600113.

(87) Saiardi, A.; Bhandari, R.; Resnick, A. C.; Snowman, A. M.; Snyder, S. H. Phosphorylation of Proteins by Inositol Pyrophosphates. *Science* **2004**, *306* (5704), 2101–2105. https://doi.org/10.1126/science.1103344.

(88) Bhandari, R.; Saiardi, A.; Ahmadibeni, Y.; Snowman, A. M.; Resnick, A. C.; Kristiansen, T. Z.; Molina, H.; Pandey, A.; Werner, J. K.; Juluri, K. R.; et al. Protein Pyrophosphorylation by Inositol Pyrophosphates Is a Posttranslational Event. *Proc. Natl. Acad. Sci.* **2007**, *104* (39), 15305–15310. https://doi.org/10.1073/pnas.0707338104.

(89) Veiga, N.; Torres, J.; Domínguez, S.; Mederos, A.; Irvine, R. F.; Díaz, A.; Kremer, C. The Behaviour of Myo-Inositol Hexakisphosphate in the Presence of Magnesium(II) and Calcium(II): Protein-Free Soluble InsP6 Is Limited to 49 MM under Cytosolic/Nuclear Conditions. *J. Inorg. Biochem.* **2006**, *100* (11), 1800–1810. https://doi.org/10.1016/j.jinorgbio.2006.06.016.

(90) Hager, A.; Wu, M.; Wang, H.; Brown, N. W.; Shears, S. B.; Veiga, N.; Fiedler, D. Cellular Cations Control Conformational Switching of Inositol Pyrophosphate Analogues. *Chem. - A Eur. J.* **2016**, *22* (35), 12406–12414. https://doi.org/10.1002/chem.201601754.

(91) Azevedo, C.; Saiardi, A. Extraction and Analysis of Soluble Inositol Polyphosphates from Yeast. *Nat. Protoc.* **2006**, *1* (5), 2416–2422. https://doi.org/10.1038/nprot.2006.337.

(92) Mayr, G. W. A Novel Metal-Dye Detection System Permits Picomolar-Range h.p.l.c. Analysis of Inositol Polyphosphates from Non-Radioactively Labelled Cell or Tissue Specimens. *Biochem. J.* **1988**, *254*, 585–591. https://doi.org/10.1042/bj2540585.

(93) Losito, O.; Szijgyarto, Z.; Resnick, A. C.; Saiardi, A. Inositol Pyrophosphates and Their Unique Metabolic Complexity: Analysis by Gel Electrophoresis. *PLoS One* **2009**, *4* (5). https://doi.org/10.1371/journal.pone.0005580.

(94) Wilson, M. S. C.; Bulley, S. J.; Pisani, F.; Irvine, R. F.; Saiardi, A. A Novel Method for the Purification of Inositol Phosphates from Biological Samples Reveals That No Phytate Is Present in Human Plasma or Urine. *Open Biol.* **2015**, *5* (3), 150014. https://doi.org/10.1098/rsob.150014.

(95) Duong, Q. H.; Clark, K. D.; Lapsley, K. G.; Pegg, R. B. Quantification of Inositol Phosphates in Almond Meal and Almond Brown Skins by HPLC/ESI/MS. *Food Chem.* **2017**, *229*, 84–92. https://doi.org/10.1016/j.foodchem.2017.02.031.

(96) McIntyre, C. A.; Arthur, C. J.; Evershed, R. P. High-Resolution Mass Spectrometric Analysis of Myo-Inositol Hexakisphosphate Using Electrospray Ionisation Orbitrap. *Rapid Commun. Mass Spectrom.* **2017**, *31* (20), 1681–1689. https://doi.org/10.1002/rcm.7935.

(97) Ito, M.; Fujii, N.; Wittwer, C.; Sasaki, A.; Tanaka, M.; Bittner, T.; Jessen, H. J.; Saiardi, A.; Takizawa, S.; Nagata, E. Hydrophilic Interaction Liquid Chromatography–Tandem Mass Spectrometry for the Quantitative Analysis of Mammalian-Derived Inositol Poly/Pyrophosphates. *J. Chromatogr. A* **2018**, *1573*, 87–97. https://doi.org/10.1016/j.chroma.2018.08.061.

(98) Couso, I.; Evans, B. S.; Li, J.; Liu, Y.; Ma, F.; Diamond, S.; Allen, D. K.; Umen, J. G. Synergism between Inositol Polyphosphates and TOR Kinase Signaling in Nutrient Sensing, Growth Control, and Lipid Metabolism in Chlamydomonas. *Plant Cell* **2016**, *28* (9), 2026–2042. https://doi.org/10.1105/tpc.16.00351.

(99) Mulugu, S.; Bai, W.; Fridy, P. C.; Bastidas, R. J.; Otto, J. C.; Dollins, D. E.; Haystead, T. A.; Ribeiro, A. A.; York, J. D. A Conserved Family of Enzymes That Phosphorylate Inositol Hexakisphosphate. *Science* **2007**, *316* (5821), 106–109. https://doi.org/10.1126/science.1139099.

(100) Fridy, P. C.; Otto, J. C.; Dollins, D. E.; York, J. D. Cloning and Characterization of Two Human VIP1-like Inositol Hexakisphosphate and Diphosphoinositol Pentakisphosphate Kinases. *J. Biol. Chem.* **2007**, *282* (42), 30754–30762. https://doi.org/10.1074/jbc.M704656200.

(101) Zhu, J.; Lau, K.; Harmel, R. K.; Puschmann, R.; Broger, L.; Dutta, A. K.; Jessen, H. J.; Hothorn, L. A.; Fiedler, D.; Hothorn, M. Two Bifunctional Inositol Pyrophosphate Kinases/Phosphatases Control Plant Phosphate Homeostasis. *bioRxiv* **2018**, 467076. https://doi.org/10.1101/467076.

Chapter 2: Synthesis of [$^{13}C_6$]*myo*-inositol and [$^{13}C_6$]inositol pyrophosphates[b]

2.1 Introduction

Nuclear magnetic resonance (NMR) spectroscopy is a widely used method for the analysis of diverse substances. In the context of metabolomics, NMR spectroscopy is a powerful tool that can provide valuable information on the status of a cell.[1–3] However, NMR suffers from its inherently low sensitivity, especially for nuclei other than ^{1}H and ^{19}F. The sensitivity and hence the applicability of carbon-NMR measurements are greatly limited by two factors: the low gyromagnetic constant of ^{13}C (γ_C = 67.2828 rad s^{-1} T^{-1}) and the low natural abundance of ^{13}C of only 1.1 %.[4] The low sensitivity can be partially overcome by the use of adequate pulse sequences that exploit the higher gyromagnetic constant of ^{1}H (γ_H = 267.5222 rad s^{-1} T^{-1}) by transferring the magnetization to ^{1}H before detection.[5] The low abundance can be improved by using isotopically enriched compounds that contain > 99 % ^{13}C. The selective labeling of compounds of interest also exploits the low background signal intensity in ^{13}C 1D or 2D experiments and greatly enhances the achievable signal-to-noise ratio, rendering such experiments highly informative, especially in complex mixtures.

For the study of PP-InsPs, scientists have relied on radioactive labeling of *myo*-inositol or the corresponding inositol phosphates for cellular and biochemical assays, respectively.[6] The drawbacks and limitations of this technique are discussed in depth in chapter three. By using a benign label in the form of ^{13}C nuclei, NMR spectroscopy not only overcomes these limitations, it also offers an additional layer of information in the form of structural data, such as the distinction of PP-InsP isomers.

For the application of ^{13}C-labeled *myo*-inositol in metabolic labeling experiments and biochemical characterization of enzymes, large quantities of pure compound

[b] The results of this chapter were partially published in "Puschmann, R. ‡; Harmel, R. K. ‡; Nguyen Trung, M.; Saiardi, A.; Schmieder, P.; Fiedler, D. Harnessing ^{13}C-Labeled *Myo*-Inositol to Interrogate Inositol Phosphate Messengers by NMR. *Chem. Sci*. **2019**, *10* (20), 5267–5274." and "Puschmann R.‡, Harmel R.K.‡, Dorothea Fiedler. 'Scalable Chemoenzymatic Synthesis of Inositol Pyrophosphates' *Biochemistry*. **2019**, *submitted*" (‡ authors contributed equally). To provide a cohesive account, results obtained by RKH are included in this chapter and highlighted as such.

are essential. To date, synthetic approaches have relied either on expensive starting material in the form of [$^{13}C_6$]glucose-6-phosphate (7000 € per g[c]) or were low yielding (9.9 % and 6.7 %).[7–9] In addition, all methods lacked scalable purification strategies, reducing their practical use. In order to make ^{13}C-labeled *myo*-inositol readily accessible and a viable tool, it is necessary to devise an efficient, scalable synthesis for it.

While genetic studies have unraveled a plethora of biological processes regulated by PP-InsPs (Table 1.1), the mechanism of action remains unknown in most cases. Whenever a biochemical mechanism was provided, the researchers relied heavily on synthetic PP-InsP standards. Although the synthetic strategy for the preparation of PP-InsPs, especially 5PP-InsP_5, has been vastly improved over the past years, the synthesis is still time consuming and low yielding (30 % starting from *myo*-inositol).[10–12] In order to advance the study of PP-InsPs, it is essential to gain access to an easy, high-yielding, scalable, and time efficient synthetic route.

In the past, enzymatic approaches were applied whenever the preparation of radioactive PP-InsPs was required. The synthesis was high-yielding and time efficient, however, this approach is limited to a few micrograms of product due to the employed purification strategy *via* SAX-HPLC.[13,14]

In order to render the enzymatic synthesis of 5PP-InsP_5, and PP-InsPs in general, more viable, a new purification strategy has to be developed and a robust expression system for a highly active IP6K and PPIP5K has to be established.

This chapter describes a scalable, enzymatic synthesis of ^{13}C-labeled *myo*-inositol starting from ^{13}C-labeled glucose. The [$^{13}C_6$]*myo*-inositol was used to optimize the chemoenzymatic synthesis of all mammalian PP-InsPs. By taking advantage of the high propensity of PP-InsPs to precipitate with Mg^{2+} ions, a scalable purification strategy for all mammalian PP-InsPs could be realized. The new synthetic route coupled with the precipitation procedure will provide large amounts of pure PP-InsP for the research community.

[c] The price at Eurisotop as of 2018.

2.2 Synthesis of ^{13}C-labeled *myo*-inositol

In order to analyze inositol-derived signaling molecules by NMR, my goal was to prepare large amounts of [$^{13}C_6$]*myo*-inositol (**1**). The synthetic strategy built upon the enzymatic route published by Saiardi and coworkers and was adapted to a scalable procedure by starting from inexpensive [$^{13}C_6$]glucose (**2**) (Figure 2.1).[7] To further simplify the synthesis, commercially available hexokinase was used in the first step for the conversion of **2** to [$^{13}C_6$]glucose-6-phosphate (**3**).[15] The key step, the isomerization of **3** to [$^{13}C_6$]*myo*-inositol-3-phosphate (**4**) is centered around inositol phosphate synthase (IPS) from *Archaeoglobus fulgidus*. The enzyme's origin from a hyperthermophilic organism renders the purification of this enzyme exceedingly simple (after boiling of the lysate only IPS remains in the supernatant), adding to the ease of adaptability of the synthesis for other research groups.[16] The isomerization procedure of Saiardi and colleagues was modified to work with Mg^{2+} instead of paramagnetic Mn^{2+} to enable reaction progress monitoring by NMR (Figure 2.2). The monitoring ensured full conversion during this key step and enabled the usage of commercially available *bovine* alkaline phosphatase (AP) instead of the self-made and inositol-3-phosphate specific inositol monophosphatase for the dephosphorylation of **4** to **1**.

The resulting [$^{13}C_6$]*myo*-inositol contained significant amounts of buffer components and salts, hence it was not pure enough to carry it over into the next

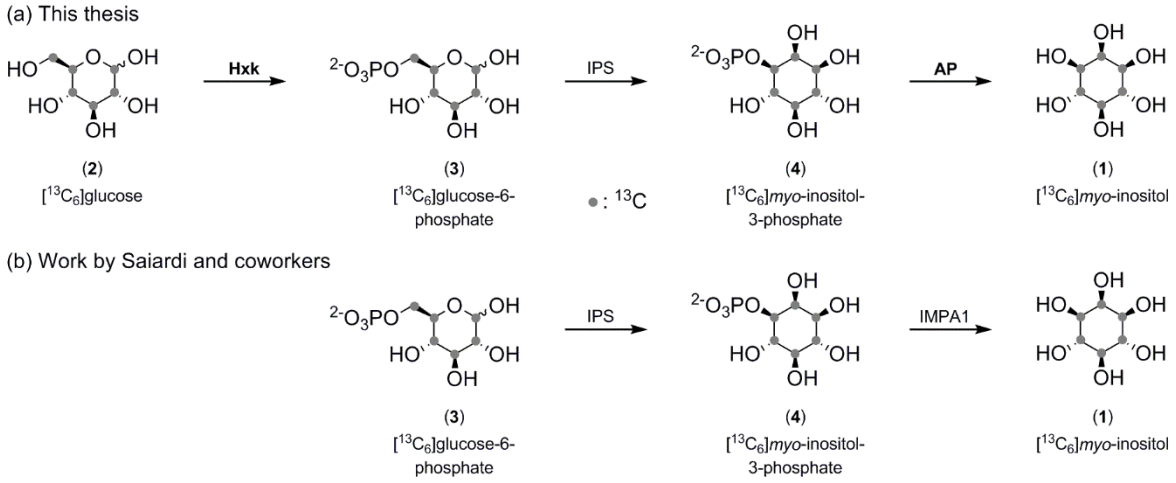

Figure 2.1. Enzymatic synthesis of [$^{13}C_6$]*myo*-inositol. (a) Improved synthetic route starting from [$^{13}C_6$]glucose. (b) Original synthetic route as published by Saiardi and coworkers. IPS: *Archeoglobus fulgidus* inositol phosphate synthase (expressed), IMPA: *human* inositol monophosphatase (expressed), Hxk: *Saccharomyces cerevisiae* hexokinase (commercial), AP: *bovine* alkaline phosphatase (commercial).

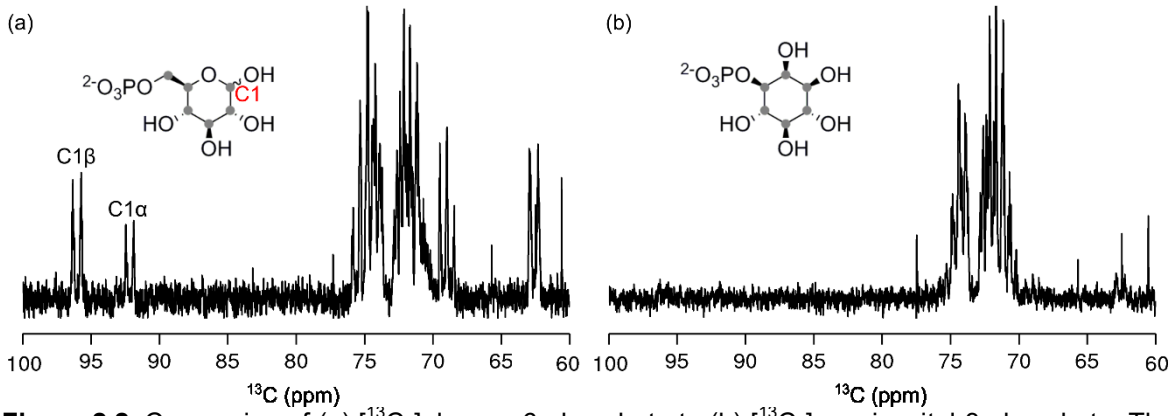

Figure 2.2. Conversion of (a) [$^{13}C_6$]glucose-6-phosphate to (b) [$^{13}C_6$]*myo*-inositol-3-phosphate. The reaction progress can be monitored via the peaks of the anomeric C1 atom at 92 and 96 ppm, respectively.

reactions towards the various InsPs. Because purification attempts *via* ion exchange, normal-phase, and reverse-phase chromatography proved difficult[d], a chemical derivatization strategy was employed. The crude mixture from the dephosphorylation reaction was acetylated using acetic anhydride in pyridine. The resulting [$^{13}C_6$]*myo*-inositol hexakisacetate (**S1**) could then be purified by silica chromatography. After basic deprotection and subsequent precipitation **1** was obtained in high purity and 50 % overall yield.

This method can be extended for other ^{13}C labeling patterns of glucose as well, and [4-^{13}C]- and [4,5-$^{13}C_2$]*myo*-inositol have been prepared from [1-^{13}C]glucose and [1,2-$^{13}C_2$]glucose respectively.

[d] These tests were conducted by RKH.

2.3 Synthesis of [$^{13}C_6$]InsP$_5$ and [$^{13}C_6$]InsP$_6$

With pure **1** in hand, the syntheses of [$^{13}C_6$]InsP$_5$[e] (**5**) and [$^{13}C_6$]InsP$_6$ (**6**), the most abundant soluble InsPs were conducted.[17,18] Standard literature procedures for the unlabeled compounds were used and both compounds were obtained in good yield (Figure 2.3a). The ^{1}H,^{13}C-HMQC spectra for both compounds **5** and **6** displayed four signals each, due to their plane of symmetry. Notably, the spectra in Figures 2.3b and 2.3c were recorded at an InsP concentration of 5 µM with 32 scans, highlighting the remarkable sensitivity provided by ^{13}C-labeling. This feature encouraged us to continue with the development of a NMR based method for the analysis of InsPs and PP-InsPs.

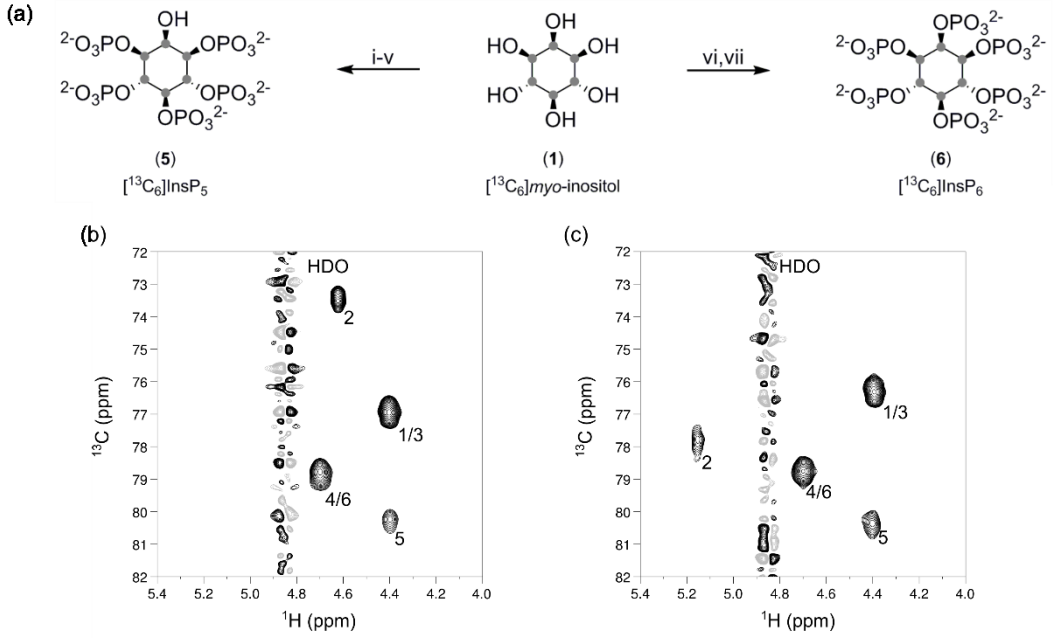

Figure 2.3. Synthesis and characterization of [$^{13}C_6$]inositol polyphosphates. (a) reagents and conditions: (i) CSA, trimethyl orthobenzoate, TEA in DMSO at 80 °C; 85 % yield (ii) TFA in H_2O at rt; quantitative yield (iii) 5-phenyltetrazole, xylyl phorsphoramidite, *m*CPBA in DCM at rt; 79 % yield (iv) $Pd(OH)_2$/C in MeOH/H_2O at rt; 88 % yield (v) NH_3 (aq.) at 60 °C; 65 % yield (vi) Xylyl phosphoramidite, 1*H*-tetrazole, *m*CPBA in DCM at rt; 38 % yield (vii) $Pd(OH)_2$/C in MeOH/H_2O at rt; 83 % yield (b) ^{1}H,^{13}C-HMQC spectrum of [$^{13}C_6$]InsP$_5$ at 5 µM. (c) ^{1}H,^{13}C-HMQC spectrum of [$^{13}C_6$]InsP$_6$ at 5 µM. The positions of the carbon atoms and the solvent signal are indicated.

[e] [$^{13}C_6$]InsP$_5$ was synthesized by RKH.

2.4 Synthesis of [$^{13}C_6$]PP-InsPs

For the best characterized PP-InsP, [$^{13}C_6$]5PP-InsP_5 (**7**), the chemical synthesis, despite recent advances, still requires several steps and promises yields of only 20-25 % starting from *myo*-inositol.[19,20] While this low yield is acceptable for unlabeled substance, the precious nature of the labeled starting material rendered this approach unusable. As an alternative, we envisioned – similar to [$^{13}C_6$]*myo*-inositol – an enzymatic route for a simple and scalable one-step preparation of [$^{13}C_6$]5PP-InsP_5 from **6**.

To this end, *eh*IP6KA was utilized as it is the IP6K with the highest known activity.[21] Stephen Shears (National Institute of Environmental Health Sciences, National Institutes of Health, USA) kindly provided us with the required expression plasmid, which contained IP6Ka in a pDest-556 vector (with a His-MBP-tag). The IP6KA open reading frame (ORF) was sub-cloned into a pET15b vector (with a His-tag), yielding good expression results. By employing an ATP-regenerative system based on creatine phosphate and creatine kinase, the reaction equilibrium was shifted towards 5PP-InsP_5. Further optimization of the conditions using NMR lead to full conversion within 45 minutes.

The isolation of enzymatically produced PP-InsPs previously relied either on SAX-HPLC purification or separation *via* preparative PAGE.[13,14] Both methods, while providing the desired material, lack scalability and contaminate the product with large amounts of salt. To overcome this limitation, I took advantage of the propensity of PP-InsPs to form insoluble salts with Mg^{2+} ions under alkaline

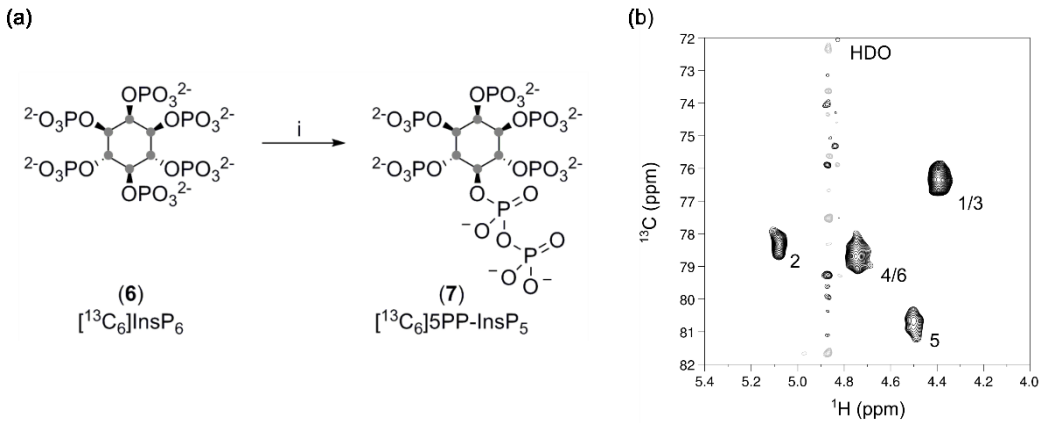

Figure 2.4. Synthesis and characterization of [$^{13}C_6$]5PP-InsP_5. (a) Reagents and conditions: MES pH 6.4, NaCl, ATP, creatine phosphate, $MgCl_2$, DTT, IP6KA in H_2O at 37 °C; quantitative yield. (b) ^{1}H,^{13}C-HMQC spectrum of [$^{13}C_6$]5PP-InsP_5 at 5 µM. The positions of the carbon atoms and the solvent signal are indicated.

conditions.[22,23] Indeed, the addition of $MgCl_2$ to the reaction mixture resulted in the selective precipitation of all InsPs, while all other reaction components remained in solution, including ATP and creatine phosphate. The 5PP-$InsP_5$–Mg salt was collected, washed and resolubilized by treatment with metal ion chelating resin, affording 5PP-$InsP_5$ in excellent yield (quantitatively on a 50 mg scale and 79 % on a 350 mg scale) and high purity as the ammonium salt (Figure 2.4).

The underlying ideas of the synthesis and purification for **7** can also be applied to make $[^{13}C_6]$1,5(PP)$_2$-$InsP_4$ (**8**) and $[^{13}C_6]$1PP-$InsP_5$ (**9**). Human diphosphoinositol pentakisphosphate kinase 2 (PPIP5K2) phosphorylates **7** to **8** and **6** to **9**, respectively (Figure 1.1). However, compared to IP6KA, PPIP5K2 is a less efficient enzyme and to obtain the large amounts of PPIP5K2 required, a codon optimized ORF was ordered and sub-cloned into a pSUMO plasmid to generate a His_6-sumo-PPIP5K2 fusion protein. Sumo-PPIP5K2 displayed adequate activity despite the tethered sumo protein and was therefore used as such without cleavage of the tag. The catalytic activity of PPIP5K2 varies for both its substrates, with 5PP-$InsP_5$ being the better substrate compared to $InsP_6$.[24] Therefore, the enzyme concentration in the reaction was raised and the reaction time prolonged to 5.5 hours (to make **8**) and 18 hours (to make **9**), respectively (Figure 2.5). After precipitation, **8** was obtained in excellent purity and good yield

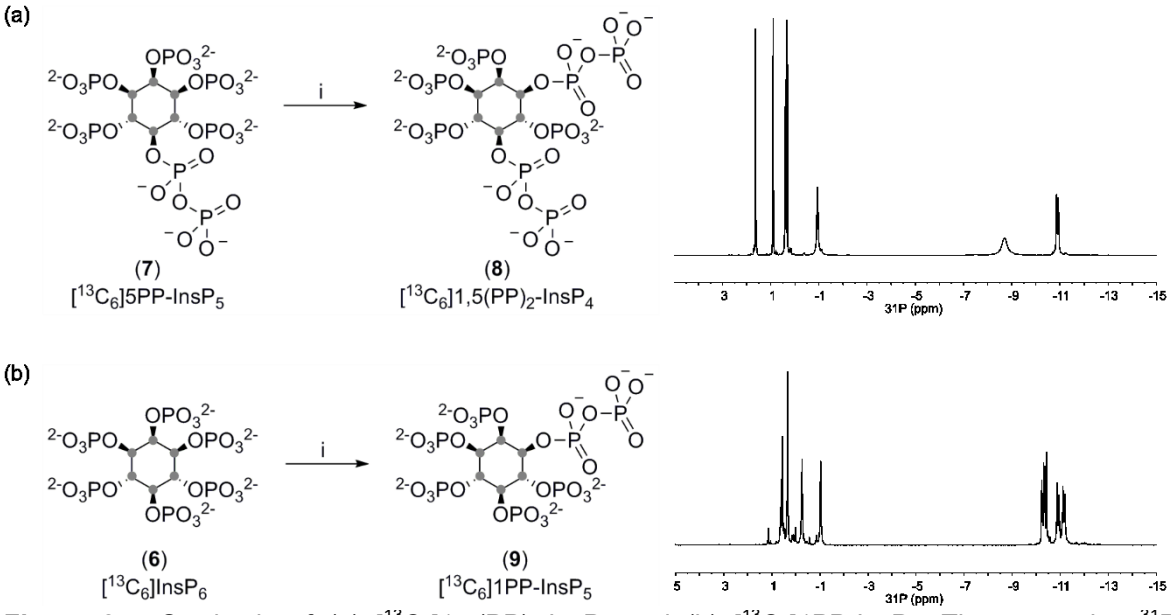

Figure 2.5. Synthesis of (a) $[^{13}C_6]$1,5(PP)$_2$-$InsP_4$ and (b) $[^{13}C_6]$1PP-$InsP_5$. The respective ^{31}P spectrum is displayed on the right. Reagents and conditions: MES pH 6.4, NaCl, ATP, creatine phosphate, $MgCl_2$, DTT, PPIP5K2 in H_2O at 37 °C.

(77 % on a 130 mg scale). [$^{13}C_6$]1PP-InsP_5, however, was contaminated with byproducts, probably a consequence of the long reaction time (18 hours). Therefore, the product was separated from the mixture by means of SAX-FPLC (Fast Protein Liquid Chromatography) with a NH_4HCO_3 gradient and after lyophilization pure **9** was obtained in good yield (68 %).[f]

2.5 Synthesis of 5PP-InsP_5-β^{32}P

Radioactive tracers have played a pivotal role in the field of inositol pyrophosphates, both in the form of tritiated *myo*-inositol and ^{32}P-labeled 5PP-InsP_5. The latter being the only option for identification of protein pyrophosphorylation targets *in vitro*.

To ensure the highest labeling efficiencies, the published protocol used an excess of InsP_6 over ATP to force the incorporation of ^{32}P from ATPγ^{32}P into 5PP-InsP_5. The method required a subsequent purification by SAX-HPLC to separate the unreacted InsP_6 and residual ATPγ^{32}P from the product, as those contaminants could potentially interfere with subsequent assays. The limited scale is not an issue in this context, however, the high amount of salt contaminations, and especially the requirement of a dedicated radioactive HPLC instrument restrict this tool to a few select groups. In order to facilitate access to ^{32}P-labeled compounds, I envisioned a modified procedure for the preparation of ^{32}P containing PP-InsPs based on the precipitation protocol established for the [$^{13}C_6$]5PP-InsP_5 (Figure 2.6a).

Separating the 5PP-InsP_5-β^{32}P (**10**) from the reaction mixture *via* precipitation would render the limiting SAX-HPLC separation obsolete. To ensure proper precipitation the reaction volume had to be increased 10-fold compared to the established ^{32}P-labeling approach. Furthermore, to guarantee full conversion and hence limit inseparable InsP_6 contamination to a minimum, the ATP concentration had to be increased, while also incorporating a creatine kinase-based ATP-regenerating system. With minor adjustments to the reaction time and $MgCl_2$ content, the reaction proceeded to full conversion, as tested with nonradioactive compound.

[f] The synthesis and purification was performed by RKH.

After the initial precipitation/chelation, the purified 5PP-InsP$_5$-β^{32}P solution was subjected to SAX-HPLC separation and scintillation counting for testing its purity (Figure 2.6b). Unexpectedly, the putative product contained significant amounts of ATPγ^{32}P and over-phosphorylated InsP$_8$ species. The InsP$_8$ species was not a major concern, however, the residual ATPγ^{32}P could lead to a false positive signal if a kinase would transfer the γ^{32}P-phosphate to a protein. To tackle this issue, I tested apyrase treatments at two different points in the protocol to degrade ATPγ^{32}P. When apyrase was added before the initial precipitation, a significant amount of the liberated phosphate, including the ^{32}P-phosphate, was co-precipitated, resulting in a large amount of radioactive contaminants and low yield. However, if the apyrase treatment was applied after the precipitation, only the carried-over ATPγ^{32}P was further degraded, enabling the isolation of highly pure 5PP-InsP$_5$-β^{32}P after a second precipitation step (Figure 2.6b).

The major drawback of this procedure is the relatively low specific activity (ca. 50-fold lower) of the generated radiolabeled 5PP-InsP$_5$ as compared to the traditional method. To test if the activity was high enough to observe protein pyrophosphorylation, a fragment of yeast NSR1, an established

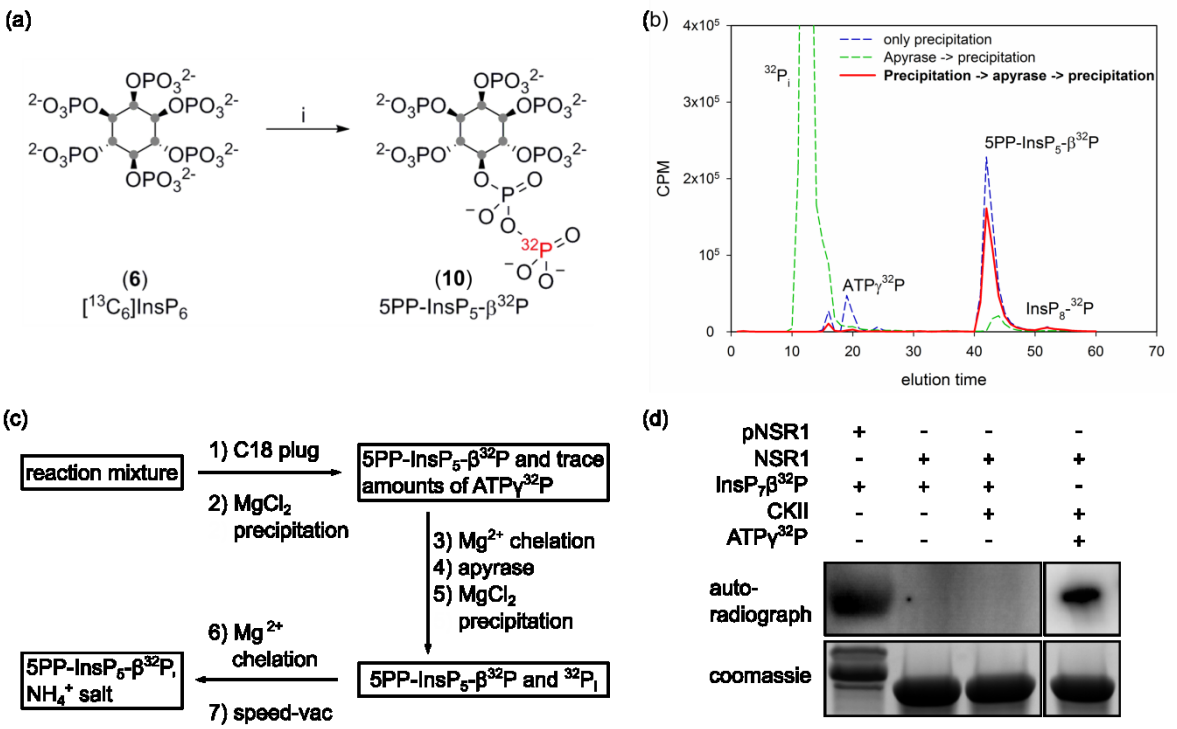

Figure 2.6. Synthesis of 5PP-InsP$_5$-β^{32}P. (a) Reagents and conditions: (i) MES pH 6.4, NaCl, ATP, creatine phosphate, MgCl$_2$, DTT, IP6KA in H$_2$O at 37 °C. (b) Chromatogram of of 5PP-InsP$_5$-β^{32}P after different purification methods. (c) Final procedure for the preparation of 5PP-InsP$_5$-β^{32}P. (d) Protein pyrophosphorylation of phospho-NSR1 to test purity of the prepared 5PP-InsP$_5$-β^{32}P.

pyrophosphorylation target, was incubated with the prepared radioactive 5PP-$InsP_5$-$\beta^{32}P$ (Figure 2.6d). Pre-phosphorylated NSR1 (pNSR1) was modified by **10** as expected, while non-phosphorylated NSR1 was not. More importantly, a control of NSR1 and casein kinase 2 showed no signal, highlighting that the apyrase treatment removed all detectable ATP$\gamma^{32}P$ from the reaction product (Figure 2.6d).

The benefit of this route is the easy accessibility to radiolabeled compounds for groups without specialized equipment and although the specific activity of the product is reduced compared to the literature method, the achievable signal is strong enough to detect protein pyrophosphorylation (Figure 2.6c).

2.6 Discussion and Outlook

The reliable production of all major mammalian PP-InsPs on a 100 mg scale is not limited to ^{13}C-labeled compounds but is, of course, also amenable for unlabeled material as well. The newly found accessibility to PP-InsPs will enable the research community to pursue new avenues in their research that have so far been inaccessible due to a lack of the required materials. High-throughput screens for IP6K and PPIP5K inhibitors are now, for example, possible. Another pressing question is the existence of additional PP-InsP phosphatases. Only now is enough substrate available to test a large array of potential candidates and define their substrate specificity. Recently, a study described a group of $InsP_6$ and 5PP-$InsP_5$ interacting proteins in yeast.[25] In order to elucidate how these interactions influence the protein's activity sufficient PP-InsP quantities are needed.

The main application for ^{13}C-labeled *myo*-inositol and PP-InsPs, however, will be in NMR spectroscopy. Replacing radioactive inositol with [$^{13}C_6$]*myo*-inositol in cell labeling experiments would be a great improvement as ^{13}C is a benign label. Furthermore, the samples could be analyzed without the need for a separation step, possibly capturing interactions that are otherwise inaccessible.

^{13}C-PP-InsPs can be a valuable tool to follow reactions *in vitro,* as well. Currently, no method is capable to replace a radioactive assay in all biochemical applications. Here, ^{13}C-PP-InsP could provide an alternative approach, be it for kinetic studies or in a binding assay.

The main bottlenecks in the presented methodology are the large amounts of IP6KA and especially PPIP5K2 that are required. However, the proteins express well and groups with biological experience will have no problem obtaining sufficient amounts of these proteins.

During the method development, we realized that clean $InsP_6$ starting material is essential to obtaining pure product. All commercially available $InsP_6$ that we tested was not clean enough to be used as starting material and so we prepared it ourselves. Although the synthesis is not difficult, it requires standard chemistry equipment and is low yielding, making it inaccessible for biological groups. These problems could be circumvented with pure commercially available $InsP_6$. I did not test all available vendors and hence, give no final recommendation.

2.7 Methods

General Information

All chemicals were purchased from Sigma Aldrich, VWR, Carl Roth, Thermo Fisher Scientific, Alfa Aesar, TCI and used without further purification unless stated otherwise. All dry solvents were purified using a solvent purification system MBRAUN MB-SPS-5 by passing through activated alumina columns. Deuterated solvents were purchased from Euriso-Top. The C18 Sep-Pak columns were purchased from Waters. Telos® was ordered from Kinesis. Normal phase flash chromatography was performed using analytical grade solvents and silica gel from VWR (40-63 µm) as stationary phase. Automated flash chromatography was performed using gradient grade solvents on a CombiFlash® Rf from Teledyne Isco using prepacked CombiFlash® columns (40-63 µm). Reversed phase flash chromatography was performed on C18 reversed phase silica gel from Teledyne Isco (40-63 µm) as stationary phase. LC-MS analysis was carried out with an Agilent 1260 Infinity Binary LC system connected to an Agilent 6130 Quadrupole LC/MS system with a ZORBAX Rapid Resolution HT Narrow Bore SB-C18 1.8 µm column (2.1 x 50mm) at 30 °C using API-ESI (atmospheric pressure ionization-electrospray) in positive ion mode. The eluent consisted of 10% ACN in water with 0.1% formic acid at 0.7 mL/min flow rate.

NMR spectra were recorded on Bruker spectrometers operating at 300 or 600 MHz for proton nuclei, 75 or 151 MHz for carbon nuclei or 122 and 244 MHz for phosphorous nuclei. NMR data are given as follows: chemical shift δ in ppm (multiplicity, coupling constant(s) J Hz, relative integral) where multiplicity is defined as: s = singlet, d = doublet, t = triplet, q = quartet, m = multiplet, br = broad or combinations of the above. The software used to control the spectrometer was topspin 3.5 pl6. Temperature had been calibrated using d_4-methanol and the formula of Findeisen et al.[26]

High-resolution mass spectrometer was performed by direct inject on an Orbitrap™ Q-Exactive mass spectrometer (Thermo Fisher Scientific).

For the purification *via* FPLC an NGC Quest™ 10 Chromatography System from Bio-Rad was used with an integrated NGC™ Sample Pump Module and a BioFrac™ Fraction Collector. For the spin filtration Amicon Ultra 0.5 mL centrifugal filters with a cut off of 10 kDa or 3 kDa from Merck Millipore were used.

Recombinant Protein Expression

Inositol phosphate Synthase (IPS)

The IPS-gene from *A. fulgidus* cloned into a pET23a vector (Prof. Helena Santos, Universidade Nova de Lisboa)[27] was transformed into *E. coli* BL21(DE3). Two 0.8 liter overnight cultures (37 °C) in Terrific Broth (TB) supplemented with Ampicillin were each diluted with 400 mL TB, prewarmed to 37 °C. After 30 min the expression was induced with 0.25 mM IPTG. After 4 hours the cells were harvested by centrifugation (3,000 g for 10 min at 4 °C) and washed with ice cold water. The pellet was stored at -80 °C until further use.

The frozen cells were resuspended in lysis buffer (50 mM Tris HCl pH 8, 250 mM NaCl). For 1 g cell pellet wet weight, 5 mL lysis buffer was used. The cell suspension was supplemented with lysozyme and DNase I, and incubated for 15 min on ice. The cells were lysed with a Microfluidizer™ LM10 at 15,000 psi with five iterations. The lysate was clarified by centrifugation (30,000 g for 30 min at 4 °C). The supernatant was incubated for 30 min at 80 °C and the precipitate was removed by centrifugation (30,000 g for 30 min at 4 °C). The volume of the heat-treated supernatant was reduced to 22 mL with spin filtration (Amicon® Ultra 15 mL 10K) and the solution was dialyzed against lysis buffer overnight. The protein solution was adjusted to 33 % (v/v) glycerol, aliquoted, frozen in liquid nitrogen, and stored at -80 °C.

Inositol hexakisphosphate kinase A (IP6KA)

The codon optimized IP6KA-gene from *E. histolytica* was subcloned from a pDest-566 vector (a kind gift from Stephen B. Shears)[28] into a pET15b plasmid using NdeI and BamHI restriction sites that were introduced by PCR (forward primer (NdeI): GGCAGCCATATGAACACGAAAATCAAACGCG, reverse primer (BamHI): GCAGCCGGATCCTTACAGTGACTTAAATTCGTTTTCG). The resulting pET15b-IP6KA plasmid was transformed into *E. coli* BL21 Arctic Express (DE3) and an overnight culture was diluted into 1 L of TB medium supplemented with Ampicillin to a final density of OD_{600} 0.1. The cells were grown for 6 h at 37 °C. The culture was then switched to 18 °C for 30 min before induction with 0.1 mM IPTG for 18 hours. The cells were harvested by centrifugation (3,000 g for 10 min at 4 °C) and washed with ice cold water. The cell pellet was resuspended in lysis

buffer (25 mM Tris HCl pH 7.4, 500 mM NaCl, 50 mM imidazole). For 1 g wet weight 10 mL lysis buffer was used. The cell suspension was supplemented with lysozyme, DNase I, and 1 tablet cOmplete™ protease inhibitor (Roche), and incubated for 15 min on ice. The cells were lysed with a microfluidizer™ LM10 at 15,000 psi with five iterations. The lysate was clarified by centrifugation (30,000 g for 30 min at 4 °C). The supernatant was filtered (VWR® vacuum filter, PES 0.45 µm), and loaded onto a Ni-NTA column (GE, 5 mL, HiTrap IMAC HP) equilibrated with lysis buffer with a flowrate of 2.5 mL/min. The column was washed with lysis buffer until the absorption was constant. IP6KA was eluted with a gradient of elution buffer (25 mM Tris HCl pH 7.4, 200 mM NaCl, 500 mM imidazole) in lysis buffer from 0-100 % over 10 CV. 1.5 mL fractions were collected. The fractions containing IP6KA were concentrated by spin filtration (Amicon® Ultra 0.5 mL 10K) and dialyzed overnight against dialysis buffer (20 mM Tris HCl pH 7.4, 200 mM NaCl, 1 mM DTT). The following day the protein was adjusted to 25 % glycerol, frozen in liquid nitrogen and stored at -80 °C.

Synthesis of [$^{13}C_6$]*myo*-inositol

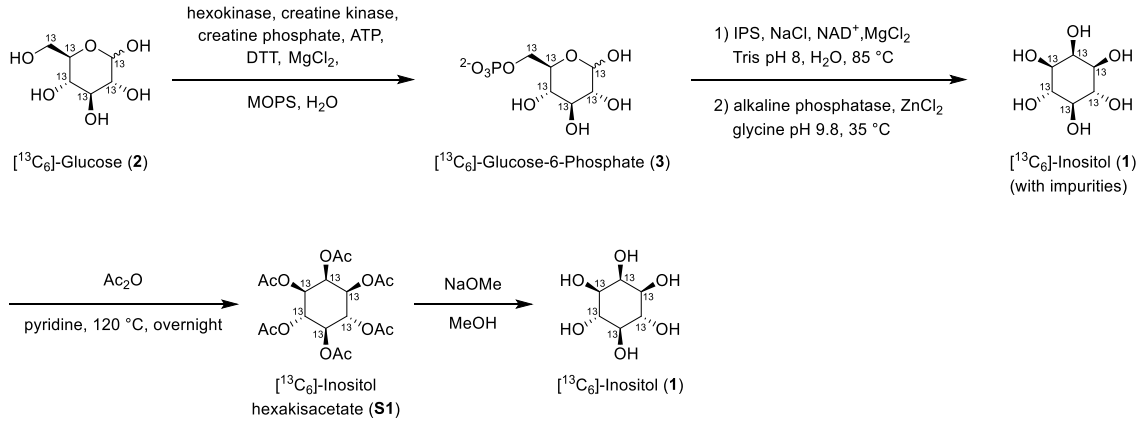

The following stock solutions were prepared:

Hexokinase stock solution: 1000 U/mL in 50 mM citrate pH 7, 10 mM $MgCl_2$, 1 mg/mL BSA.

Creatine kinase stock solution: 350 U/mL in 200 mM MOPS pH 6.5, 20 mM $MgCl_2$, 20 mM DTT.

Inositol phosphate synthase stock solution: 4 mg/mL in 20 mM Tris HCl pH 7.4, 200 mM NaCl, 1 mM DTT.

Alkaline phosphatase stock solution: 100 U/mL, 10 mM Tris pH 8.5, 5 mM $MgCl_2$, 0.2 mM $ZnCl_2$, 50 % (v/v) glycerol.

A solution containing D-[$^{13}C_6$]glucose (2) (83 mM, 1000 mg, 5.4 mmol), MOPS (100 mM, pH 6.5), creatine phosphate (87 mM), ATP (1 mM), DTT (20 mM) and $MgCl_2$ (20 mM) in MilliQ® water (65 mL total reaction volume) was prepared and evenly split (32.5 mL each) into two 50 mL conical tubes. Hexokinase (1 U/mL) and creatine kinase (1.75 U/mL) were added and the reaction incubated at 30 °C overnight. The resulting solution was monitored by TLC (MeOH:H_2O:NH_4OH:AcOH, 50:30:15:5; stained by $KMnO_4$ or excessive heating) and upon completion diluted 5-fold with 320 mL of water. An anion-exchange column (DOWEX® 1X8) was equilibrated with 1 M $(NH_4)HCO_3$ and washed with water. The reaction mixture was loaded onto the column followed by washing with water to remove unreacted 2. [$^{13}C_6$]glucose-6-phosphate (3) was eluted by 0.1 M $(NH_4)_2CO_3$ and lyophilized to obtain the product 3 in combination with high amount of salts (4 g) as a white solid.

The product/salt mixture was redissolved in 40 mL MilliQ® water and added to a solution of Tris (50 mM, pH 8.0), NAD^+ (0.5 mM), NaCl (50 mM) and $MgCl_2$ (2 mM) in MilliQ® (196 mL total reaction volume). The pH was adjusted to 8.0, if necessary, and the mixture was evenly split (49 mL each) into four 50 mL conical tubes. Recombinantly expressed inositol-3-phosphate synthase (IPS) (500 µL of 4 mg/mL stock) was added to each tube and the reaction mixture was incubated at 85 °C monitoring conversion by NMR. After 4 h, NAD^+ (10 mg, 0.8 mM total) and IPS (500 µL, 4 mg/mL) were added to each tube and the mixture was incubated for additional 4 h at 85 °C. After full conversion of 3 into [$^{13}C_6$]*myo*-inositol-3-phosphate (4) was observed by ^{13}C NMR the reaction mixture was directly used for the subsequent dephosphorylation reaction.

For the dephosphorylation reaction, the 200 mL reaction mixture was split evenly across 5 conical tubes (40 mL each). For a total reaction volume of 50 mL, glycine (50 mM, pH 9.8) was added and the pH adjusted to 9.8. $ZnCl_2$ (0.25 mM) and alkaline phosphatase (0.5 U/mL) were added and the solution was filled up to 50 mL with MilliQ® water. After incubation at 35 °C overnight, all tubes were combined (250 mL total) and diluted with 300 mL MilliQ® water and the reaction mixture was applied to an ion exchange column (DOWEX® 1X8 in HCO_3^- form).

The flow-through was collected and lyophilized to afford [$^{13}C_6$]*myo*-inositol (1) with salts (7.5 g) as a brown solid which was directly used for the acetylation reaction.

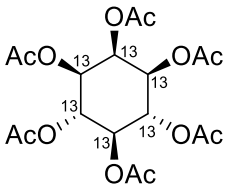

[$^{13}C_6$]Inositol hexakisacetate (S1)

The crude material of 1 (7.5 g) was suspended in pyridine (161 mL) and treated with acetic anhydride (68.5 mL) at 120 °C overnight. The black solution was concentrated to minimize the amount of pyridine, re-dissolved in DCM (500 mL), and 1 M HCl was added. The resulting suspension was filtered and the filter washed with DCM and water. All filtrates were combined and organic and aqueous phase were separated. (Note: Phase separation is hard to see because of the black solution so use a flash light to find the separation layer.) The aqueous layer was extracted twice with DCM and the combined organic layers were washed with 1 M $NaHCO_3$. The aqueous layer was washed twice with DCM and the combined organic layers were washed with brine, dried with Na_2SO_4 and concentrated under reduced pressure. The residue was immobilized on Telos® and purified by column chromatography on silica gel changing the eluent step wise (hexane:EtOAc, 10:1 → 5:1 → 1:1 → 1:2) assisted by analysis of the fractions by LCMS to afford compound S1 (1200 mg, 2.7 mmol) as a white solid in 50% overall yield from 2.

^{1}H NMR (600 MHz, $CDCl_3$) δ 5.79 – 5.54 (m, 1.5H), 5.53 – 5.32 (m, 1.5H), 5.32 – 5.12 (m, 1.5H), 5.11 – 4.82 (m, 1.5H), 2.20 (s, 3H), 2.01 (s, 3H), 2.01 (s, 6H), 2.00 (s, 6H).

^{13}C NMR (151 MHz, $CDCl_3$) δ 169.94, 169.81, 169.56, 71.68 – 70.65 (m), 70.11 – 69.15 (m), 69.11 – 67.90 (m), 20.89, 20.69, 20.60.

HRMS (ESI/Orbitrap) m/z: $[M + K]^+$ calcd. for $C_{12}{}^{13}C_6H_{24}KO_{12}$ 477.1101; Found 477.1091.

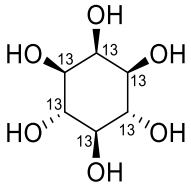

[$^{13}C_6$]*myo*-Inositol (1)

To a solution of S1 (1200 mg, 2.7 mmol) in methanol (249 mL), 5.4 M NaOMe in MeOH (3.35 mL, 18.1 mmol) was added and the reaction was left to stir for 2 hours. The resulting suspension was neutralized by the addition of DOWEX 50W x 8 (H^+ form) followed by filtration. The residue was washed with methanol (100 mL) and water (100 mL) to dissolve all precipitated [$^{13}C_6$]*myo*-inositol and the filtrate was evaporated. The resulting solids were redissolved in H_2O and precipitated by the addition of MeCN. Subsequently, the solids were redissolved in H_2O and lyophilized to afford 1 (505 mg, 2.7 mmol) as white solid in 99% yield.

^{1}H NMR (600 MHz, D_2O, pD 7.0) δ 4.29 – 4.14 (m, 0.5H), 4.03 – 3.90 (m, 0.5H), 3.82 – 3.60 (m, 2H), 3.59 – 3.34 (m, 2.5H), 3.25 – 3.12 (m, 0.5H).

^{13}C NMR (151 MHz, D_2O, pD 7.0) δ 74.96 – 73.80 (m), 72.86 – 71.71 (m), 71.60 – 70.50 (m).

HRMS (ESI/Orbitrap) m/z: $[M - H]^-$ Calcd for $^{13}C_6H_{11}O_6$ 185.0762; Found 185.0814.

Chemical synthesis of [$^{13}C_6$]inositol polyphosphates

Synthesis of xylyl phosphoamidite

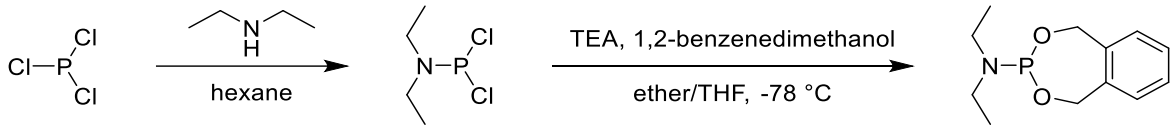

(**S2**) (**S3**)

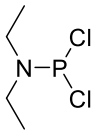

N,*N*-diethylaminodichlorophosphine (S2)

N,*N*-diethylaminodichlorophosphine was synthesized according to a procedure of Drent and coworkers.[29] S2 was obtained in 68% yield (12.9 g, 74.37 mmol) in good purity. ^{1}H-, ^{13}C- and ^{31}P NMR are in agreement with the literature procedure.

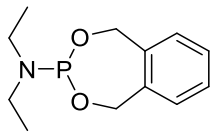

Xylyl phosphoramidite (S3)

Xylyl phosphoamidite was synthesized according to a modified procedure of Gregory and coworkers[30]. S2 (11.1 g, 63.79 mmol) was dissolved in dry THF (425 mL) and cooled to -78 °C. A solution of triethylamine (12.9 g, 17.8 mL, 127.59 mmol) and phenyldimethanol (8.8 g, 63.79 mmol) in dry THF (425 mL) was prepared and added to the stirring reaction mixture with a dropping funnel over 30 min. The cooling was removed and the reaction left to stir overnight at room temperature. The resulting precipitates were removed by filtration and washed with dry THF (2 × 100 mL) and the filtrate was concentrated to 500 mL. TEA (5 mL) was added to the solution and it was passed through a silica plug (equilibrated with 1% TEA in dry THF). Subsequently, 1% TEA in THF (2.0 L) was passed through the silica plug and the combined organic fractions were concentrated to afford the product (14.9 g, 62.09 mmol) as colorless oil in 97 % yield. The product can be stored at -20 °C under N_2 for several months. ^{1}H-, ^{13}C- and ^{31}P NMR are in agreement with the literature procedure.

Synthesis of [$^{13}C_6$]inositol hexakisphosphate (6)

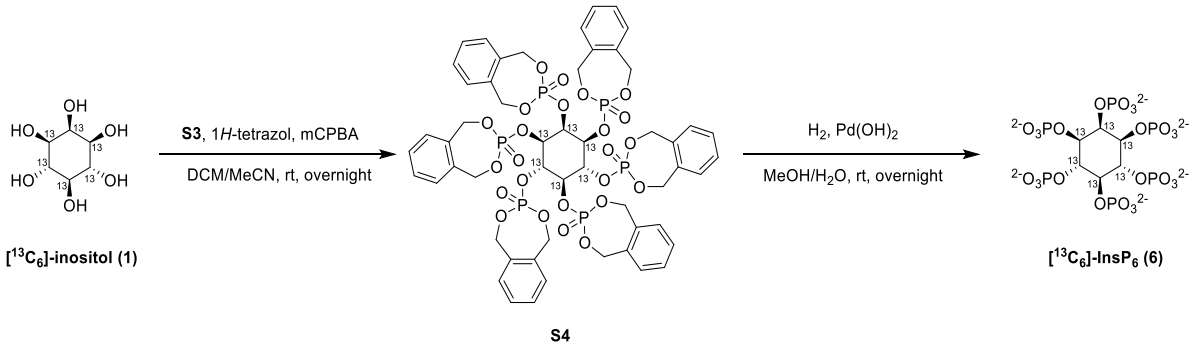

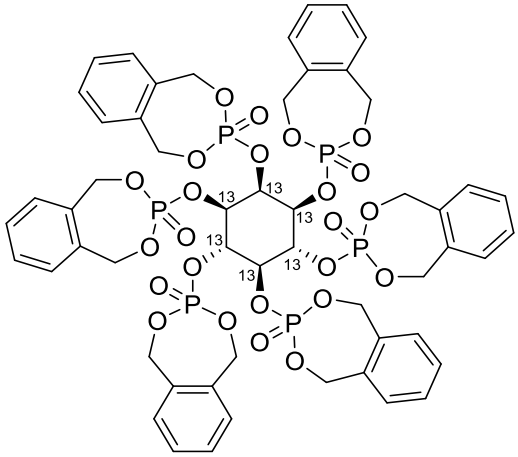

Xylyl protected [$^{13}C_6$]inositol hexakisphosphate (S4)

Xylyl protected [$^{13}C_6$]inositol hexakisphosphate (S4) was synthesized according to a modified procedure of Podeschwa and coworkers[31]. Under nitrogen atmosphere a suspension of 1 (100 mg, 0.54 mmol) and S3 (900 mg, 3.76 mmol) in dry DCM (38.65 mL) was prepared and sonicated for 1 min. 1*H*-tetrazole in anhydrous MeCN (14.33 mL, 6.45 mmol, 0.45 M) was added and the solution was stirred at rt overnight. For workup the solution was cooled to -40 °C and an anhydrous solution of *m*CPBA in DCM (30 mL dried with Na_2SO_4) was added. The solution was allowed to warm to rt, and the stirring was continued for another hour. The reaction mixture was diluted with DCM (300 mL) and washed consecutively with aqueous sodium bisulfite (20%, 2 × 50 mL), saturated $NaHCO_3$ (3 × 100 mL), and then with brine. After evaporation of the solvents, the crude was immobilized on Telos® and purified by CombiFlash® chromatography on silica gel (12 g column, gradient: 0% → 2% → 4% → 10% MeOH in DCM) and afforded the product (221 mg, 0.173 mmol) as a white solid in 32% yield.

^{1}H NMR (600 MHz, Chloroform-*d*) δ 7.60 – 7.49 (m, 18H), 7.44 (d, *J* = 7.7 Hz, 6H), 5.93 (dd, *J* = 13.8, 9.5 Hz, 2.5H), 5.84 (dd, *J* = 13.7, 9.1 Hz, 2H), 5.79 – 5.70 (m,

6H), 5.66 (s, 0.5H), 5.55 (dd, *J* = 13.9, 12.4 Hz, 3H), 5.50 – 5.16 (m, 15H), 5.12 (s, 1H).

^{13}C NMR (151 MHz, Chloroform-*d*) δ 135.94, 135.91, 135.73, 135.69, 135.52, 134.62, 129.72, 129.60, 129.47, 129.45, 129.42, 129.40, 129.39, 129.36, 129.19, 129.13, 78.48 – 76.20 (m), 73.92 (dd, *J* = 43.9, 34.0 Hz), 69.84, 69.79, 69.68, 69.62, 69.57, 69.51, 69.45.

^{31}P NMR (122 MHz, Chloroform-*d*) δ -2.80, -3.57, -4.48, -4.71.

HRMS (ESI/Orbitrap) m/z: $[M + H]^+$ Calcd for $C_{48}{}^{13}C_6H_{54}O_{24}P_6$ 1279.1705; Found 1279.1676.

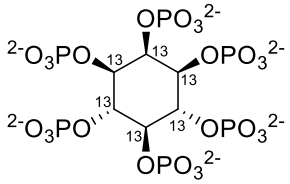

[$^{13}C_6$]inositol hexakisphosphate (6)

[$^{13}C_6$]inositol hexakisphosphate (6) was synthesized according to a modified procedure of Godage and coworkers[32]. Compound S4 (148 mg 0.12 mmol) was dissolved in methanol (10.53 mL) and water (2.63 mL) and 20% $Pd(OH)_2$/C (50% wetted with water) (68 mg, 0.49 mmol) was added. The resulting suspension was stirred at room temperature overnight under hydrogen atmosphere. The reaction mixture was passed through a PTFE syringe filter and the filtrate was evaporated under reduced pressure. The free acid was treated with NaOH (1 M) to afford the dodecasodium salt of 6 as a white solid (136 mg, 0.10 mmol, 66 w/w%) in 83% yield.

^{1}H NMR (600 MHz, Deuterium Oxide, pD 7.0) δ 5.01 – 4.90 (m, 0.5H), 4.71 – 4.63 (m, 0.5H), 4.48 – 4.34 (m, 1H), 4.22 – 4.04 (m, 2.5H), 3.95 – 3.78 (m, 1.5H).

^{13}C NMR (151 MHz, Deuterium Oxide, pD 7.0) δ 79.99 (d, *J* = 35.7 Hz), 78.52 (t, *J* = 40.0 Hz), 77.60 – 74.58 (m).

^{31}P NMR (122 MHz, Deuterium Oxide, pD 7.0) δ 1.99, 1.04, 0.77.

HRMS no ion detected.

Synthesis of and [$^{13}C_6$]inositol pentakisphosphate

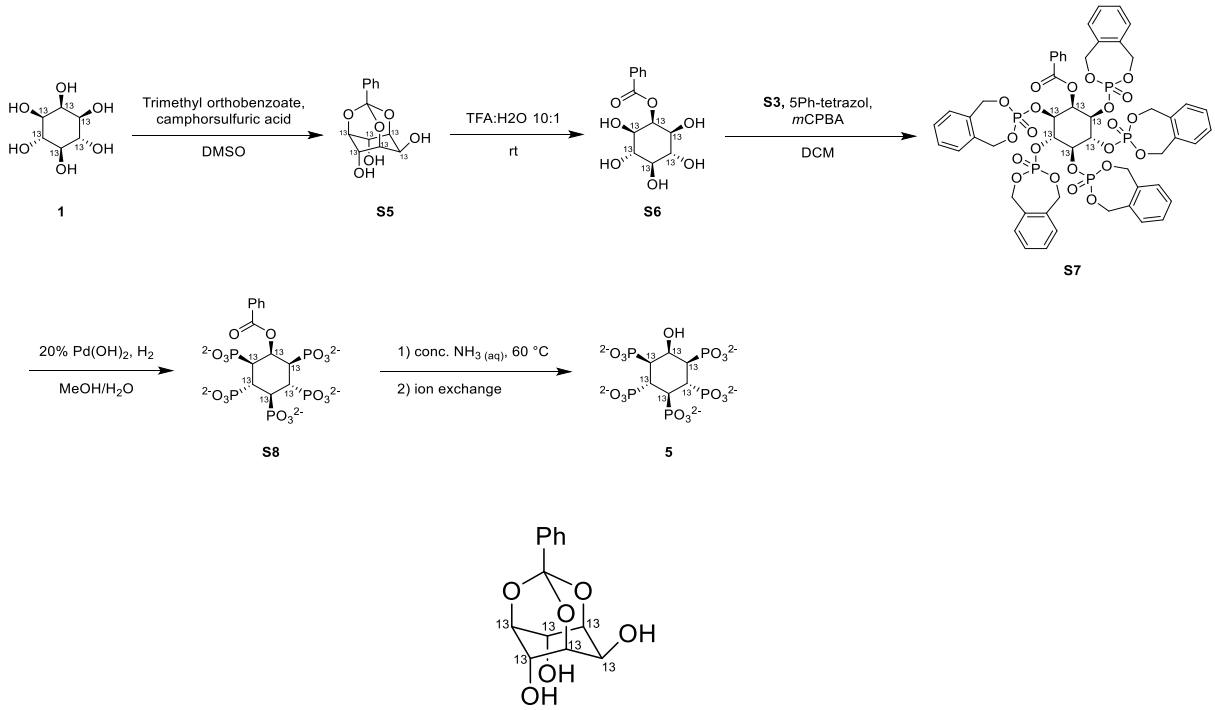

[$^{13}C_6$]inositol-(1,3,5)-orthobenzoate ester (S5)

[$^{13}C_6$]inositol-(1,3,5)-orthobenzoate (S5) ester was synthesized according to a modified procedure of Godage and coworkers[32]. A suspension of 1(1.045 g, 5.61 mmol) and CSA (26.08 mg, 0.11 mmol) in DMSO (3.74 mL) was heated to 80 °C under vacuum (Rotovap, 30-40 mbar) to remove residual water. Upon the addition of trimethyl orthobenzoate (1.125 g, 6.17 mmol, 1.061 mL), the mixture was left at 80 °C under vacuum (Rotovap, 30-40 mbar) until the suspension became clear. The resulting solution was quenched with TEA (62.5 mg, 0.62 mmol, 86 µL). (Note: Quenching of acid is highly important to assure the stability of the formed orthoester during the workup.) The product was slowly precipitated through the addition of water (16 mL) at 4 °C and the solids were filtered and washed with ice cold water 3 times. The mother lye was combined with the washings and applied to reversed phase chromatography changing the eluent step wise (5 % → 25 % → 50 % MeCN in H_2O) to separate residual product from DMSO. The product containing fractions were lyophilized and the precipitates were dissolved in 50 % MeCN in H_2O and lyophilized to afford the product S5 (1.300 g, 4.78 mmol) as white solid in 85% yield.

^{1}H NMR (600 MHz, Methanol-d_4) δ 7.71 – 7.64 (m, 2H), 7.42 – 7.30 (m, 3H), 4.70 (s, 1H), 4.45 (s, 2.5H), 4.37 (s, 0.5H), 4.18 (s, 1.5H), 4.13 (s, 0.5H).

^{13}C NMR (151 MHz, Methanol-d_4) δ 130.12, 128.58, 126.74, 77.50 (t, *J* = 37.2 Hz), 71.63 (t, *J* = 37.7 Hz), 68.98 (t, *J* = 37.7 Hz), 60.20 (t, *J* = 36.8 Hz).
HRMS no ions detected.

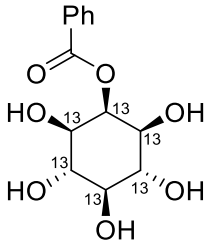

2-Benzoyl [$^{13}C_6$]inositol (S6)

[$^{13}C_6$]benzoyl inositol (S6) was synthesized according to a procedure of Godage and coworkers[32]. A mixture of TFA (1.8 mL) and water (180 µL) was added to S5 (300 mg, 1.1 mmol) and the solution was stirred for 1 h and the conversion was followed by TLC (100 % EtOAc; starting material R_f 0.6; product R_f 0.0). The reaction mixture was then co-evaporated with water *in vacuo*, redissolved in water and lyophilized to obtain the product S6 (314 mg, 1.08 mmol) as a white solid in quantitative yield.
^{1}H NMR (600 MHz, Deuterium Oxide, pD 7.0) δ 8.10 (d, *J* = 7.8 Hz, 2H), 7.74 (d, *J* = 7.5 Hz, 1H), 7.59 (t, *J* = 7.7 Hz, 2H), 5.86 (s, 0.5H), 5.60 (s, 0.5H), 4.02 – 3.89 (m, 2H), 3.78 – 3.66 (m, 2H), 3.58 – 3.51 (m, 0.5H), 3.36 – 3.28 (m, 0.5H).
^{13}C NMR (151 MHz, Deuterium Oxide, pD 7.0) δ 170.73, 136.84, 132.46, 131.52, 77.85 (t, *J* = 38.6 Hz), 77.09 (t, *J* = 38.6 Hz), 75.62 (t, *J* = 38.8 Hz), 72.63 (td, *J* = 38.8, 6.6 Hz).
HRMS (ESI/Orbitrap) m/z: $[M + H]^+$ calcd. for $C_7{}^{13}C_6H_{17}O_7$ 291.1170; Found 291.1166.

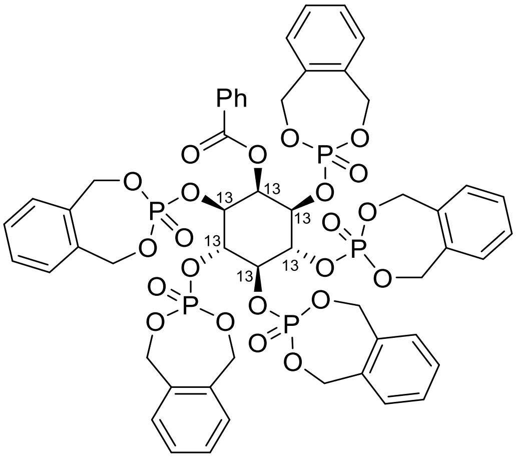

Xylyl protected [$^{13}C_6$]benzoyl inositol (S7)

Xylyl protected [$^{13}C_6$]benzoyl (S7) inositol was synthesized according to a procedure of Godage and coworkers[32]. To a solution of S6 (200 mg, 0.7 mmol) and 5-phenyltetrazole (1.01 g, 6,89 mmol) in dry DCM (4.9 mL) under nitrogen atmosphere was added S3 (1.24 g, 5.17 mmol). The suspension was sonicated (1 min) and further stirred overnight at rt. The reaction mixture was cooled to -40 °C, and *m*CPBA (1.70 g, 6.89 mmol) was added portion-wise while stirring. The cooling bath was removed, and the mixture was allowed to reach rt and diluted with DCM (50 mL), washed with 10% sodium sulfite solution (2 × 100 mL), dried and solvent evaporated *in vacuo*. The crude was immobilized on Telos® and purified by CombiFlash® chromatography on silica gel (120 g column, gradient: 1% → 4% → 10% MeOH in DCM) to afford the product S7 (651 mg, 0.54 mmol) as white solid in 79% yield

^{1}H NMR (600 MHz, Chloroform-*d*) δ 8.06 (d, *J* = 7.1 Hz, 2H), 7.61 – 7.53 (m, 1H), 7.49 – 7.45 (m, 2H), 7.43 – 7.35 (m, 10H), 7.35 – 7.30 (m, 6H), 7.29 – 7.27 (m, 1H), 7.26 – 7.23 (m, 2H), 6.53 (s, 0.5H), 6.27 (s, 0.5H), 5.64 (ddd, *J* = 17.9, 13.9, 8.1 Hz, 4H), 5.58 – 5.47 (m, 3H), 5.41 (dd, *J* = 13.7, 9.4 Hz, 2H), 5.27 (s, 1H), 5.21 (dd, *J* = 13.5, 10.9 Hz, 3.5H), 5.16 (d, *J* = 9.8 Hz, 1H), 5.12 (d, *J* = 8.7 Hz, 1H), 5.05 (ddd, *J* = 22.1, 13.8, 5.8 Hz, 8H), 4.96 (s, 1.5H).

^{13}C NMR (151 MHz, Chloroform-*d*) δ 78.00 – 76.46 (m), 74.25 (td, *J* = 38.4, 36.8, 6.5 Hz), 70.59 (t, *J* = 38.5 Hz).

^{31}P NMR (122 MHz, $CDCl_3$) δ -3.32, -4.25, -4.90.

HRMS (ESI/Orbitrap) m/z: $[M + Na]^+$ Calcd for $C_{47}{}^{13}C_6H_{51}NaO_{22}P_5$ 1223.1613; Found 1223.1613.

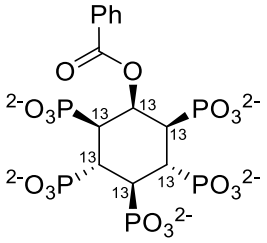

Benzoyl [$^{13}C_6$]inositol pentakisphosphate (S8)

[$^{13}C_6$]benzoyl inositol pentakisphosphate (S8) inositol was synthesized according to a procedure of Godage and coworkers[32]. S7 (50 mg, 0.04 mmol) was dissolved in methanol (3.8 mL), and water (0.95 mL) and 20% $Pd(OH)_2/C$ (50% wetted with water) (25 mg, 0.18 mmol) were added. The resulting suspension was stirred at rt overnight under hydrogen atmosphere. The catalyst was filtered through a PTFE syringe filter, and the filtrate neutralized by the addition of 1 M Et_3NHCO_3 until the pH 7.5 was reached. Lyophilization afforded the product S8 (50 mg, 0.037 mmol, 8 × EtN_3 salt) as white solid in 88% yield. The amount of the TEA-counter ion was determined by NMR spectroscopy.

^{1}H NMR (600 MHz, Deuterium Oxide, pD 7.0) δ 8.19 (dd, *J* = 8.2, 1.9 Hz, 2H), 7.74 (t, *J* = 7.2 Hz, 1H), 7.61 (dd, *J* = 9.0, 6.6 Hz, 2H), 6.10 (s, 0.5H), 5.84 (s, 0.5H), 4.58 – 4.45 (m, 2H), 4.39 (s, 0.5H), 4.27 (s, 1H), 4.16 (d, *J* = 11.1 Hz, 0.5H), 3.21 (qd, *J* = 7.3, 2.5 Hz, EtN_3), 1.30 (td, *J* = 7.3, 2.6 Hz, EtN_3).

^{13}C NMR (151 MHz, Deuterium Oxide, pD 7.0) δ 77.65 (t, *J* = 39.7 Hz), 76.46 (t, *J* = 39.7 Hz), 73.93 (t, *J* = 38.6 Hz), 72.53 (t, *J* = 39.9 Hz), 46.60, 8.23.

^{31}P NMR (122 MHz, Deuterium Oxide, pD 7.0) δ 0.33, -0.00, -0.80.

HRMS (ESI/Orbitrap) m/z: $[M - 2H]^{2-}$ calcd. for $C_7{}^{13}C_6H_{19}O_{22}P_5$ 343.9634; Found 343.9954.

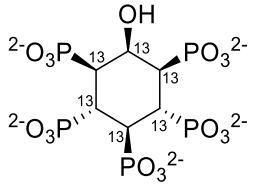

[$^{13}C_6$]inositol pentakisphosphate (5)

[$^{13}C_6$]inositol pentakisphosphate (5) was synthesized according to a procedure of Godage and coworkers[32]. Compound S8 (50 mg, 0.037 mmol) was dissolved in concentrated aqueous ammonia solution (2.0 mL) and heated at 60 °C overnight in a Pyrex pressure tube. After evaporation of the solution under vacuum, the

residue was dissolved in water and the benzamide byproduct was removed by washing with DCM. The ammonium salt of the product was obtained by evaporation of the ammonia and converted into the free acid by quick filtration (Note: Prolonged exposure causes phosphoryl group migration.) through DOWEX 50W x 8 (H^+ form) (10-fold molar excess, previously washed with MilliQ® water) and then to its hexasodium salt by titration to pH 7.40 with 0.1 M sodium hydroxide solution. Lyophilization afforded the product 5 (17 mg, 0.024 mmol) as white solid in 65% yield.

^{1}H NMR (300 MHz, Deuterium Oxide, pD 7.5) δ 4.72 – 4.53 (m, 1.5H), 4.47 – 4.25 (m, 1.5H), 4.24 – 4.02 (m, 1.5H), 3.96 – 3.74 (m, 1.5H).

^{13}C NMR (75 MHz, Deuterium Oxide, pD 7.5) δ 78.28 – 74.98 (m), 73.92 (t, *J* = 37.7 Hz), 70.68 (t, *J* = 37.6 Hz).

^{31}P NMR (122 MHz, D_2O, pD 7.5) δ 1.49, 1.23, 0.86.

HRMS no ions detected.

Enzymatic synthesis of [$^{13}C_6$]inositol pyrophosphates

Synthesis of [$^{13}C_6$]5-diphosphoinositol pentakisphosphate (7)

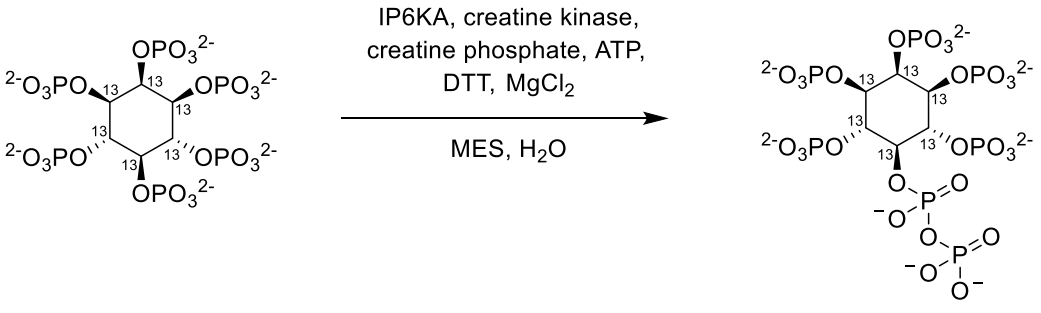

[$^{13}C_6$]InsP$_6$ (**6**) [$^{13}C_6$]5PP-InsP$_5$ (**7**)

The following stock solutions were prepared:

Creatine kinase stock solution: 350 U/mL creatine kinase in 200 mM MOPS pH 6.5, 20 mM $MgCl_2$, 20 mM DTT

IP6KA stock solution: 10 mg/mL IP6KA in 20 mM Tris HCl pH 7.4, 200 mM NaCl, 1 mM DTT

ATP stock solution: 50 mM in MilliQ® water pH 6.4; (Note: Concentration was determined via UV-Vis analysis at 259 nm; ε_{259} = 15.4 E/mmol/cm).

A solution of 6 (dodecasodium salt, 70 mg, 250 µM, 66 w/w%), MES (20 mM, pH 6.4), NaCl (50 mM), ATP (disodium salt, 2 mM), creatine phosphate (5 mM), $MgCl_2$ (7 mM), DTT (1 mM) in 199 mL MilliQ® water was prepared. The pH was adjusted to 6.4 and the mixture was split into four 50 mL conical tubes. The individual tubes were then equilibrated to 37 °C within 30 min without shaking. IP6KA (1 µM) and creatine kinase (1 U/mL) were added, the tube was gently inverted several times to homogenize and left to react for exactly 45 min without shaking. (Note: The correct temperature was essential to assure full conversion of the starting material within 45 min. Prolonged reaction times above 1 h led to side reactions. However, the speed of the reaction will depend on the batch and quality of the recombinantly expressed IP6KA.)

Purification: The reaction was stopped by cooling the reaction mixture down to 4 °C within 5 min with the help of a dry ice isopropanol bath. Four short C18 columns (SepPak V C18 500 mg) were each washed and equilibrated with 9 mL MeCN, then 9 mL H_2O. To remove protein, the reaction mixture was filtered through the SepPak columns (1 column per 50 mL reaction) and each column was washed with 20 mL water. The flow through was combined (~280 mL) and the pH adjusted to 9.0-9.2 by dropwise addition of a 10 M NaOH-solution (roughly 180 µL). 2.3 mL of a 1 M $MgCl_2$ solution was added which led to precipitation of InsPs as magnesium complex. The suspension was left shaking at room temperature overnight to facilitate complete precipitation. The suspension was centrifuged (5 min at 3000 g), the supernatant removed and the precipitate washed 3 times with 15 mL $MgCl_2$ solution (8 mM, pH 9 adjusted with NaOH)

The precipitate was resuspended in 10 mL NH_4HCO_3 buffer (10 mM, pH 8) and mixed with Amberlite IRC-748 (10 mL wetted bed volume, pre-equilibrated with NH_4HCO_3, pH 8) until the precipitate dissolved. (Note: The Amberlite resin should be washed with 500 mL of MeOH and 500 mL of H_2O before use.) The buffer/resin suspension was added to a short Amberlite IRC-748 column (5 mL bed volume, pre-equilibrated with NH_4HCO_3, pH 8) to remove excess Mg^{2+}. The product was flushed through the column with 50 mL water and all eluents were collected and lyophilized to afford the ammonium salt of the product (100 mg, 0.14 mmol, 35.5 w/w%) as white solid in quantitative yield.

^{1}H NMR (600 MHz, Deuterium Oxide, pD 7.5) δ 5.05 – 4.95 (m, 0.5H), 4.69 – 4.58 (m, 1H), 4.49 – 4.36 (m, 1.5H), 4.35 – 4.26 (m, 1H), 4.25 – 4.15 (m, 0.5H), 4.12 – 4.00 (m, 1H).

^{13}C NMR (151 MHz, Deuterium Oxide, pD 7.5) δ 80.74 – 79.46 (m), 79.32 – 77.17 (m), 76.03 (t, *J* = 38.7 Hz).

^{31}P NMR (243 MHz, D_2O) δ -1.45, -2.00, -2.45, -10.32, -13.41.

HRMS no ions detected.

Synthesis of [$^{13}C_6$]1,5-bisdiphosphoinositol tetrakisphosphate (8)

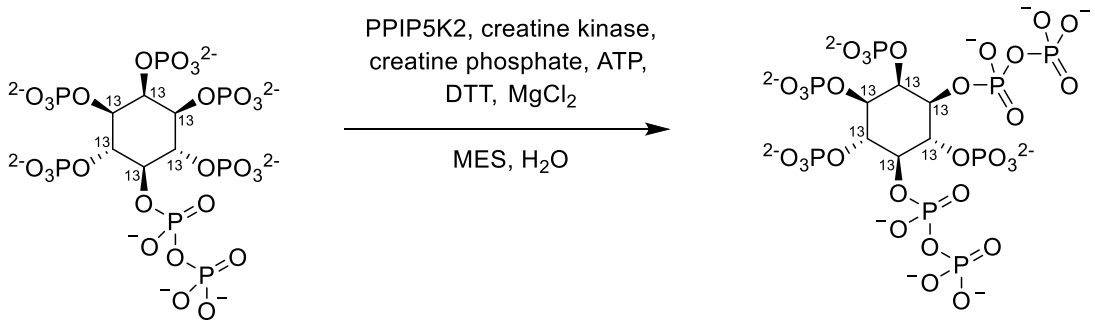

[$^{13}C_6$]5PP-InsP$_5$ (**7**) [$^{13}C_6$]1,5(PP)$_2$-InsP$_4$ (**8**)

MilliQ® water was prewarmed to 37 °C by incubation in a water bath. A solution of 5PP-InsP$_5$ (250 µM, 100 mg based on free acid 726.9 g/mol), MES (20 mM, pH 6.4), NaCl (250 mM), ATP (disodium salt, 2 mM), creatine phosphate (5 mM), $MgCl_2$ (5 mM), DTT (1 mM) in 715 mL prewarmed MilliQ® water was prepared in a 1 L Schott bottles and incubated in the water bath at 37 °C for 10 min. PPIP5K2^{KD} (1.5 µM) and creatine kinase (1 U/mL) were added and bottle gently inverted several times to homogenize and left to react overnight for 5.5 h without shaking.

Purification: The reaction was stopped by cooling the reaction mixture down to 4 °C within 5 min with the help of a dry ice isopropanol bath. A fritted filter was loaded with 6 g of C18 reversed phase silica gel suspended in MeCN and sand was added on top. The C18 plug was washed with 30 mL MeCN and 30 mL H_2O and the complete reaction mixture was passed through the filter under vacuum. The C18 plug was washed with 2 × 30 mL H_2O and all the combined flow through was supplemented with 12.5 mM $MgCl_2$. The pH was adjusted to 8.8–9.0 by drop wise addition of 10 mM NaOH solution which leads to precipitation of the PP-InsPs as magnesium complex within 1 h at room temperature. (The precipitation can also be performed overnight at room temperature.) The suspension was collected in 2 canonical 50 mL tubes by centrifugation (2 min at 3000 g) and the supernatant

was removed. The precipitates of each tube were washed 3 times with 15 mL $MgCl_2$ solution (8 mM, pH 9 adjusted with NaOH).

The precipitate of each tube was resuspended in 15 mL NH_4HCO_3 buffer (10 mM, pH 8) and vortexed with Amberlite® IRC-748 (15 mL wetted bed volume, pre-equilibrated with NH_4HCO_3, pH 7.5–8) until the precipitate dissolved. The buffer/resin suspension of each tube was added to a short Amberlite® IRC-748 column (5 mL bed volume, pre-equilibrated with NH_4HCO_3, pH 8) to remove excess Mg^{2+}. The product was flushed through the column with 40 mL H_2O and all eluents were collected, combined and lyophilized in a round-bottom flask to afford the ammonium salt of the product as white solid. The solids were dissolved in D_2O and the concentration of the solution was determined by NMR against a standard (phosphonoacetic acid) to determine yield and purity: 12 mL of 12.7 mM solution were obtained which corresponds to 111 mg (77% yield, purity > 95%) 1,5(PP)$_2$-InsP_4 based on the free acid 805.9 g/mL.

^{1}H NMR (600 MHz, Deuterium Oxide) δ 5.01 (d, *J* = 9.6 Hz, 1H), 4.55 (p, *J* = 9.9 Hz, 2H), 4.36 (q, *J* = 9.8 Hz, 1H), 4.25 (t, *J* = 9.4 Hz, 1H).
^{31}P NMR (243 MHz, Deuterium Oxide) δ 0.56, 0.33, -0.26, -1.04, -10.34 (dd, *J* = 29.9, 19.2 Hz), -11.03 (dd, *J* = 60.0, 19.3 Hz).
^{13}C NMR (151 MHz, D_2O) δ 77.42, 76.05, 75.53, 74.78, 73.53, 73.18.
HRMS no ions detected.

Synthesis of [$^{13}C_6$]1-diphosphoinositol pentakisphosphate (9)

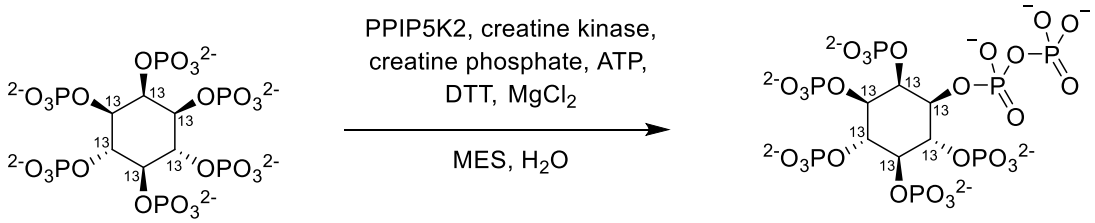

[$^{13}C_6$]InsP_6 (**6**) [$^{13}C_6$]1PP-InsP_5 (**9**)

MilliQ® water was prewarmed to 37 °C by incubation in a water bath. A solution of InsP_6 (250 µM, 100 mg based on free acid 647.9 g/mol), MES (20 mM, pH 6.4), NaCl (250 mM), ATP (disodium salt, 2 mM), creatine phosphate (5 mM), $MgCl_2$ (6 mM), DTT (1 mM) in 617 mL prewarmed MilliQ® water was prepared in a 1 L

Schott bottles and incubated in a water bath at 37 °C for 10 min. PPIP5K2^{KD} (2 μM) and creatine kinase (1 U/mL) were added and bottle gently inverted several times to homogenize and left to react overnight for 18 h without shaking.

Purification: The reaction was stopped by cooling the reaction mixture down to 4 °C within 5 min with the help of a dry ice isopropanol bath. A fritted filter was loaded with 6 g of C18 reversed phase silica gel suspended in MeCN and sand was added on top. The C18 plug was washed with 30 mL MeCN and 30 mL H_2O and the complete reaction mixture was passed through the filter under vacuum. The C18 plug was washed with 2 × 30 mL H_2O and all the combined flow through was supplemented with 12.5 mM $MgCl_2$. The pH was adjusted to 8.8–9.0 by drop wise addition of 10 mM NaOH solution which leads to precipitation of the PP-InsPs as magnesium complex within 1 h at room temperature. (The precipitation can also be performed overnight at room temperature.) The suspension was collected in 2 canonical 50 mL tubes by centrifugation (2 min at 3000 g) and the supernatant was removed. The precipitates of each tube were washed 3 times with 15 mL $MgCl_2$ solution (8 mM, pH 9 adjusted with NaOH).

The precipitate of each tube was resuspended in 15 mL NH_4HCO_3 buffer (10 mM, pH 8) and vortexed with Amberlite® IRC-748 (15 mL wetted bed volume, pre-equilibrated with NH_4HCO_3, pH 7.5–8) until the precipitate dissolved. The buffer/resin suspension of each tube was added to a short Amberlite® IRC-748 column (5 mL bed volume, pre-equilibrated with NH_4HCO_3, pH 8) to remove excess Mg^{2+}. The product was flushed through the column with 40 mL H_2O and all eluents were collected, combined and lyophilized in a round-bottom flask. The resulting white solid was purified in 2 runs using a strong anion exchange column (HiPrep^{TM} Q HP 16/10, GE Healthcare) and H_2O as buffer A and 1 M NH_4HCO_3 as buffer B. The column was washed with 100% B and equilibrated at 1% B. The sample was dissolved and loaded in 1% B and, followed by a gradient from 1% to 20% in 1 CV. The product was eluted in a gradient from 20%–40% over 10 CV. Fractions were analyzed by a metal dye detection assay[33] in a 96-well plate format and product containing fractions were combined and lyophilized in a round-bottom flask. The solids were dissolved in D_2O and the concentration of the solution was determined by NMR against a standard (phosphonoacetic acid) to determine yield

and purity: 20 mL of 5.3 mM solution were obtained which corresponds to 77 mg (68% yield, purity > 95%) 1PP-InsP$_5$ based on the free acid 726.9 g/mol.

^{1}H NMR (600 MHz, Deuterium Oxide) δ 5.08 (d, *J* = 9.8 Hz, 1H), 4.40 (p, *J* = 9.7 Hz, 2H), 4.21 (t, *J* = 9.8 Hz, 1H), 4.15 (q, *J* = 9.5 Hz, 1H), 4.09 (t, *J* = 9.2 Hz, 1H).
^{13}C NMR (151 MHz, D_2O) δ 77.32, 76.11, 75.68, 75.58, 73.70, 73.08.
^{31}P NMR (243 MHz, Deuterium Oxide) δ 1.64, 0.90, 0.40, 0.32, -0.94, -8.70, -10.89 (d, *J* = 18.7 Hz).
HRMS no ions detected.

Enzymatic synthesis of 5PP-InsP$_5$-β^{32}P (10)

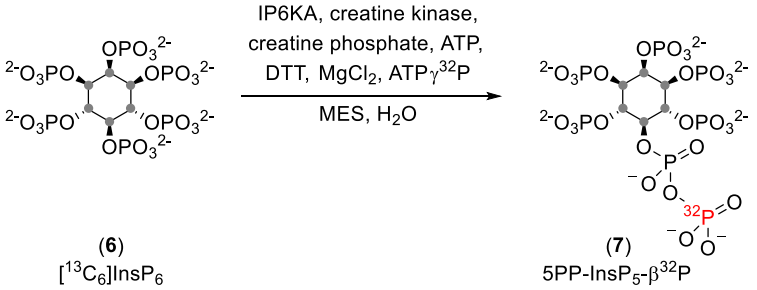

Reaction conditions: 20 mM MES pH 6.4, 50 mM NaCl, 1 mM DTT, 5 mM creatine phosphate, 200 µCi ATPγ^{32}P (6000Ci/mmol 10mCi/ml from Perkin Elmer), 0.2 mM ATP, 2 mM $MgCl_2$, 0.3 µM IP6KA, 1 U/ml creatine kinase, 0.2 mM InsP$_6$.
Volume: 500 µl reaction
time: 1 h for IP6KA at 37 °C.
For Purification: The solution was centrifuged (2 min at 5000 g) to separate possible precipitates (with these conditions I usually don't observe precipitation). Remove the supernatant and check if you have a precipitate with a geiger counter (this is recommended as the precipitate might not be visible). If you have a precipitate wash it with 0.2 ml water 3 times and add the washes to the supernatant. Keep the precipitate for combining it with the reaction solution after the C18 column.

One short C18 column (SepPak Vac RC tC18 100 mg, Waters, WAT043410) was washed and equilibrated with 5 mL MeCN, then 5 mL H_2O. The reaction mixture was filtered through the SepPak column and the column was washed with 0.25 mL water aliquots until no radioactivity (low radioactivity compared to the filtrate) remained on the column. The filtrate and the precipitate

from the previous step were combined and 0.25 M $MgCl_2$ was added to a final concentration of 16 mM. The pH was adjusted to 8.5 - 9 by dropwise addition of a 0.1 M NaOH-solution (the pH was checked with pH-stripes. The Solution is radioactive). The mixture is left at rt overnight to facilitate complete precipitation.

The next day the suspension was centrifuged (5 min at 5000 g) and the supernatant was removed. The precipitate was washed three times in 0.25 mL MgCl2 solution (8 mM, pH 9 adjusted with NaOH) and the suspensions were centrifuged (5 min at 5000 g). The precipitate was resuspended in 0.1 mL NH_4HCO_3 buffer (10 mM, pH 8) and mixed with chelex 100 (0.3 mL wetted bed volume, pre-equilibrated with 10 mM NH_4HCO_3, pH 8, column: BD PP reactor 2 ml with PE frit) until the precipitate dissolved (this will take up to one hour). The buffer/resin suspension was added to a short chelex 100 column (1 mL bed volume, pre-equilibrated with 10 mM NH_4HCO_3, pH 8) to remove excess Mg^{2+}. The product was flushed through the column with water until no radioactivity remained on the column and the eluent was collected (you should have < 3 ml). To the solution 10X apyrase buffer and 4 U/ml apyrase (NEB) were added and the reaction was incubated overnight at rt. Another precipitation and chelation followed. The elution of the chelex column was collected and concentrated in a speed-vac to afford the ammonium salt of the product as a concentrated solution (I usually end up with 50-100 µl).

Protein pyrophosphorylation

The 15 µl reactions contained 25 mM Tris HCl pH 7.4, 50 mM NaCl, 6 mM $MgCl_2$, 1 mM DTT, and 4 µg either pNSR1 or NSR1. If needed 500 U Casein kinase II (NEB) or 0.1 µCi ATPγ^{32}P (6000 Ci/mmol, Perkin Elmer) was added.

The reactions were started by the addition of 10 µl 5PP-InsP_5-β^{32}P and the samples were incubated for 30 min at 45 °C. The reactions were quenched by the addition of 5 µl 4X Laemmli sample buffer and heating to 95 °C for 5 min. The samples were loaded onto an SDS-PAGE and resolved. The gel was fixed, stained with colloidal coomassie, and dried before the radioactivity was detected using a phosphor imager screen.

2.7 References

(1) Reo, N. V. NMR-Based Metabolomics. In *Drug and Chemical Toxicology*; 2002; Vol. 25, pp 375–382.

(2) Bingol, K.; Bruschweiler-Li, L.; Li, D.; Zhang, B.; Xie, M.; Brüschweiler, R. Emerging New Strategies for Successful Metabolite Identification in Metabolomics. *Bioanalysis*. March 2016, pp 557–573.

(3) Markley, J. L.; Brüschweiler, R.; Edison, A. S.; Eghbalnia, H. R.; Powers, R.; Raftery, D.; Wishart, D. S. The Future of NMR-Based Metabolomics. *Current Opinion in Biotechnology*. February 2017, pp 34–40.

(4) Ardenkjaer-Larsen, J. H.; Boebinger, G. S.; Comment, A.; Duckett, S.; Edison, A. S.; Engelke, F.; Griesinger, C.; Griffin, R. G.; Hilty, C.; Maeda, H.; et al. Facing and Overcoming Sensitivity Challenges in Biomolecular NMR Spectroscopy. *Angew. Chemie - Int. Ed.* **2015**, *54* (32), 9162–9185.

(5) Claridge, T. D. W. *High-Resolution NMR Techniques in Organic Chemistry.*; 1999; Vol. 122.

(6) Azevedo, C.; Saiardi, A. Extraction and Analysis of Soluble Inositol Polyphosphates from Yeast. *Nat. Protoc.* **2006**, *1* (5), 2416–2422.

(7) Saiardi, A.; Guillermier, C.; Loss, O.; Poczatek, J. C.; Lechene, C. Quantitative Imaging of Inositol Distribution in Yeast Using Multi-Isotope Imaging Mass Spectrometry (MIMS). *Surf. Interface Anal.* **2014**, *46* (S1), 169–172.

(8) Sahai, P.; Chawla, M.; Vishwakarma, R. A. 13C Labelling and Electrospray Mass Spectrometry Reveal a de Novo Route for Inositol Biosynthesis in Leishmania Donovani Parasite. *J. Chem. Soc. Perkin Trans. 1* **2000**, *0* (8), 1283–1290.

(9) Moure, M. J.; Zhuo, Y.; Boons, G. J.; Prestegard, J. H. Perdeuterated and 13 C-Enriched Myo-Inositol for DNP Assisted Monitoring of Enzymatic Phosphorylation by Inositol-3-Kinase. *Chem. Commun.* **2017**, *53* (92), 12398–12401.

(10) Pavlovic, I.; Thakor, D. T.; Bigler, L.; Wilson, M. S. C.; Laha, D.; Schaaf, G.; Saiardi, A.; Jessen, H. J. Prometabolites of 5-Diphospho-Myo-Inositol Pentakisphosphate. *Angew. Chemie - Int. Ed.* **2015**, *54* (33), 9622–9626.

(11) Wild, R.; Gerasimaite, R.; Jung, J. Y.; Truffault, V.; Pavlovic, I.; Schmidt, A.; Saiardi, A.; Jacob Jessen, H.; Poirier, Y.; Hothorn, M.; et al. Control of Eukaryotic Phosphate Homeostasis by Inositol Polyphosphate Sensor Domains. *Science* **2016**, *352* (6288), 986–990.

(12) Riley, A. M.; Godage, H. Y.; Mahon, M. F.; Potter, B. V. L. Chiral Desymmetrisation of Myo-Inositol 1,3,5-Orthobenzoate Gives Rapid Access to Precursors for Second Messenger Analogues. *Tetrahedron Asymmetry* **2006**, *17* (2), 171–174.

(13) Loss, O.; Azevedo, C.; Szijgyarto, Z.; Bosch, D.; Saiardi, A. Preparation of Quality Inositol Pyrophosphates. *J. Vis. Exp.* **2011**, No. 55, e3027.

(14) Saiardi, A.; Bhandari, R.; Resnick, A. C.; Snowman, A. M.; Snyder, S. H. Phosphorylation of Proteins by Inositol Pyrophosphates. *Science* **2004**, *306* (5704), 2101–2105.

(15) Morin, L. G. Creatine Kinase: Re-Examination of Optimum Reaction Conditions. *Clin. Chem.* **1977**, *23* (9), 1569–1575.

(16) Chen, L.; Zhou, C.; Yang, H.; Roberts, M. F. Inositol-1-Phosphate Synthase from Archaeoglobus Fulgidus Is a Class II Aldolase. *Biochemistry* **2000**, *39* (40), 12415–12423.

(17) Thota, S. G.; Bhandari, R. The Emerging Roles of Inositol Pyrophosphates in Eukaryotic Cell Physiology. *J. Biosci.* **2015**, *40* (3), 593–605.

(18) Barker, C. J.; Wright, J.; Hughes, P. J.; Kirk, C. J.; Michell, R. H. Complex Changes in Cellular Inositol Phosphate Complement Accompany Transit through the Cell Cycle. *Biochem. J.* **2004**, *380* (Pt 2), 465–473.

(19) Zhang, H.; Thompson, J.; Prestwich, G. D. A Scalable Synthesis of the IP7isomer, 5-PP-Ins(1,2,3,4,6) P5. *Org. Lett.* **2009**, *11* (7), 1551–1554.

(20) Pavlovic, I.; Thakor, D. T.; Vargas, J. R.; McKinlay, C. J.; Hauke, S.; Anstaett, P.; Camunã, R. C.; Bigler, L.; Gasser, G.; Schultz, C.; et al. Cellular Delivery and Photochemical Release

of a Caged Inositol-Pyrophosphate Induces PH-Domain Translocation in Cellulo. *Nat. Commun.* **2016**, *7* (1), 10622.

(21) Löser, B.; Nalaskowski, M. M.; Fanick, W.; Lin, H.; Tannich, E.; Mayr, G. W. A Novel Entamoeba Histolytica Inositol Phosphate Kinase Catalyzes the Formation of 5PP-Ins(1,2,3,4,6)P 5. *Mol. Biochem. Parasitol.* **2012**, *181* (1), 49–52.

(22) Hager, A.; Wu, M.; Wang, H.; Brown, N. W.; Shears, S. B.; Veiga, N.; Fiedler, D. Cellular Cations Control Conformational Switching of Inositol Pyrophosphate Analogues. *Chem. - A Eur. J.* **2016**, *22* (35), 12406–12414.

(23) Veiga, N.; Torres, J.; Domínguez, S.; Mederos, A.; Irvine, R. F.; Díaz, A.; Kremer, C. The Behaviour of Myo-Inositol Hexakisphosphate in the Presence of Magnesium(II) and Calcium(II): Protein-Free Soluble InsP6 Is Limited to 49 MM under Cytosolic/Nuclear Conditions. *J. Inorg. Biochem.* **2006**, *100* (11), 1800–1810.

(24) Fridy, P. C.; Otto, J. C.; Dollins, D. E.; York, J. D. Cloning and Characterization of Two Human VIP1-like Inositol Hexakisphosphate and Diphosphoinositol Pentakisphosphate Kinases. *J. Biol. Chem.* **2007**, *282* (42), 30754–30762.

(25) Wu, M.; Chong, L. S.; Perlman, D. H.; Resnick, A. C.; Fiedler, D. Inositol Polyphosphates Intersect with Signaling and Metabolic Networks via Two Distinct Mechanisms. *Proc. Natl. Acad. Sci.* **2016**, *113* (44), E6757–E6765.

(26) Findeisen, M.; Brand, T.; Berger, S. A 1H-NMR Thermometer Suitable for Cryoprobes. *Magn. Reson. Chem.* **2007**, *45* (2), 175–178.

(27) Rodrigues, M. V.; Borges, N.; Henriques, M.; Lamosa, P.; Ventura, R.; Fernandes, C.; Empadinhas, N.; Maycock, C.; Da Costa, M. S.; Santos, H. Bifunctional CTP:Inositol-1-Phosphate Cytidylyltransferase/CDP-Inositol: Inositol-1-Phosphate Transferase, the Key Enzyme for Di-Myo-Inositol-Phosphate Synthesis in Several (Hyper)Thermophiles. *J. Bacteriol.* **2007**, *189* (15), 5405–5412.

(28) Wang, H.; Derose, E. F.; London, R. E.; Shears, S. B. IP6K Structure and the Molecular Determinants of Catalytic Specificity in an Inositol Phosphate Kinase Family. *Nat. Commun.* **2014**, *5*, 4178.

(29) Drent, E.; van Dijk, R.; van Ginkel, R.; van Oort, B.; Pugh, R. I. The First Example of Palladium Catalysed Non-Perfectly Alternating Copolymerisation of Ethene and Carbon Monoxide. *Chem. Commun.* **2002**, *2* (9), 964–965.

(30) Gregory, M.; Catimel, B.; Yin, M. X.; Condron, M.; Burgess, A. W.; Holmes, A. B. Synthesis of a Tethered Myo -Inositol (1,3,4,5,6)Pentakisphosphate (IP5) Derivative as a Probe for Biological Studies. *Synlett* **2016**, *27* (1), 121–125.

(31) Podeschwa, M.; Plettenburg, O.; Vom Brocke, J.; Block, O.; Adelt, S.; Altenbach, H. J. Stereoselective Synthesis of Myo-, Neo-, L-Chiro, D-Chiro, Allo-, Scyllo-, and Epi-Inositol Systems via Conduritols Prepared from p-Benzoquinone. *European J. Org. Chem.* **2003**, *2003* (10), 1958–1972.

(32) Godage, H. Y.; Riley, A. M.; Woodman, T. J.; Thomas, M. P.; Mahon, M. F.; Potter, B. V. L. Regioselective Opening of Myo-Inositol Orthoesters: Mechanism and Synthetic Utility. *J. Org. Chem.* **2013**, *78* (6), 2275–2288.

(33) Mayr, G. W. A Novel Metal-Dye Detection System Permits Picomolar-Range h.p.l.c. Analysis of Inositol Polyphosphates from Non-Radioactively Labelled Cell or Tissue Specimens. *Biochem. J.* **1988**, *254* (2), 585–591.

Chapter 3: Analysis of inositol phosphates *in vitro* and *ex vivo* by NMR spectroscopy[g]

3.1 Introduction

Biochemical analysis of PP-InsP metabolizing enzymes

Small molecule networks play a crucial part in cell homeostasis. To better understand how the small molecules function in a biological context and to tie them to observable phenotypes, their concentrations and dynamics have to be measured. In order to fully comprehend the underlying mechansims, it is necessary to fully characterize the enzymes catalyzing the reactions that make up a particular pathway. For example, the ability of IP6Ks to directly respond to ATP availability is caused by its relatively high $K_{M,ATP}$ of about 0.5 mM, near physiological concentrations, highlighting the need to know these kinetic properties. For determining kinetic parameters of kinases two approaches are commonly pursued: measuring either the consumption of ATP or the conversion of substrate.

ATP consumption can be detected by several methods, including coupling ATP turnover to NADH oxidation via pyruvate kinase and lactate dehydrogenase or by ADP-Glo^{TM} (Figure 3.1a,b).[1] Such an approach, however, is problematic, as InsP- and PP-InsP kinases are known to possess an ATPase activity as well, uncoupling ATP consumption from product formation.[2] This enzyme property mostly disqualifies the approach of ATP measurement. A better alternative is the direct monitoring of InsP conversion. In the past, this has been achieved by three different methods (Figure 3.1c-e).

Radioactive labeling of InsPs with tritium (^{3}H) provides a sensitive analytical handle that can be exploited by scintillation counting after SAX-HPLC separation

[g] The results of this chapter were partially published in "Robert K. Harmel[‡], Robert Puschmann[‡], Minh Nguyen Trung, Adolfo Saiardi, Peter Schmieder, Dorothea Fiedler. 'Harnessing ^{13}C-labeled *myo*-inositol to interrogate inositol phosphate messengers by NMR' *Chem. Sci.* **2019**, doi: 101039/C9SC00151D" ([‡] authors contributed equally) and "Jinsheng Zhu, Kelvin Lau, Robert Harmel, Robert Puschmann, Larissa Broger, Ludwig A. Hothorn, Dorothea Fiedler, Michael Hothorn. "Two bifunctional inositol pyrophosphate kinases/phosphatases control plant phosphate homeostasis", *bioRxiv* **2018**, doi: 10.1101/467076; *elife under revision*". To provide a cohesive account, results obtained by RKH are included in this chapter and highlighted as such.

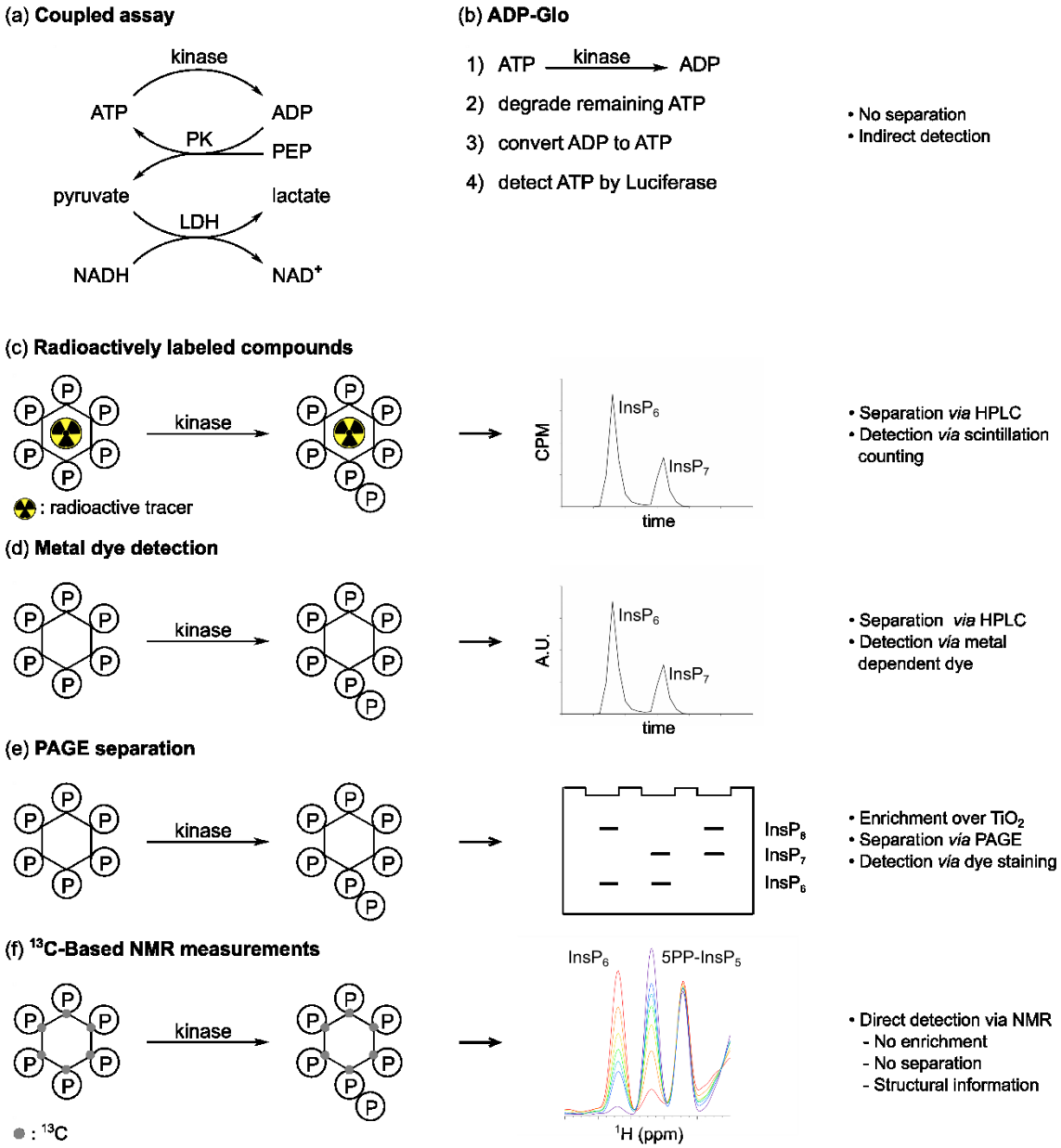

Figure 3.1. Methods for the *in vitro* characterization of InsP kinases. (a) ATP-consumption can be measured by coupling the oxidation of NADH to the production of ADP. PK: pyruvate kinase, LDH: lactate dehydrogenase. (b) The amount of generated ADP can be determined by removing unreacted ATP, converting the ADP to ATP and quantifying it by bioluminescence. (c) Radioactively labeled InsPs can be resolved via SAX-HPLC and the amount of radioactivity in each fraction is analyzed. (d) Instead of a radioactive handle, the InsPs can be detected by a metal dependent dye. (e) InsPs are enriched with TiO_2-beads from complex mixtures, subsequently resolved via PAGE, and detected by staining with toluidine blue. (f) ^{13}C-labeled InsPs can be directly measured in complex samples using NMR spectroscopy.

(Figure 3.1c). This method has enabled seminal findings in the field but is dependent on dedicated radioactive HPLC equipment, a commitment not every group can make. Furthermore, the only supplier of [^{3}H]InsPs has discontinued their distribution, rendering this method unavailable for most laboratories.

Research groups developed alternative methods to detect InsP conversion, one of which aimed to replace the radioactivity read-out with a more benign detection method while still retaining the SAX-HPLC based separation (Figure 3.1d). Mayr and co-workers exploited the metal chelation property of InsPs by using a metal dependent dye. This method is sensitive but suffers from high variability and has seen no use by the field.[3]

Saiardi and coworkers, on the other hand, adapted high percentage polyacrylamide gels used in polyphosphate research for the analysis of PP-InsPs (Figure 3.1e). Here, the extracted InsPs and PP-InsPs have to be enriched over TiO_2 beads, and are then resolved on a high-percentage polyacrylamide gel (PAGE) and stained by an cationic dye.[4] Although the independence from radioactive tracers has allowed more laboratories to employ this approach, the lack of an InsP-specific analytical handle requires a more elaborate sample preparation and it is limited to the detection of only the most highly phosphorylated InsPs ($InsP_6$ – $InsP_8$). Furthermore, the limit of detection is not as good as for radioactive labeling.

While all methods mentioned above have been instrumental to date, they do not provide structural information about the InsPs and PP-InsPs, such as the clear distinction of the structural isomers of PP-InsPs. The methods also lack the ability to monitor conversion of InsP species in real time *in vitro*, thereby losing informative kinetic insight contained within biochemical experiments. Desired properties of an InsP detection assay are high sensitivity for InsPs, while differentiating between isomers (e.g. 1PP-$InsP_5$ and 5PP-$InsP_5$), and not requiring specialized equipment.

NMR spectroscopy can provide detailed information about the chemical and structural environment of a nucleus solely based on the chemical shift. For example, two-dimensional $^{1}H,^{31}P$-NMR has been used to elucidate the structure of PP-InsPs.[5,6] Since experiments utilizing the $^{3}J(^{1}H,^{31}P)$ coupling are of limited sensitivity due to the inefficient magnetization transfer *via* these couplings, high analyte concentrations were necessary. In addition, the low chemical shift dispersion and the broad lines of ^{31}P can limit the information content.[5,6] By contrast, the chemical shift dispersion of the NMR-active nucleus ^{13}C is superior to ^{31}P.Additionally, the sensitivity of two-dimensional experiments is much better due to an efficient magnetization transfer *via* $^{1}J(^{1}H,^{13}C)$ one-bond couplings.

Consequently, ^{13}C-labeled InsPs and PP-InsPs, should enable NMR measurements at low, biologically relevant analyte concentrations (Figure 3.1f).

Ex vivo analysis of cellular PP-InsP pools.

To comprehensively understand a biological pathway, it is not enough to solely characterize it *in vitro*. Proteins and enzymes might behave differently *in vivo*, making it necessary to analyze them in their endogenous settings. For InsP metabolism this requirement means to analyze and quantify InsP and PP-InsP levels inside the cell. To date, two methods are available for the analysis of cellular InsP pools: radioactive labeling of cell using tritiated *myo*-inositol, followed by extraction and SAX-HPLC, or alternatively, PP-InsP resolution by PAGE after extraction and TiO_2 enrichment (Figure 3.2a). These methods are virtually identical to their counterparts for *in vitro* characterization and therefore suffer from the same drawbacks.

NMR spectroscopy can take advantage of the natural abundance of ^{13}C of only approx. 1 %, by isotopic labeling of selected compounds to provide targeted information on these labeled molecules in complex environments. Indeed, labeling of small molecules and metabolites with ^{13}C has been applied widely to elucidate various metabolic pathways and processes.[7–9] Thus, metabolic labeling of cells with [$^{13}C_6$]*myo*-inositol (**1**), should enable NMR measurements of complexed, un-resolved cell extracts an reveal unprecedented information about InsP metabolism (Figure 3.2b).

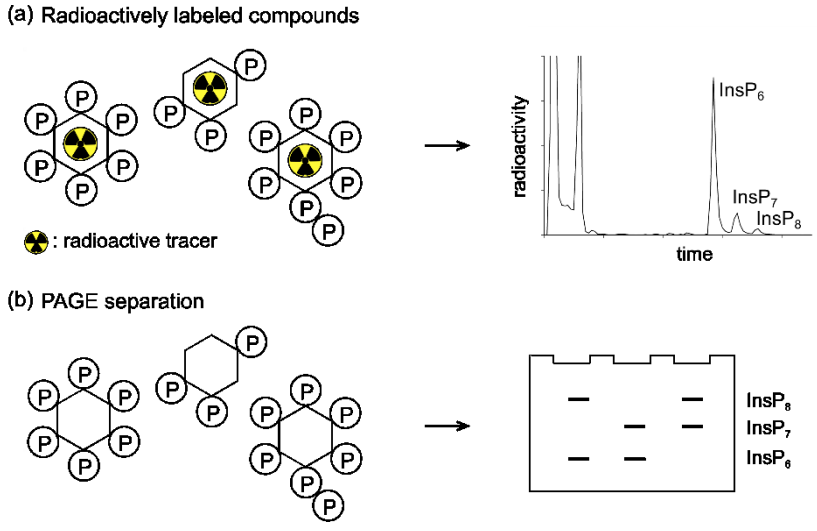

Figure 3.2. Methods for the *ex vivo* analysis of inositol polyphosphates. (a) Radioactively labeled InsPs can be resolved via SAX-HPLC and the amount of radioactivity in each fraction is analyzed. (b) InsPs are enriched with TiO_2-beads from complex mixtures, subsequently resolved via PAGE, and detected by staining with toluidine blue.

3.2 *In vitro* characterization of InsP metabolizing enzymes

While optimizing the enzymatic synthesis of **7**, we noted that the progression of the reaction could be followed readily by NMR spectroscopy, even in the presence of high concentrations of non-deuterated buffer and ATP (Figure 3.3). Specifically, the diagnostic signals for the protons at the 2-position of the inositol ring of [$^{13}C_6$]InsP$_6$ and [$^{13}C_6$]5PP-InsP$_5$ were baseline-separated in the ^{1}H-dimension (5.05 ppm for **6**, 4.95 ppm for **7**) and showed no overlap with signals from other compounds within the mixture (Figure 3.3). The ability to resolve the ^{1}H-signals at the 2-position provided the opportunity to monitor the enzymatic reaction in a time-resolved fashion, using a pseudo-2D spin-echo difference experiment. This pulse sequence is similar to a ^{1}H,^{13}C-HMQC experiment and results in a series of time-resolved one-dimensional spectra that only display resonances for ^{1}H-nuclei that are bound to ^{13}C-nuclei. By plotting the peak intensity of the ^{1}H-nuclei at the 2-position against time (each experiment required only 75 seconds at a substrate concentration of 175 µM) the progress of the kinase reaction could be observed (Figure 3.4). The non-invasive nature of the NMR measurements allowed for continuous reaction monitoring, providing time-resolved data from a single sample. Nevertheless, this method suffered from an unavoidable dead time of ca. 5 min at the beginning of each experiment due to locking, shimming, tuning and matching, precluding the measurement of fast reactions.

Considering our ability to reliably measure kinase activity by NMR, we next wanted to determine the kinetic parameters for *human* IP6K1. However,

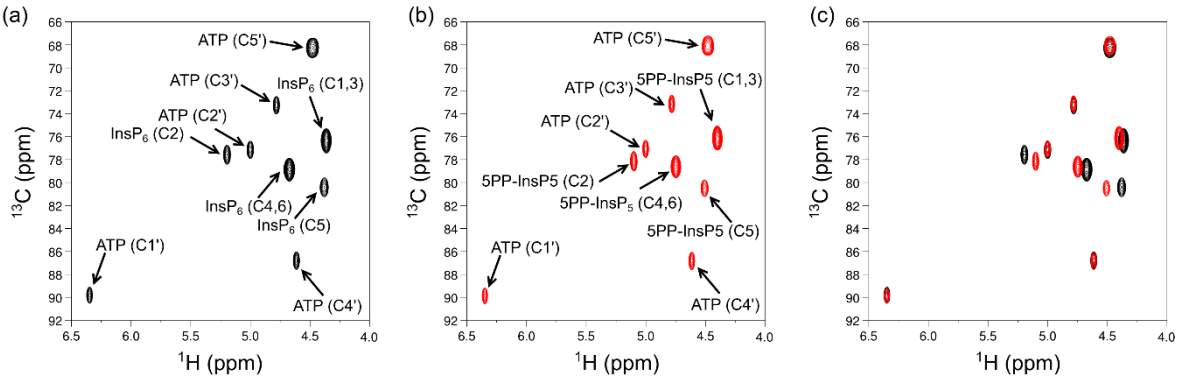

Figure 3.3. HMQC-Spectra to determine conversion to [$^{13}C_6$]5PP-InsP$_5$. (a) Control reaction without IP6KA shows no conversion of [$^{13}C_6$]InsP$_6$. (b) Full conversion of [$^{13}C_6$]InsP$_6$ to [$^{13}C_6$]5PP-InsP$_5$. (c) Overlay of a and b to illustrate that the C2 peaks are well resolved and can be used to monitor the reaction progress.

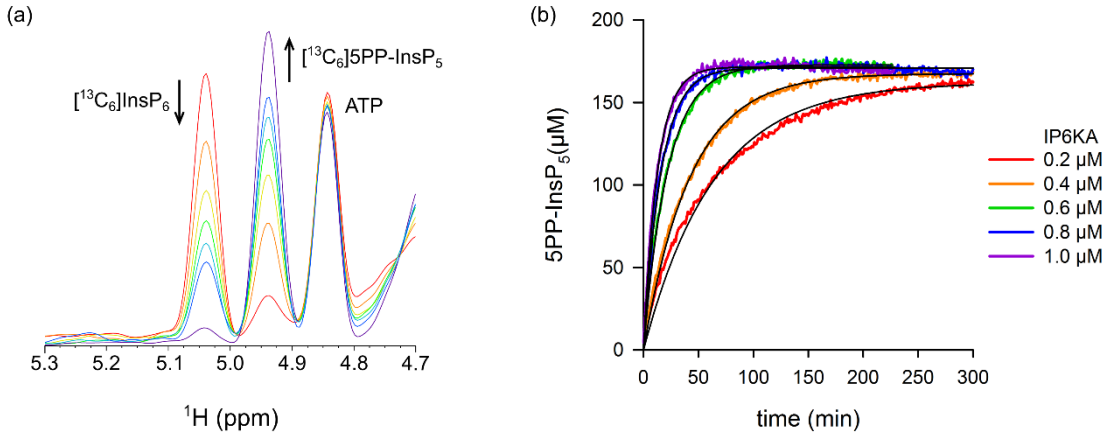

Figure 3.4. NMR-based measurements of IP6KA activity. (a) Superimposed pseudo-2D spin-echo difference spectra at different time points (6 min, 28 min, 50 min, 73 min, 95 min, 118 min, 455 min; red to purple). The $InsP_6$ and 5PP-$InsP_5$ peaks are labeled and the change over time is indicated by the arrows. The intensity of the ATP-peak hardly changed due to the ATP regenerating system. (b) Progress curves of [$^{13}C_6$]5PP-$InsP_5$ synthesis at different IP6KA concentrations. An individual NMR-spectrum was recorded every 75 seconds. The [$^{13}C_6$]5PP-$InsP_5$ peak height was normalized against the HEPES signal and the data was fitted with a first order decay model.

measurement of time courses at different ATP concentrations in triplicate would require long allocations of NMR time. To circumvent this shortcoming, the reactions were quenched with EDTA after ca. 20 % conversion. In this way, the measurement time could be reduced to 10 min per sample instead of up to an hour. Furthermore, fast reactions that would exceed 20 % conversion within the first 5 min are amenable for characterization.

The resulting initial rates for *h*IP6K1 at constant $InsP_6$ concentration (175 µM) and varying ATP concentrations (62.5 µM to 8 mM) provided the Michalis-Menten constant (K_M) for ATP and the maximum velocity (V_{max}) for IP6K1 (Figure 3.5).
The K_M measured for ATP (353 ± 167 µM) was comparable to previous reports and is close to cellular ATP concentrations, which supports the assertion that the IP6Ks are uniquely sensitive to ATP availability.[1,10] The V_{max} value (192 ± 41 nmol min^{-1} mg^{-1}) for IP6K1 was also within the range of published literature values, which varied greatly depending on the protein-tag and purification strategy (37.3 nmol min^{-1} mg^{-1} to 1410 nmol min^{-1} mg^{-1}).[10,11] Interestingly, we found that ATP concentrations above 2 mM led to substrate inhibition of IP6K1 (K_i 7.48 mM), which had not been quantified before (Figure 3.5).[11] The robust measurement of InsP conversion by NMR spectroscopy has provided kinetic data with low experimental error, which, in turn, has allowed the observation of substrate inhibition by ATP.

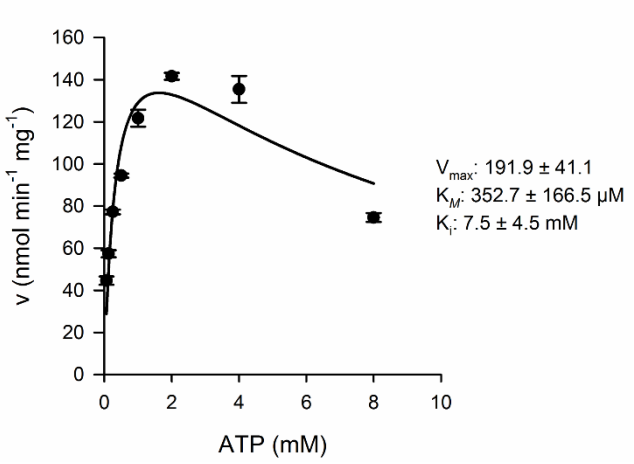

Figure 3.5. Michaelis-Menten kinetics for IP6K1. The initial velocity was measured in triplicates at different ATP concentrations and fitted against a model for substrate inhibition.

IP6Ks regulate important aspects of metabolism and signaling in mammals and in pathogenic microorganisms like *Trypanosoma brucei* and therefore increased efforts to identify selective inhibitors have been made.[1,12,13] Thus far, two molecules, TNP (N^2-(*m*-Trifluorobenzyl)-N^6-(*p*-nitrobenzyl)purine), and myricetin have been shown to inhibit IP6K1 activity at low micromolar concentrations. The potency of the inhibitors was characterized using radiolabeled InsPs in the case of TNP, and an indirect ATP-consumption assay for myricetin.[1,12] Given that we could directly measure product formation, we expanded the scope of our NMR method towards the characterization of IP6K1 inhibitors. Indeed, we found that TNP and myricetin inhibited IP6K1 with IC_{50} values of 2.25 µM and 0.6 µM, respectively, while wortmannin, a PI3K inhibitor, did not affect enzyme activity, even at high concentrations (Figure 3.6). While the NMR-based method is not compatible with high-throughput screening to identify new kinase inhibitors, it provides a direct read-out of the substrate and the reaction product and is highly reliable. This type of assay can thus serve as a platform to develop suitable high-throughput screening approaches for the kinases and phosphatases involved in InsP metabolism and can ultimately provide the necessary validation for the discovered inhibitors.

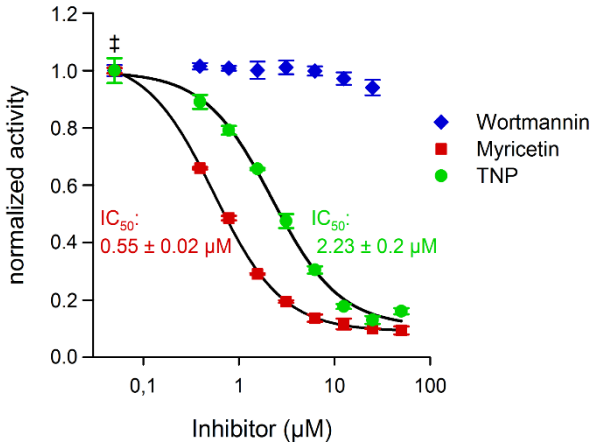

Figure 3.6. Inhibition of IP6K1. The inhibitory effect of TNP (N^2-(*m*-Trifluorobenzyl)-N^6-(*p*-nitro-benzyl)purine), Myricetin, and Wortmannin were tested at different concentrations and the IC_{50} values were determined. The ATP concentration was 2.5 mM for all inhibitor measurements. (‡ enzyme activity at 0 µM inhibitor).

Indeed, the developed NMR-based method has been used in the Fiedler group to develop a high-throughput assay to identify inhibitors for IP6Ks and it is now routinely used to characterize PP-InsP pyrophosphatases as well.

3.3 Characterization of *A. thaliana* VIH2

Phosphate (P_i) homeostasis is an essential process in all organism (and especially in plants) that relies on intricate mechanisms for the sensing, uptake, transport and storage of P_i. Among the proteins involved in these processes, the SPX domain is a common motif. The small four helix bundle domain can be a part of larger proteins (yeast VTC2 or human XPR1) or exist as stand-alone proteins.[14–16] It has been shown, that PP-InsPs can specifically interact with SPX domains and regulate their activity.[16,17] Interestingly, stand-alone SPX proteins interact with phosphate starvation response (PHR) transcription factors in a PP-InsP-dependent manner, establishing a link between P_i homeostasis and PP-InsP metabolism.[16,18–21] PHR1 is a master regulator of the phosphate starvation response in plants. Upon binding to DNA, it upregulates transcription of P_i starvation induced genes, enabling the plant to survive under phosphate limited conditions. However, PHR1 is sequestered from the DNA by binding to SPX in an $InsP_7$ dependent fashion (Figure 3.7a). This connection suggests that PP-InsPs might be major regulators of P_i homeostasis in plants. For mammals and yeast, such a connection has already been established.[15,16]

In order to further investigate the phosphate starvation response in plants, it is essential to know the biosynthetic enzymes responsible for the synthesis of PP-InsPs. While the respective enzymes in yeast and human have been known for several years, identification and characterization of the plant enzymes is lacking behind (Figure 3.7b). VIH 1 and VIH2 have been recently identified to be the plant PPIP5K homologs and they were proposed to possess the same catalytic activity as their mammalian counterpart.[22,23] So far, no enzymes with IP6K functionality have been described in plants (Figure 3.7b).

Professor Hothorn approached the Fiedler group as he was interested in the connection between P_i starvation response and VIH1/2. They had found that VIH1/2 knockout plants (*vih1-2 vih2-4*) responded sensitively to external phosphate and exhibited severe growth phenotypes (Figure 3.8a,b). Furthermore, the P_i storage regulation seemed to be impaired as *vih1-2 vih2-4* hyper-accumulated large amounts of phosphate (Figure 3.8c). Genetic complementation experiments showed that a mutant of VIH2 that targeted the predicted kinase

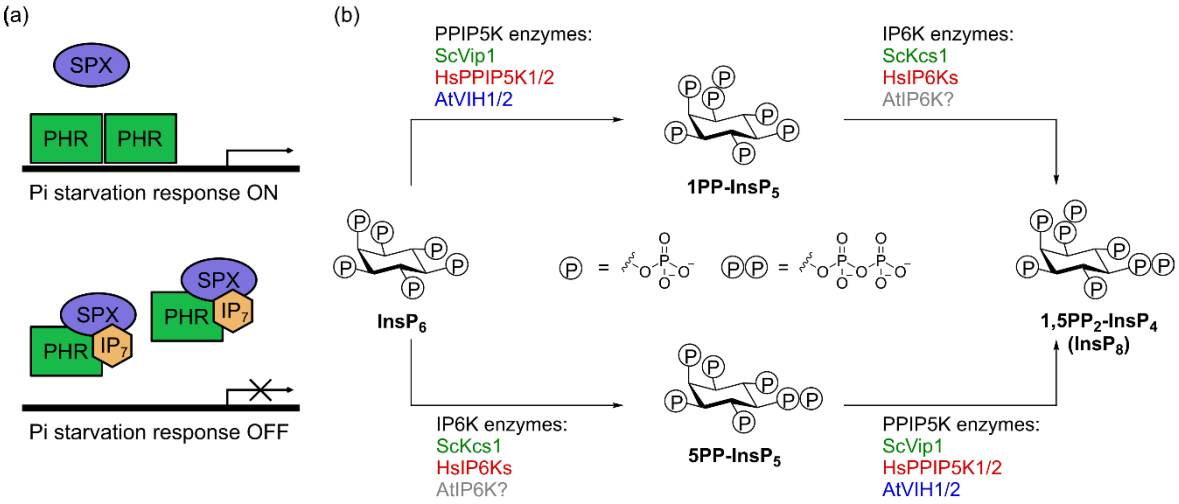

Figure 3.7. The role of inositol pyrophosphates in phosphate starvation response and PP-InsP biosynthetic pathway in plants. (a) Schematic representation of phosphate starvation response regulation by PP-$InsP_5$ (IP_7). (b)Two classes of inositol pyrophosphate kinases, PPIP5K and IP6K, are responsible for the synthesis of inositol pyrophosphates. The schematic describes PPIP5K enzymes from *Saccharomyces cerevisiae* ScVip1, *Homo sapiens* HsPPIP5K11 and 2, *Arabidopsis thaliana* VIH1 and VIH2. These enzymes synthesize 1PP-$InsP_5$ and 1,5$(PP)_2$-$InsP_4$ ($InsP_8$) by phosphorylating $InsP_6$ at the 1 position, and by phosphorylating 5PP-$InsP_5$ at the 1 position, respectively. IP6K enzymes from *Saccharomyces cerevisiae* KCS1 and *Homo sapiens* IP6Ks synthesize 5PP-$InsP_5$ and $InsP_8$ by phosphorylating $InsP_6$ at the 5 position, and by phosphorylating 1PP-$InsP_5$ at the 5 position, respectively. However, plant IP6Ks have not been reported yet.

active site (VIH2$^{KD/AA}$, Lys219Ala and Asp298Ala, based on homology to yeast vip1, Mulugu et al.[24]) was not able to rescue the plants. However, a mutant targeting the phosphatase domain (VIH2$^{RH/AA}$, Arg372Ala and His373Ala, based on homology to yeast vip1, Mulugu et al.[24]) was able to rescue the growth defect (Figure 3.8d). Furthermore, overexpression of VIH2 and VIH2$^{RH/AA}$ in wildtype plants had only a minor effect on the P_i content, while VIH2$^{KD/AA}$ led to a marked increase in phosphate (Figure 3.8e). All of these observations (and more, as found in [25]) implied a strong connection between PP-InsP metabolism and the phosphate starvation response.

To better understand the processes involved in the regulation, RKH characterized in a first step the products of VIH2 and confirmed that the kinase, indeed, belongs to the PPIP5K family (data not shown). I continued by interrogating the enzymatic activity of VIH2-phosphatase domain (PD) and VIH2-PD$^{RH/AA}$ *via* a progress curve (Figure 3.9a). Surprisingly, both enzymes exhibited the same activity although the Arg to Ala, His to Ala mutation had been described as catalytically dead in ScVip1.[24] This result was reproduced by Jinsheng Zhu in the Hothorn group *via* a malachite green assay.[25] Next, ScVip1-PD and its mutant

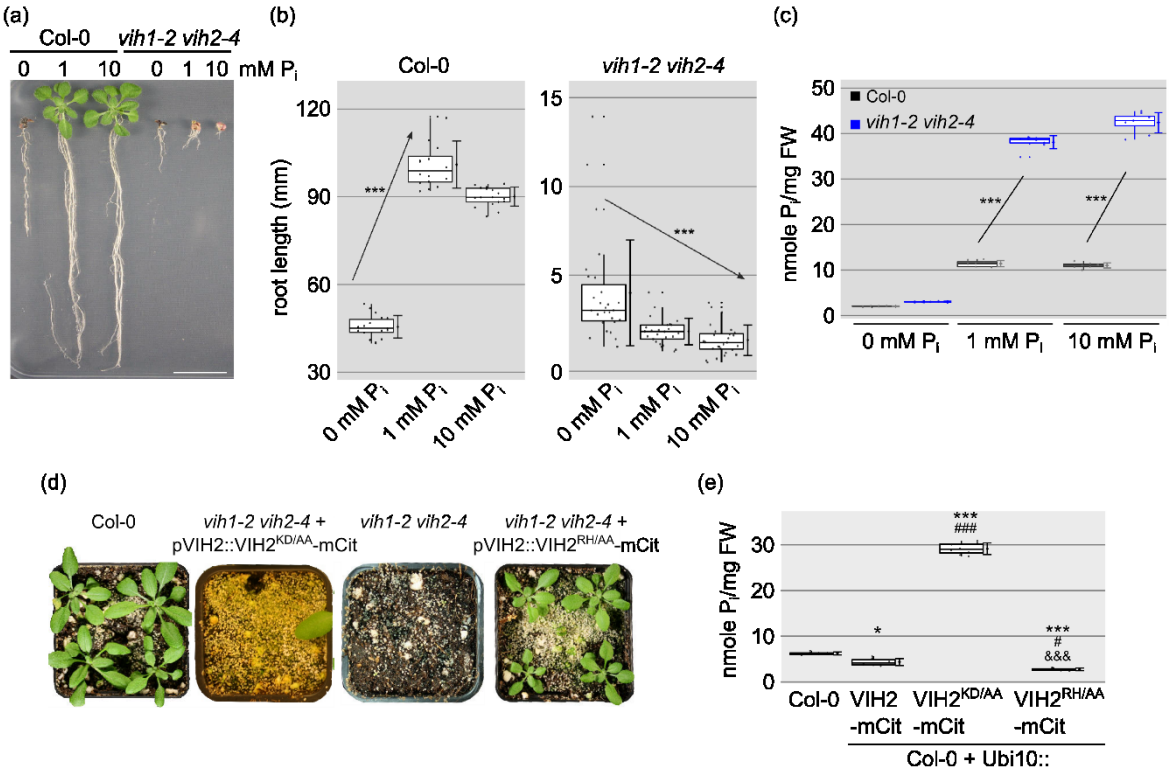

Figure 3.8. *vih1 vih2* loss-of-function mutants show severe growth phenotypes and hyper-accumulate phosphate. (a) Root growth phenotypes of Col-0 wild-type and *vih1-2 vih2-4* seedlings grown in different P_i concentrations. Plants were germinated in vertical $^{1/2}$MS plates for 8 d, transferred into P_i-deficient $^{1/2}$MS plates supplemented with either 0 mM, 1 mM or 10 mM P_i and grown for additional 12 d. Scale bars correspond to 2 cm. (b) Quantification of (a). For each boxed position, at least 16 independent measurements were performed for roots of seedlings from 3 different MS plates. (c) Shoot P_i content of the wild-type (black) and *vih1-2 vih2-4* (blue) seedlings grown under different P_i conditions as shown in (a). For each boxed position, at least 3 ndependent measurements were performed for shoots of seedlings from 3 different MS plates. (d) Expression of pVIH2::VIH2$^{RH/AA}$-mCit (Arg372Ala and His373Ala) but not pVIH2::VIH2$^{KD/AA}$-mCit (Lys219Ala and Asp298Ala) rescues the *vih1-2 vih2-4* mutant phenotype. Plants were transferred to soil 7 DAG and grown for 20 d. (e) Shoot P_i content of plants 20 DAG, over-expressing VIH2-mCit, VIH2$^{KD/AA}$-mCit or VIH2$^{RH/AA}$-mCit with a Ubi10 promoter in the Col-0 wild-type background. 4 independent plants were measured with 2 technical replicates each. The figure was taken from [25].

ScVip1$^{RH/AA}$ were measured as a control and as expected, the mutant displayed a drastically reduced activity. It is noteworthy, that the activity level of wildtype VIH-PD was comparable to mutant ScVip1$^{KH/AA}$ but this might have been an artifact of the protein being shipped in dry ice as the VIH2-PD was unstable. In light of these results, it is not surprising that complementation of *vih1-2 vih2-4* with VIH2-PD$^{RH/AA}$ mostly rescued the wildtype growth phenotype and that overexpression of VIH2-PD$^{RH/AA}$ had almost no effect on P_i content (Figure 3.8d,e).

In animal and yeast cells PP-InsP levels are downregulated upon phosphate starvation, it therefore seemed natural to tested if the phosphatase activity of

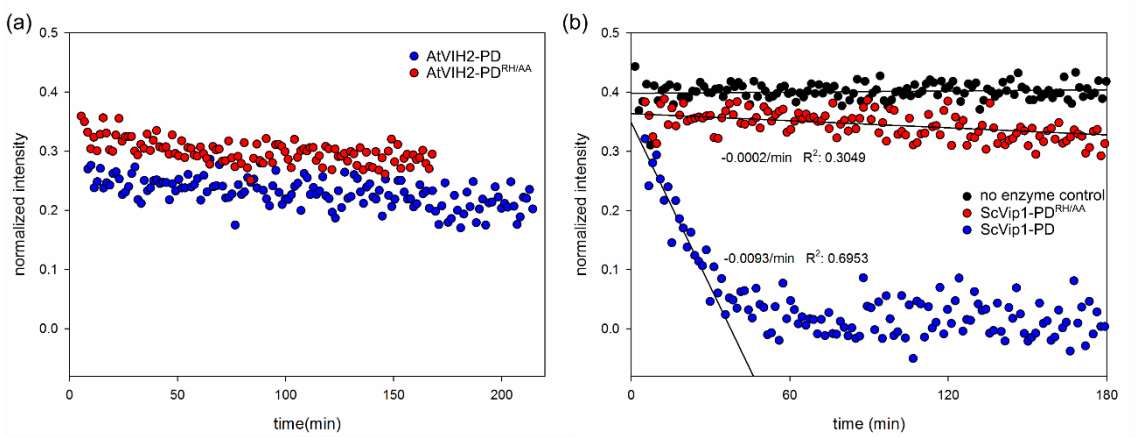

Figure 3.9. AtVIH2$^{RH/AA}$ is not a phosphatase dead allele. (a) The catalytic activity of VIH2 phosphatase domain (PD) and VIH2-PD$^{RH/AA}$ against [$^{13}C_6$]5PP-InsP$_5$ was tested by NMR spectroscopy. (b) The catalytic activity of ScVip1 phosphatase domain (PD) and ScVip1-PD$^{RH/AA}$ against 5PP-InsP$_5$ was tested by NMR spectroscopy. 20 mM HEPES pH* 7, 150 mM NaCl, 1 mg/ml BSA, 175 µM [$^{13}C_6$]5PP-InsP$_5$, 37 °C.

VIH2-PD was responsive to P_i concentration.[16,26,27] However, the protein expression was low yielding and the enzyme unstable (personal correspondence with Jinsheng Zhu), so we decided to continue with the homolog ScVip1-PD and characterize its response to phosphate concentration as a proxy. At 10 mM P_i the phosphatase activity was slightly downregulated when compared to 0 mM, and 1 mM P_i (Figure 3.10).

After characterizing the impact of P_i concentration on the phosphatase domain's activity, the question emerged how the full length (FL) enzyme would react to different phosphate concentrations. Such an assay proved to be logistically

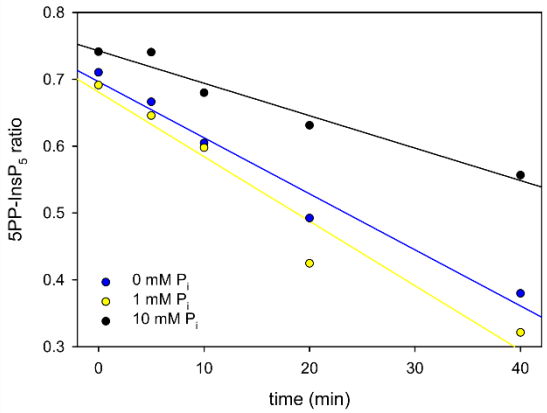

Figure 3.10 ScVip1-PD phosphatase activity is sensitive for phosphate concentration. The reactions contained 20 mM HEPES pH* 7, 150 mM NaCl, 1 mg/ml BSA, 40 µM [$^{13}C_6$]5PP-InsP$_5$, and 0/1/10 mM Pi, respectively. Samples were taken at the indicated time points and the reaction was quenched by heating to 90 °C for 5 min. The samples were measured using a pseudo-2D spin-echo difference experiment and the integrals corresponding to the C2 of 5PP-InsP$_5$ and InsP$_6$ were quantified.

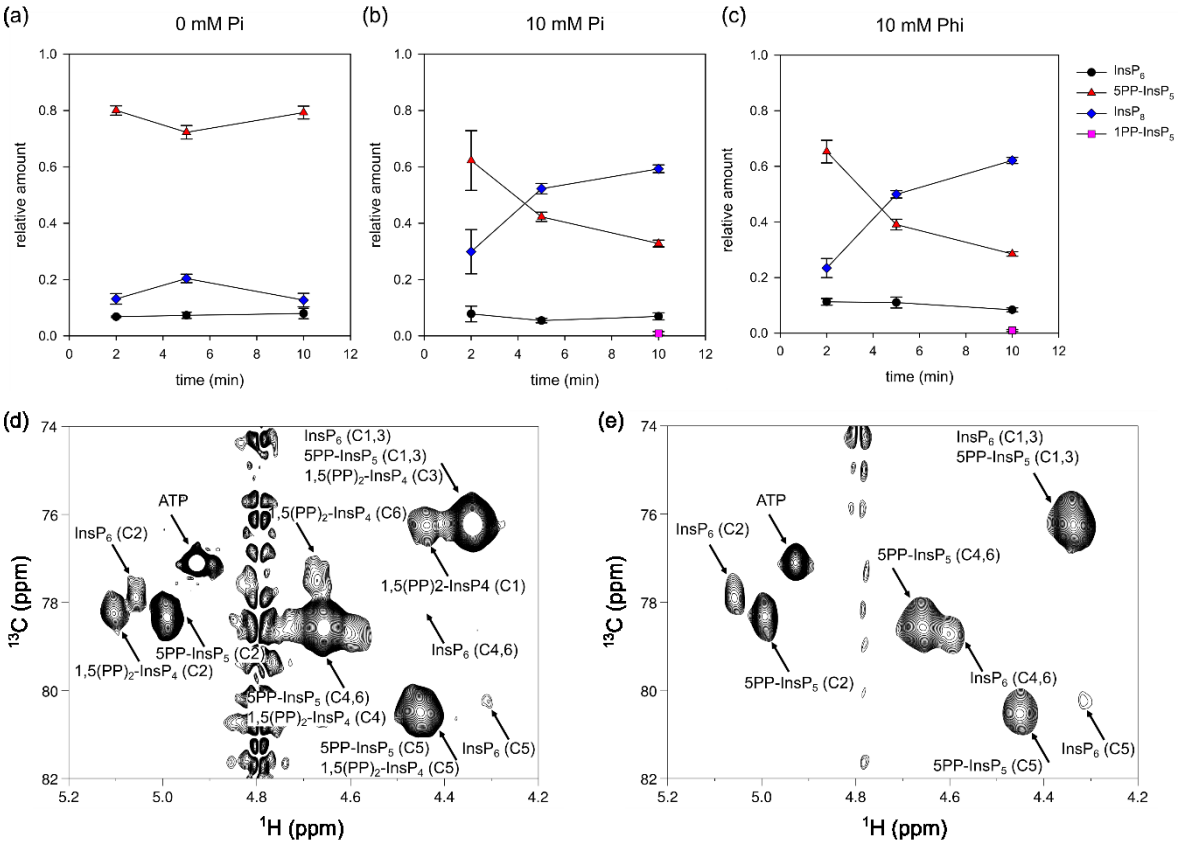

Figure 3.11. Phosphate stimulates the kinase activity of ScVip1-FL. ScVip1-FL was incubated with 40 µM [$^{13}C_6$]5PP-InsP5 in the presence of (a) 0 mM P_i, (b) 10 mM P_i, and (c) 10 mM Ph_i. The reactions were quenched after the indicated time points, measured by NMR spectroscopy, and the C2 peaks of $InsP_6$, 1PP-$InsP_5$, 5PP-$InsP_5$, and 1,5(PP)$_2$-$InsP_4$ were quantified. (d) Representative spectrum from (a). The C2 signals are well resolved. (e) Control sample after 0 min.

difficult, as the full length protein lost all kinase activity during transport from Geneva to Berlin. To circumvent this problem, the biochemical experiment was conducted in Geneva by Jinsheng Zhu and the samples were lyophilized before sending them to Berlin. In preparation for NMR spectroscopy measurements, the samples were reconstituted in D_2O and all residual enzyme activity was quenched by a heat shock. A pseudo-2D spin-echo difference experiment was not suitable to analyze the samples as it would not allow for the differentiation of $InsP_6$ and $InsP_8$ (the spectral resolution in the ^1H dimension is not sufficient to resolve both signals), instead, the samples were quantified utilizing ^1H,^{13}C-HMQC spectra (Figure 3.11c,d). In the absence of P_i, the substrate and product concentrations of 5PP-$InsP_5$, and $InsP_6$ and $InsP_8$ remained constant over time with only little $InsP_8$ being made (Figure 3.11a). However, in the presence of 10 mM P_i, the concentration of $InsP_8$ increased in a time dependent manner to constitute the majority of PP-InsPs in the sample after 10 min, while 5PP-$InsP_5$ levels decreased. Also after 10 min, a cross peak for 1PP-$InsP_5$ started to appear. This data

solidifies the notion that PP-InsPs and VIH1/2 are involved in plant phosphate homeostasis.

The NMR spectroscopy workflow developed previously could be applied to a question in PP-InsP metabolism. It could be shown that VIH2 is a member of the PPIP5K family and its catalytic activity in different conditions, plus and minus phosphate, was established, ascertaining the involvement of VIH1/2 in plant phosphate starvation response. It is noteworthy that $InsP_6$, 5PP-$InsP_5$, 1PP-$InsP_5$, and $InsP_8$ could be resolved and quantified in one sample, strengthening the advantage of NMR spectroscopy over radiolabeling or PAGE.

The information gained in this project, highlight the easy applicability of NMR spectroscopy for *in vitro* characterization of PP-InsP metabolizing enzymes and promises a wide adoption of the method by the inositol pyrophosphate field in the future.

3.4 Metabolic labeling of mammalian cells with [$^{13}C_6$]*myo*-inositol

To date, the most widely used method to assay cellular InsP and PP-InsP levels employs metabolic labeling of the cells with tritiated, radioactive *myo*-inositol. After incorporation into the cellular InsP and PP-InsP pools the labeled compounds are extracted, fractionated *via* SAX-HPLC chromatography, and analyzed using scintillation counting (Figure 3.2a). We envisioned to replace [^{3}H]*myo*-inositol with [$^{13}C_6$]*myo*-inositol and tested the metabolic labeling of the human colon cancer cell line HCT116. HCT116 cells were grown in DMEM and 10 % dialyzed FBS in the presence of 100 µM [$^{13}C_6$]*myo*-inositol and subsequently lysed using 1 M $HClO_4$. The extract was neutralized, lyophilized, dissolved in D_2O, and a ^{1}H,^{13}C-HMQC spectrum was recorded (Figure 3.12a). The spectrum displayed several strong peaks in the characteristic chemical shift region for InsPs and PP-InsPs (^{1}H: 5.0 – 3.6 ppm; ^{13}C: 81 – 71 ppm, Figure 3.12b). At high spectral resolution a characteristic triplet pattern emerged due to the coupling of neighboring ^{13}C nuclei in the *myo*-inositol ring. Comparison to an extract prepared with [$^{12}C_6$]*myo*-inositol

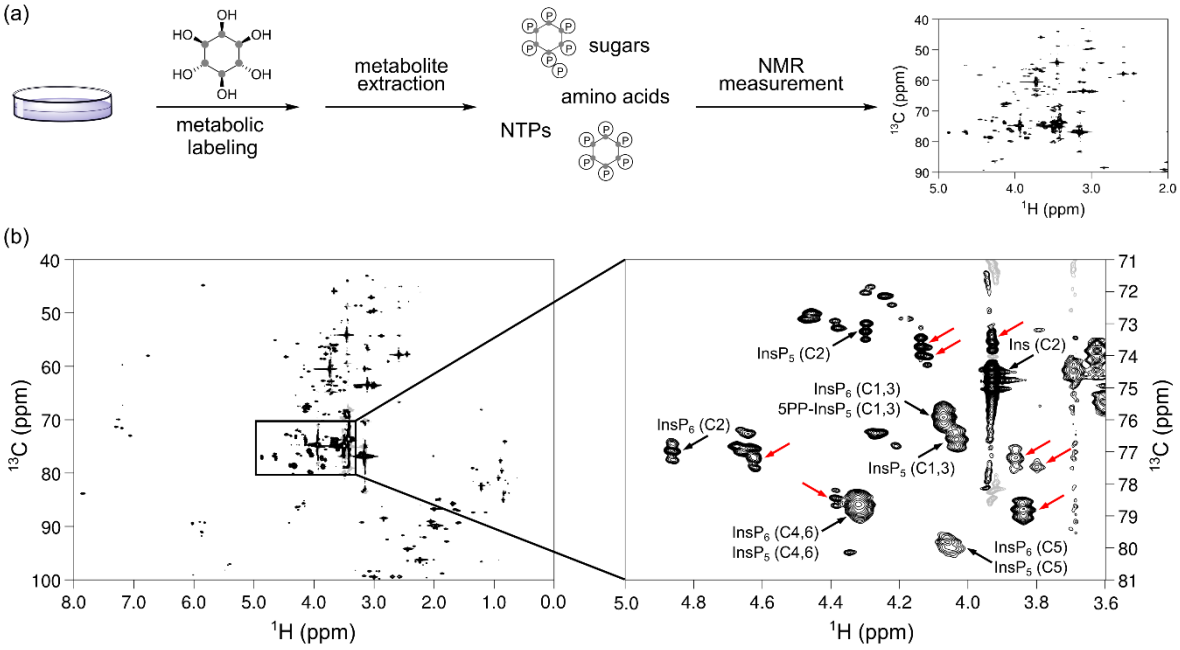

Figure 3.12. Metabolic labeling of mammalian cell line HCT116, followed by NMR analysis. (a) General workflow for the preparation of whole cell extracts for NMR spectroscopy. (b) Left: ^{1}H,^{13}C HMQC spectrum of an HCT116 extract. The peaks from 80 to 100 ppm in the F1 and between 0 and 3 ppm are folded into an empty region of the spectrum. Right: the inositol phosphate region of the spectrum is depicted in more detail. The identified InsPs are annotated while peaks that exhibit the expected splitting pattern in the carbon dimension but could not be attributed to either *myo*-inositol (Ins), $InsP_5$, $InsP_6$, nor 5PP-$InsP_5$ are highlighted by red arrows.

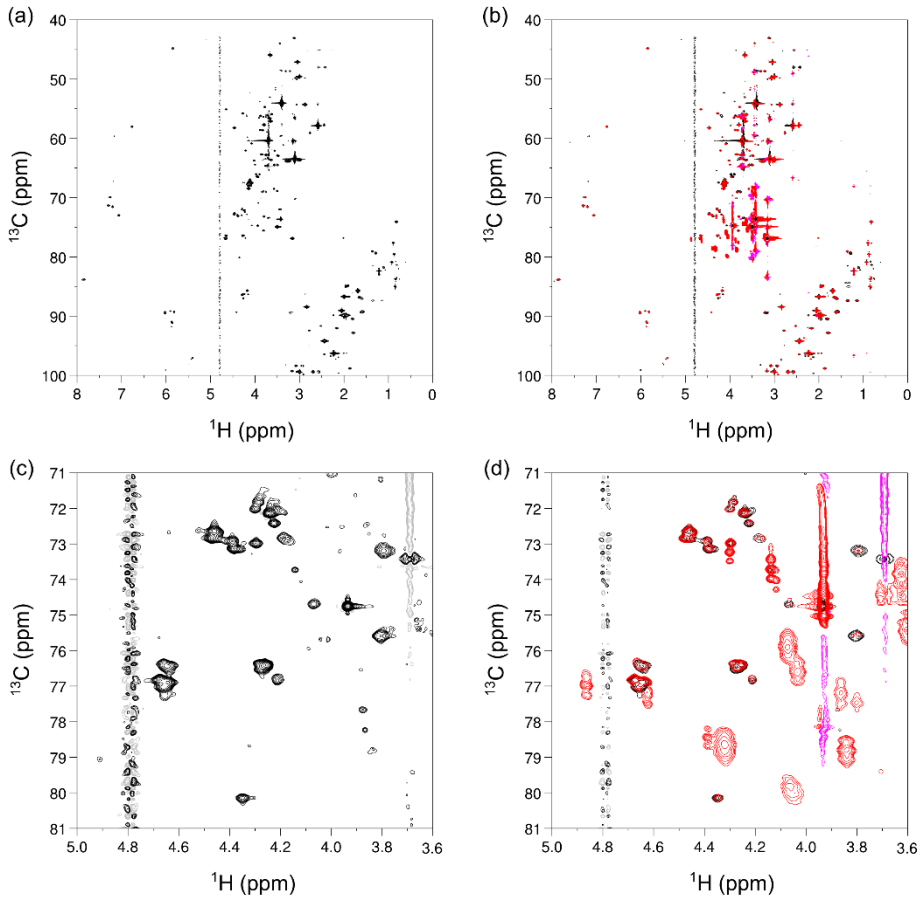

Figure 3.13. [$^{12}C_6$]*myo*-inositol labeled HCT116 wt cell extract. (a) The cells were grown in DMEM supplemented with 100 µM [$^{12}C_6$]*myo*-inositol and the InsPs were extracted. (b) Overlay of [$^{13}C_6$]*myo*-inositol-labeled (red) and unlabeled (black) HCT116 extracts. (c) Inositol phosphate region of the unlabeled HCT116 wt extract. (d) Inositol phosphate regions of overlay between [$^{13}C_6$]*myo*-inositol-labeled (red) and unlabeled (black) HCT116 wt extracts.

confirmed that these peaks were a result of labeling with [$^{13}C_6$]*myo*-inositol (Figure 3.13). To verify that the labeling success was not limited to HCT116 cells, we next treated human embryonic kidney cells (HEK293T) with [$^{13}C_6$]*myo*-inositol and again observed robust labeling (Figure 3.14).[h] When cells are labeled with radioactive [^{3}H]*myo*-inositol, their growth is slowed down. No such effect was observed during labeling with the benign [$^{13}C_6$]*myo*-inositol.

To annotate characteristic resonances for endogenous $InsP_5$, $InsP_6$ and 5PP-$InsP_5$, we performed spike-in experiments with synthetic standards (see chapter 2) on the labeled extracts (Figure 3.15) and confirmed the presence of the above mentioned InsPs (as annotated in Figure 3.12). We further added a mixture containing synthetic $InsP_5$, $InsP_6$ and 5PP-$InsP_5$ to an unlabeled extract from HCT116 and detected all signals at their expected chemical shifts (Figure 3.15).

[h] The labeling of HEK293T cells was conducted by RKH.

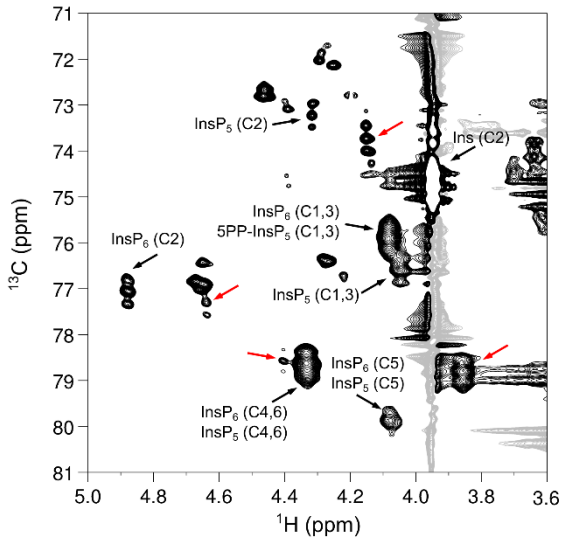

Figure 3.14. HEK293T cell extract. HEK293T cells were extracted with 1 M $HClO_4$ and the soluble fraction was measured by NMR-spectroscopy. The relevant InsP peaks are labeled and additional peaks displaying the triplet pattern are highlighted by red arrows.

For absolute quantification of $InsP_5$, $InsP_6$ and 5PP-$InsP_5$, we prepared [$^{13}C_6$]*myo*-inositol labeled HCT116 extracts containing a known concentration of an internal standard (tetramethyl phosphonium bromide, PMe_4Br). Resonances corresponding to the C2-position were integrated and referenced to a set of calibration curves (Figure 3.16). Assuming full replacement of the unlabeled InsP pools we calculated respective concentrations of 26.7 ± 2.3 µM $InsP_5$, 29.4 ± 7.6 µM $InsP_6$, and 1.9 ± 0.5 µM PP-$InsP_5$, based on packed cell volume (Figure 3.17a). The measured concentrations are consistent with previous publications with respect to $InsP_5$ and $InsP_6$, however, the amount of 5PP-$InsP_5$ determined by NMR is at least 2-fold higher.[28,29] These results underline the mild sample preparation and the quantitative nature of NMR spectroscopy and highlight its potential for future measurements of labeled cells or tissues.

The ability to quantify mixtures of InsP messengers prompted us to analyze the concentrations of $InsP_5$, $InsP_6$ and 5PP-$InsP_5$ in HCT116 cells with perturbed PP-InsP metabolism. When HCT116 cells were treated for one hour with 10 mM sodium fluoride (NaF), an agent previously shown to elevate 5PP-$InsP_5$ levels,[30] the content of 5PP-$InsP_5$ increased dramatically to an absolute concentration of 14.7 ± 2.0 µM (Figure 3.17b). Elevated concentrations of 5PP-$InsP_5$ were also

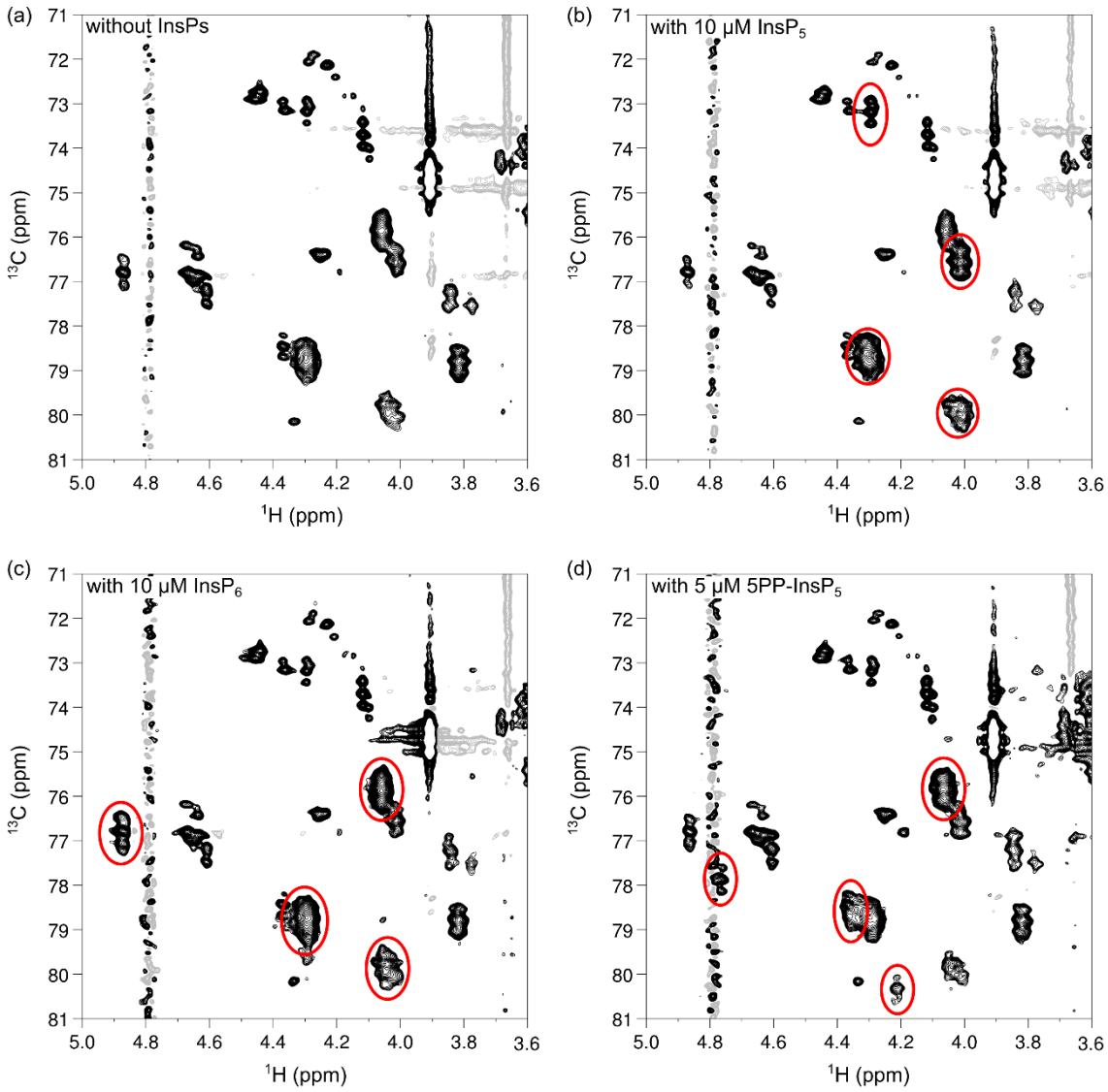

Figure 3.15. Spike in experiments to confirm the identity of $InsP_5$, $InsP_6$, and 5PP-$InsP_5$ in HCT116 extracts. (a) HCT116 extract. (b) Extract + $InsP_5$. (10 µM final concentration) (c) Extract + $InsP_6$. (10 µM final concentration) (d) Extract + 5-PP-$InsP_5$ (5 µM final concentration).

reported in cells lacking PPIP5K1 and PPIP5K2.[31] We therefore grew PPIP5K$^{-/-}$ cells and indeed, a general increase of 5PP-$InsP_5$ was detected compared to HCT116 wt cells (Figure 3.17c). Addition of NaF to this knock-out cell line resulted in extracts which contained more 5PP-$InsP_5$ than $InsP_6$ or $InsP_5$ (Figure 3.17d). These trends of increasing 5PP-$InsP_5$ concentrations had been observed before and the ratio of 5PP-$InsP_5$ to $InsP_6$ in all our samples was consistent with previous publications.[31]

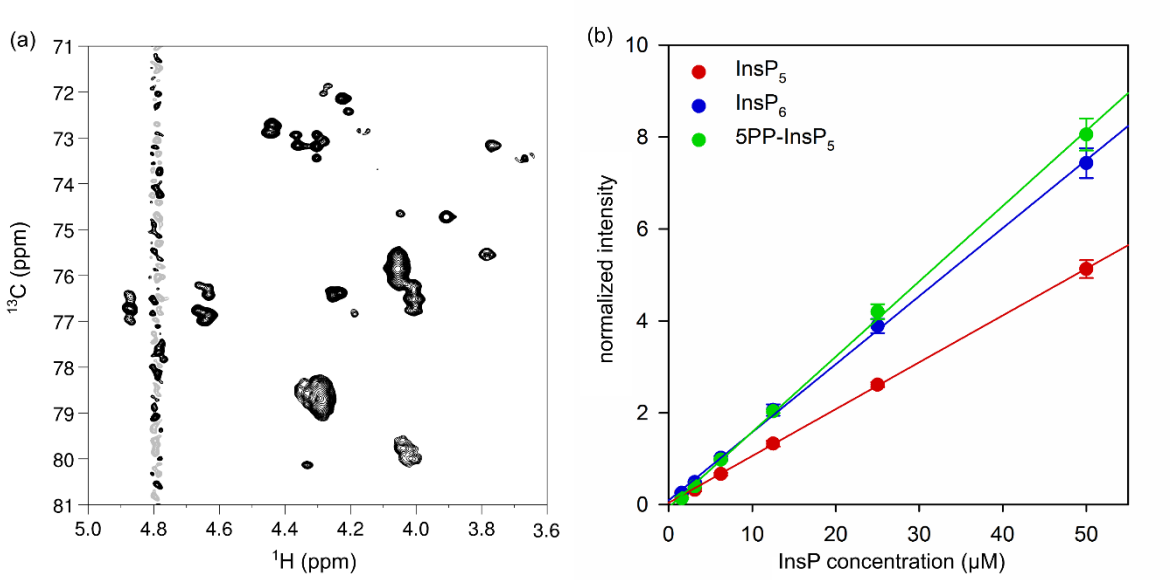

Figure 3.16. Absolute quantification of InsPs from HCT116 extracts. (a) 8 µM $InsP_5$, 10 µM $InsP_6$, 3 µM 5PP-$InsP_5$ spiked into a ^{12}C-labeled HCT116 extract. (b) Calibration curves for InsP C2 peak intensities normalized to the reference standard PMe_4Br.

To our surprise, the analysis of the mammalian extracts uncovered additional NMR signals that displayed a triplet-pattern in the carbon-dimension. These signals were absent in the corresponding samples prepared with unlabeled *myo*-inositol and must therefore stem from metabolic labeling with [$^{13}C_6$]*myo*-inositol (Figure 3.12b, Figure 3.13). Interestingly, several of these signals increased upon NaF treatment (Figure 3.17b,d). To determine whether these signals correspond to other InsP or PP-InsP species, the ^{13}C-labeled, NaF treated HCT116 wt extract was incubated with TiO_2 beads, which enrich phosphate containing molecules.[4,32] In addition to retaining $InsP_5$, $InsP_6$ and 5PP-$InsP_5$, a putative unsymmetrical InsP species ($InsP_1$ or $InsP_2$) could be observed (Figure 3.18). Nevertheless, most unassigned labeled resonances were not bound by the TiO_2 beads. To test for conversion of *myo*-inositol to related metabolites, spectra of D-*chiro*- and s*cyllo*-inositol – two inositol isomers that occur in human next to *myo*-inositol and are generated from it – and glucuronic acid, the canonic *myo*-inositol degradation product, were recorded (Figure 3.19a-c), none of which were superimposable with the unassigned labeled species.[33,34]

Lastly, we considered that the additional peaks corresponded to PtdInsPs. However, after a phospholipid extraction, the aqueous layer still contained the

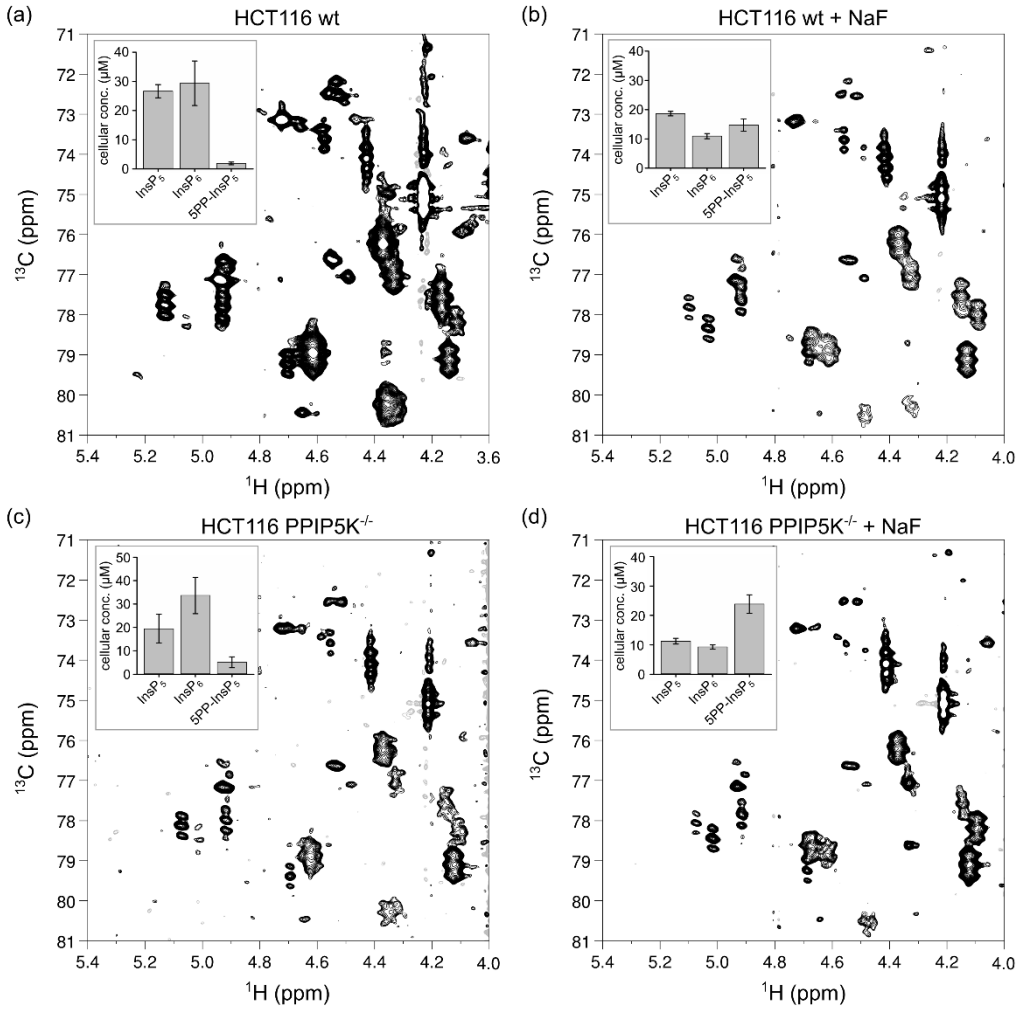

Figure 3.17. Changes in 5PP-$InsP_5$ levels can be observed by NMR spectroscopy. (a) $^{1}H,^{13}C$ HMQC spectrum of a HCT116 wt cell extract. (b) $^{1}H,^{13}C$ HMQC spectrum of an extract of HCT116 wt cells treated with 10 mM NaF before extraction. (c) $^{1}H,^{13}C$ HMQC spectrum of HCT116 $PPIP5K^{-/-}$ cell extract. (d) $PPIP5K^{-/-}$ cells were treated with 10 mM NaF for 1h prior to extraction. The inserts display triplicates of absolute cellular concentration of $InsP_5$, $InsP_6$ and 5PP-$InsP_5$ based on packed cell volume.

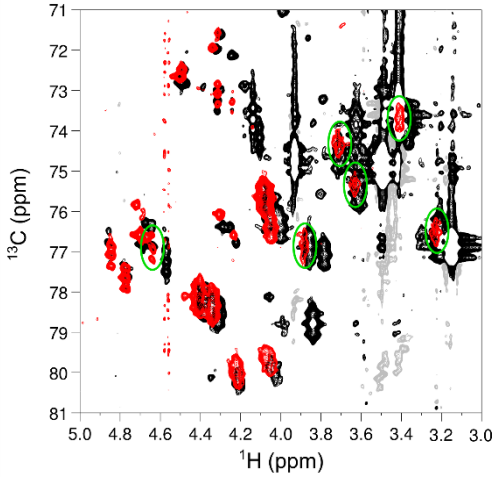

Figure 3.18. TiO_2-enrichment of NaF treated HCT116 wt cells. Overlay of TiO_2 enrichment of NaF treated, ^{13}C-labeled HCT116 wt cell extract (red) and the original NaF treated, ^{13}C-labeled HCT116 wt cell extract (black). One set of 6 peaks (green circles) was retained that corresponds to a putative unsymmetrical $InsP_1$ or $InsP_2$ species. All other labeled unassigned peaks were removed.

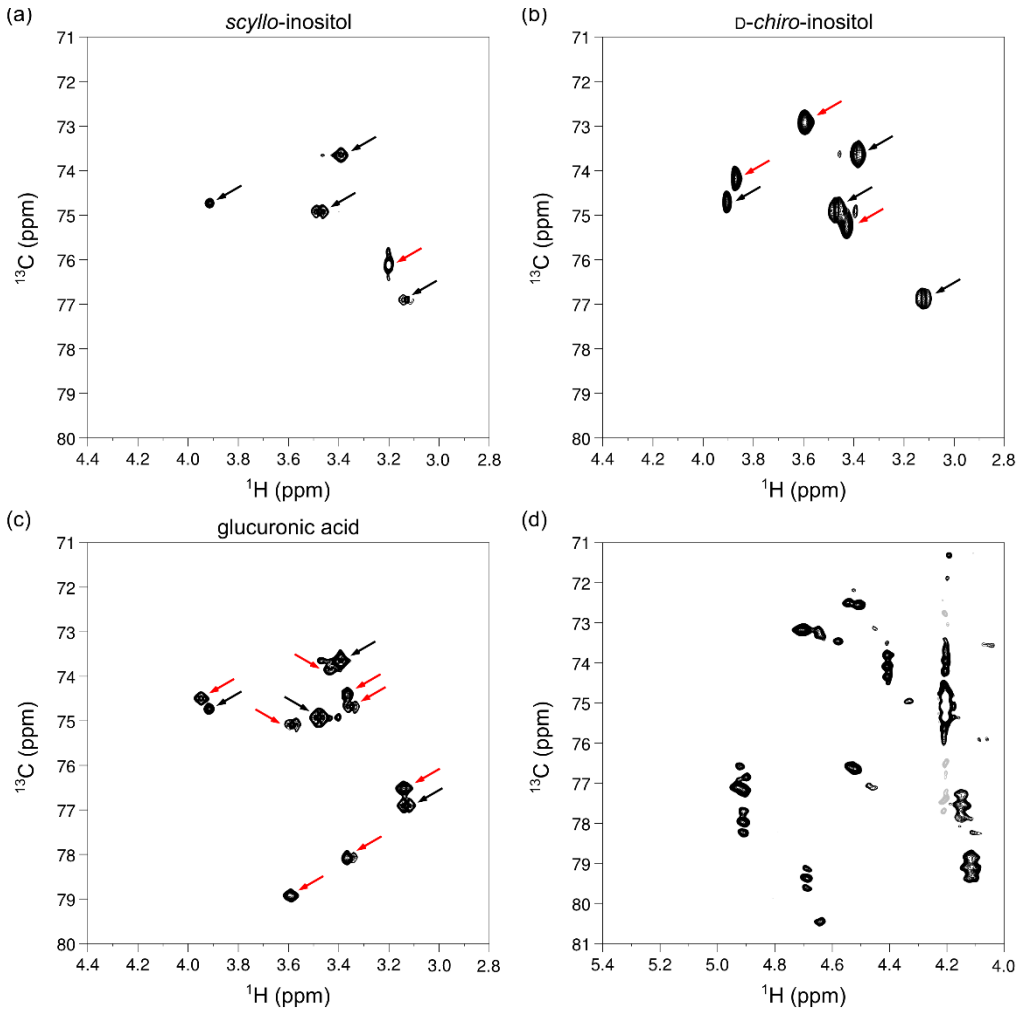

Figure 3.19. Preliminary analysis of unannotated NMR signals. HMQC spectra of 1 mM (a) *scyllo*-inositol, (b) D-*chiro*-inositol, and (c) glucuronic acid (highlighted with red arrows) in $KClO_4$ saturated D_2O. 1 mM *myo*-inositol was included as an internal reference (black arrows). (d) Aqueous phase of a lipid extraction of HCT116 wt retained all unassigned peaks except for the putative unsymmetrical $InsP_1$ or $InsP_2$ species.

unidentified resonances, strongly implying a non-lipid, hydrophilic character of these molecules (Figure 3.19d). These observations suggest that the supplemented [$^{13}C_6$]*myo*-inositol has been diverted into an unknown metabolic pathway. Detection of these unanticipated species was only possible because the NMR-analysis was conducted on the crude extract and did not require a separation step. Elucidating the structure and function of these molecules connected to inositol metabolism will be of interest in the future.

3.5 Outlook

The ability to use [$^{13}C_6$]*myo*-inositol to label mammalian cells and quantify the amount of InsPs and PP-InsPs is a powerful tool. So far, $InsP_5$, $InsP_6$ and PP-$InsP_5$ could be assigned in spectra of cell extracts. The experiments with VIH2 showed furthermore, that it is possible to detect and quantify $InsP_6$ and PP-$InsP_5$, 1PP-$InsP_5$, and $InsP_8$ in the same sample (Figure 3.11). This means that the natural abundance of these compounds in the only limiting factor for detecting them. The ^{13}C-labeling is not limited to mammalian cells but quantification of InsP levels in other organisms is feasible, as well. In collaboration with the Hothorn group, labeling of *A. thaliana* was started and should enable the first quantification of PP-InsPs in plants. Another collaboration with the group of Hartmut Oschkinat at the FMP aims to utilize ^{13}C- inositol for the labeleing and subsequent analysis of PtdInsPs with solid state NMR spectroscopy. In conclusion, the labeling of cells with ^{13}C-inositol is only limited by the ability of the organism to import the [$^{13}C_6$]*myo*-inositol and by the intracellular concentration of the inositol derived compounds of interest.

The additional peaks in HCT116 extracts that exhibit the triplet pattern, but could not be attributed to any InsPs, have to be identified. To this end, a mass spectrometry based metabolomics approach seems feasible. By comparing a ^{13}C and a ^{12}C labeled sample, the compounds responsible for the additional peaks should be identifiable.

The applicability of the developed NMR-methodology to biochemical reactions was demonstrated with the kinetic characterization of IP6K1 and its inihitors TNP and myrecitin. By empoying a pseudo-2D spin-echo difference experiment, the measurement time for an individual sample could be reduced from several hours to 5 – 10 min. However, due to the low spectral resolution of such an experiment, this pulse program is not suited for samples containing all mammalian PP-InsPs.

The major limitation of this method is its low sensitivity and the resulting requirement for higher concentrated samples. This means that, depending on spectral width and number of scans, compounds with a concentration of > 200 nM are detectable within 12 hour measurements. With a shorter measurement time of one hour, 1 micromolar concentrations are robustly detected. Nevertheless, for cells with low endogenous PP-InsPs levels or for biochemical samples that require

low substrate concentrations (e.g., for the measurement of the K_M of IP6Ks for $InsP_6$) this NMR-based method is not amenable.

3.6 Methods

General Information

All chemicals were purchased from Sigma Aldrich, VWR, Carl Roth, Thermo Fisher Scientific, Alfa Aesar, TCI and used without further purification unless stated otherwise. Deuterated solvents were purchased from Euriso-Top.

NMR spectra were recorded on Bruker spectrometers at 600 MHz for proton nuclei, 151 MHz for carbon nuclei or 244 MHz for phosphorous nuclei. NMR data are given as follows: chemical shift δ in ppm (multiplicity, coupling constant(s) J Hz, relative integral) where multiplicity is defined as: s = singlet, d = doublet, t = triplet, q = quartet, m = multiplet, br = broad or combinations of the above. Measurement of the metabolic extracts was performed on Bruker AV-III spectrometers (Bruker Biospin, Rheinstetten, Germany) at 310 K using a cryogenically cooled 5 mm TCI-triple resonance probe equipped with one-axis self-shielded gradients. The software used to control the spectrometer was topspin 3.5 pl6. Temperature had been calibrated using d_4-methanol and the formula of Findeisen et al.[35]

For the purification *via* FPLC an NGC Quest^{TM} 10 Chromatography System from Bio-Rad was used with an integrated NGC^{TM} Sample Pump Module and a BioFrac^{TM} Fraction Collector. For the spin filtration Amicon Ultra 0.5 mL centrifugal filters with a cut off of 10 kDa or 3 kDa from Merck Millipore were used.

Protein expression and purification

Inositol hexakisphosphate kinase 1 (IP6K1)

The codon optimized IP6K1-gene from human cloned into a pTrcHis vector (a kind gift from Adam Resnick) was transformed into *E. coli* BL21 (DE3). A 1 L overnight culture (37 °C) in TB supplemented with Ampicillin was diluted with 500 mL TB, prewarmed to 37 °C. After 30 min the expression was induced with 1 mM IPTG. After 4 hours the cells were harvested by centrifugation (3,000 g for 10 min at 4 °C) and washed with ice cold water. The pellet was stored at -80 °C until further use.

The frozen cells were resuspended in lysis buffer (20 mM Tris HCl pH 7.4, 150 mM NaCl). For 1 g wet weight 10 mL lysis buffer was used. The cell suspension

was supplemented with lysozyme, DNase I and 1 tablet cOmplete™ protease inhibitor (Roche), and incubated for 15 min on ice. The cells were lysed with a microfluidizer™ LM10 at 15,000 psi with five iterations. The lysate was clarified by centrifugation (30,000 g for 30 min at 4 °C). The supernatant was adjusted to 0.1 % (v/v) Triton X-100, filtered (VWR® vacuum filter, PES 0.45 µm), and loaded onto a Co-NTA column (GE, 1 mL, HiTrap IMAC HP) that was equilibrated with lysis buffer with a flowrate of 1 mL/min. The column was washed with wash buffer (20 mM Tris HCl pH 7.4, 500 mM NaCl, 50 mM imidazole, 0.1 % (v/v) Triton X-100) until the absorption was constant. IP6K1 was eluted with a gradient of elution buffer (20 mM Tris HCl pH 7.4, 500 mM NaCl, 500 mM imidazole, 0.1 % (v/v) Triton X-100) in wash buffer from 0-100 % over 10 CV. 1 mL fractions were collected. The fractions containing IP6K1 (not more than three fractions were used) were concentrated to 0.5 mL by spin filtration (Amicon® Ultra 0.5 mL 10K) and dialyzed overnight against dialysis buffer (20 mM Tris HCl pH 7.4, 500 mM NaCl, 1 mM DTT). The protein solution was used immediately and not frozen.

NMR experiments

Synthesis of inositol phosphates and inositol pyrophosphates

[$^{13}C_6$]*myo*-inositol, [$^{13}C_6$]InsP_5, [$^{13}C_6$]InsP_6, and [$^{13}C_6$]5PP-InsP_5 were prepared according to the procedures described in chapter two.

Progress curve measurement with IP6KA

Progress curves were recorded for different IP6KA concentrations ranging from 0.2 – 1 µM. The reactions contained 20 mM HEPES NaOD pH* 7.0, 50 mM NaCl, 1 mM DTT, 10 mM ATP, 11 mM $MgCl_2$, 176 µM [$^{13}C_6$]InsP_6Na_{12} (**6**), 5 mM creatine phosphate, 2 mM Me_4PBr, and 1 U/mL creatine kinase in D_2O. All stock solutions were prepared in D_2O. The reactions were run in a total volume of 650 µl and equilibrated at 37 °C. The reactions were transferred into a 5 mm NMR tube and the reaction was started by the addition of the appropriate amount of IP6KA (in D_2O buffer). The NMR tubes were inserted into the NMR instrument, locked, tuned and matched, and shimmed. A spin echo difference pulse was used to measure consecutively 75 sec spectra until the reaction was finished.

Kinetic characterization of IP6K1

The $K_{M,ATP}$ and V_{max} were determined for IP6K1. The buffer contained 20 mM HEPES NaOD pH* 7.0, 50 mM NaCl, 1 mM DTT, 1 mg/mL BSA, 1 µM IP6K1, 5 mM creatine phosphate, and 1 U/mL creatine kinase in D_2O. The ATP concentration ranged from 8 mM to 62.5 µM (two-fold dilution series) and the $MgCl_2$ concentration was adjusted to be 5 mM plus the ATP concentration. The reaction volume was 500 µL and the reaction was started after 10 min equilibration at 37 °C by the addition of 175 µM [$^{13}C_6$]$InsP_6$. The reaction was quenched with 38 µL 0.7 M EDTA (in D_2O, pH* 8.0) after approximately 20 % conversion (5 min for IP6K1). Before the NMR measurements the pH* was adjusted to 8, if needed. The conversion of [$^{13}C_6$]$InsP_6$ at different ATP concentration was determined by NMR spectroscopy. The data was fitted against a kinetic model for substrate inhibition: $v = \frac{V_{max}}{1+\frac{K_m}{S}+\frac{S}{K_i}}$ using SigmaPlot 12.5.

Determination of IC_{50} values for IP6K1 inhibitors

For the IC_{50} value determination a two-fold dilution series of the appropriate inhibitor in DMSO-d_6 was used. The reactions were run in a total volume of 500 µL and contained 20 mM HEPES NaOD pH* 7.0, 50 mM NaCl, 1 mM DTT, 2.5 mM ATP, 7.5 mM $MgCl_2$, 0.2 µM IP6K1, 1 mg/mL BSA, 5 mM creatine phosphate, and 1 U/mL creatine kinase in D_2O. The inhibitor concentration ranged from 50 µM to 195 nM (200 x stock solutions were used). The reactions were equilibrated to 37 °C for 10 min and initiated by the addition of 175 µM [$^{13}C_6$]$InsP_6$. The reactions were quenched after 3 hours by the addition of 38 µL of 0.7 M EDTA (in D_2O, pH* 8.0). Before the NMR measurements the pH* was adjusted to 8, if needed. The conversion of [$^{13}C_6$]$InsP_6$ at different inhibitor concentrations was determined by NMR spectroscopy. The data was fitted against a kinetic model for dose response inhibition: $v = \frac{bottom+(top-bottom)}{1+\frac{x}{IC_{50}}^{Hillslope}}$ using SigmaPlot 12.5.

NMR kinase assay

Proteins encoding full-length proteins of AtVIH1 and ScVIP1, and kinase-domains of AtVIH2 and HsVIP2 were used. 1 – 10 µM of proteins were incubated in a buffer containing (final concentrations) 20 mM HEPES pH 7, 50 mM NaCl, 1mM DTT, 2.5 mM ATP, 5 mM creatine phosphate, 1 U creatine kinase, 7.5 mM

$MgCl_2$ and 175 uM of [$^{13}C_6$]$InsP_6$ or [$^{13}C_6$]5PP-$InsP_5$, at a final volume of 550 µL. The reaction was incubated at 37°C overnight, quenched with 50 µL 0.7 M EDTA, lyophilized and resuspended in 600 µL of 100% D2O. Kinetic assays were performed similarly with the exception that the labelled InsPs were added just before NMR measurements and were not quenched by EDTA.

Phosphatase assay

The reactions contained 20 mM HEPES pH* 7, 150 mM NaCl, 1 mg/ml BSA, and 2 µM Vip1 in D_2O (total volume 600 µl). Depending on the experiment, the reaction also contained 1 mM or 10 mM K_2HPO_4. The reaction was pre-incubated at 37 °C and started by adding 40 µM [$^{13}C_6$]5PP-$InsP_5$. The reactions were quenched after 0, 5, 10, 20, and 40 min by boiling at 90 °C for 5 min. The samples were measured by NMR with a pseudo-2D spin-echo difference experiment and the relative intensities of the C2 peaks of $InsP_6$ and 5PP-$InsP_5$ were quantified.

Vip1-FL assay

Reactions were performed by Jinsheng Zhu. The reactions were lyophilized, dissolved in 600 µl D2O, the remaining protein was heat-inactivated for 5 min at 90 °C and the precipitated protein removed by centrifugation. $^{1}H,^{13}C$-HMQC spectra of the samples were recorded and the relative signal intensities of the C2 peaks were quantified.

Metabolic labeling of mammalian cell lines

HCT116 wt, HCT116 PPIP5K$^{-/-}$ (a kind gift from Stephen Shears)[31] and HEK293T cells were grown in DMEM lacking *myo*-inositol and supplemented with 10 % dialyzed fetal bovine serum, 100 µM either [$^{12}C_6$]- or [$^{13}C_6$]*myo*-inositol, and Penicillin/Streptomycin at 37 °C and 5 % CO_2. 1 liter DMEM w/o inositol was prepared from pre-mixed medium components (8.1 g, Dulbecco), $NaHCO_3$ (3.7 g), HEPES (10 mL of a 1 M stock, pH 7.4), l-glutamine (584 mg), l-serine (42 mg), d-glucose (4.5 g), and NaH_2PO_4 (125 mg). The cells were grown in 15 cm dishes (for one experiment we used five to ten plates) until they reached 80-90 % confluency. For harvesting, cells were washed with PBS and 0.9 % NaCl solution, and trypsinized. The trypsin was quenched with regular DMEM. The cells were collected and washed two more times with PBS before lysis and extraction. The

packed cell volume and the cell number of the preparations were determined. If needed, the cells were incubated with 10 mM NaF for one hour before harvest.

Inositol phosphate extraction

All steps were performed at 4 °C. The protocol was adapted from Azevedo et al.[36] For HCT116 wt we used ten 15 cm dishes and for HCT116 wt with NaF treatment, HCT116 PPIP5K$^{-/-}$ and HCT116 PPIP5K$^{-/-}$ with NaF treatment we used three 15 cm dishes. Cell pellets were lysed with 5 mL of 1 M $HClO_4$, containing 3 mM EDTA, by vortexing. The lysate was incubated on ice for 30 min before the precipitate was removed by centrifugation. The supernatant was neutralized with 2 M KOH, containing 3 mM EDTA, and the pH was adjusted to 5.8-6. The resulting $KClO_4$ precipitate was removed by centrifugation and the supernatant was lyophilized. After lyophilization the supernatant was redissolved in 1 mL D_2O and the resulting precipitate was removed by centrifugation. The supernatant was lyophilized again and the residue was redissolved in 600 µL D_2O containing the 50–150 µM Me_4PBr standard for absolute quantification.

TiO_2 enrichment

All steps were performed at 4 °C. The protocol was adapted from Wilson *et al*.[4] TiO_2 beads 4-5 mg were washed with 500 µL of water and 500 µL of 1 M $HClO_4$. Cell extract was adjusted to pH 1 with 1 M $HClO_4$ and added to the beads. The beads were rotated for 5 min and after centrifugation, the supernatant was discarded. The beads were washed twice with 500 µL of 1 M $HClO_4$ and the InsPs were eluted by incubating the beads twice with 200 µL 2.8 % NH_4OH solution. The eluate was lyophilized and the dry residue was dissolved in 600 µL of 1 mM MES (pH* 6.0) in D_2O.

Lipid extraction

The lipid extraction was adopted from Clark et al.[37] In summary: The cells from 3 15 cm dishes were trypsinized and washed twice with PBS. The cells were resuspended in 1.7 mL Milli-Q water and 7.5 ml quench mix (48.4 mL MeOH, 24.2 mL $CHCl_3$, 2.4 mL 1 M $HClO_4$) was added. The cells were lysed by vortexing for 30 sec. 1.7 mL 1 M $HClO_4$ and 7.25 mL $CHCl_3$ were added to induce phase separation and the mixture was vortexed for 30 sec. The sample was centrifuged

at 3000 g for 5 min to facilitate phase separation. The top aqueous layer was collected and washed with 7 mL $CHCl_3$. The aqueous layer was collected and neutralized with 2 M KOH containing 3 mM EDTA. The $KClO_4$ salt was removed by centrifugation and the sample was lyophilized. After lyophilization the supernatant was redissolved in 1 mL D_2O and the resulting precipitate was removed by centrifugation. The supernatant was lyophilized again and the residue was redissolved in 600 µL D_2O.

3.7 References

(1) Wormald, M.; Liao, G.; Kimos, M.; Barrow, J.; Wei, H. Development of a Homogenous High-Throughput Assay for Inositol Hexakisphosphate Kinase 1 Activity. *PLoS One* **2017**, *12* (11), e0188852. https://doi.org/10.1371/journal.pone.0188852.

(2) Weaver, J. D.; Wang, H.; Shears, S. B. The Kinetic Properties of a Human PPIP5K Reveal That Its Kinase Activities Are Protected against the Consequences of a Deteriorating Cellular Bioenergetic Environment. *Biosci. Rep.* **2013**, *33* (2). https://doi.org/10.1042/BSR20120115.

(3) Mayr, G. W. A Novel Metal-Dye Detection System Permits Picomolar-Range h.p.l.c. Analysis of Inositol Polyphosphates from Non-Radioactively Labelled Cell or Tissue Specimens. *Biochem. J.* **1988**, *254*, 585–591. https://doi.org/10.1042/bj2540585.

(4) Wilson, M. S. C.; Bulley, S. J.; Pisani, F.; Irvine, R. F.; Saiardi, A. A Novel Method for the Purification of Inositol Phosphates from Biological Samples Reveals That No Phytate Is Present in Human Plasma or Urine. *Open Biol.* **2015**, *5* (3), 150014. https://doi.org/10.1098/rsob.150014.

(5) Laussmann, T.; Eujen, R.; Weisshuhn, C. M.; Thiel, U. Structures of Diphospho-Myo-Inositol Pentakisphosphate and Bisdiphospho- Myo-Inositol Tetrakisphosphate from Dictyostelium Resolved by NMR Analysis. *Biochem. J.* **1996**, *315*, 715–720. https://doi.org/10.1080/00207549608905086.

(6) Laussmann, T.; Reddy, K. M.; Reddy, K. K.; Falck, J. R.; Vogel, G. Diphospho-Myo-Inositol Phosphates from Dictyostelium Identified as D-6-Diphospho-Myo-Inositol Pentakisphosphate and D-5,6-Bisdiphospho-Myo-Inositol Tetrakisphosphate. *Biochem. J.* **1997**, *322* (1), 31–33. https://doi.org/10.1042/bj3220031.

(7) Ijare, O. B.; Baskin, D. S.; Sharpe, M. A.; Pichumani, K. Metabolism of Fructose in B-Cells: A13C NMR Spectroscopy Based Stable Isotope Tracer Study. *Anal. Biochem.* **2018**, *552*, 110–117. https://doi.org/10.1016/j.ab.2018.04.003.

(8) Keshari, K. R.; Wilson, D. M.; Chen, A. P.; Bok, R.; Larson, P. E. Z.; Hu, S.; Van Criekinge, M.; Macdonald, J. M.; Vigneron, D. B.; Kurhanewicz, J. Hyperpolarized [2-13C]-Fructose: A Hemiketal DNP Substrate for in Vivo Metabolic Imaging. *J. Am. Chem. Soc.* **2009**, *131* (48), 17591–17596. https://doi.org/10.1021/ja9049355.

(9) Park, J. M.; Wu, M.; Datta, K.; Liu, S. C.; Castillo, A.; Lough, H.; Spielman, D. M.; Billingsley, K. L. Hyperpolarized Sodium [1-13C]-Glycerate as a Probe for Assessing Glycolysis in Vivo. *J. Am. Chem. Soc.* **2017**, *139* (19), 6629–6634. https://doi.org/10.1021/jacs.7b00708.

(10) Wundenberg, T.; Grabinski, N.; Lin, H.; Mayr, G. W. Discovery of InsP $_6$ -Kinases as InsP $_6$ -Dephosphorylating Enzymes Provides a New Mechanism of Cytosolic InsP $_6$ Degradation Driven by the Cellular ATP/ADP Ratio. *Biochem. J.* **2014**, *462* (1), 173–184. https://doi.org/10.1042/BJ20130992.

(11) Voglmaier, S. M.; Bembenek, M. E.; Kaplin, A. I.; Dormán, G.; Olszewski, J. D.; Prestwich, G. D.; Snyder, S. H. Purified Inositol Hexakisphosphate Kinase Is an ATP Synthase: Diphosphoinositol Pentakisphosphate as a High-Energy Phosphate Donor. *Proc. Natl. Acad. Sci. U. S. A.* **1996**, *93* (9), 4305–4310. https://doi.org/10.1073/pnas.93.9.4305.

(12) Padmanabhan, U.; Dollins, D. E.; Fridy, P. C.; York, J. D.; Downes, C. P. Characterization of a Selective Inhibitor of Inositol Hexakisphosphate Kinases. Use in Defining Biological Roles and Metabolic Relationships of Inositol Pyrophosphates. *J. Biol. Chem.* **2009**, *284* (16), 10571–10582. https://doi.org/10.1074/jbc.M900752200.

(13) Saiardi, A.; Azevedo, C.; Desfougères, Y.; Portela-Torres, P.; Wilson, M. S. C. Microbial Inositol Polyphosphate Metabolic Pathway as Drug Development Target. *Adv. Biol. Regul.* **2018**, *67*, 74–83. https://doi.org/10.1016/j.jbior.2017.09.007.

(14) Hothorn, M.; Neumann, H.; Lenherr, E. D.; Wehner, M.; Rybin, V.; Hassa, P. O.; Uttenweiler, A.; Reinhard, M.; Schmidt, A.; Seiler, J.; et al. Catalytic Core of Amembrane-Associated Eukaryotic Polyphosphate Polymerase. *Science (80-.).* **2009**, *324* (5926), 513–

516. https://doi.org/10.1126/science.1168120.
(15) Wilson, M. S.; Jessen, H. J.; Saiardi, A. The Inositol Hexakisphosphate Kinases IP6K1 and -2 Regulate Human Cellular Phosphate Homeostasis, Including XPR1-Mediated Phosphate Export. *J. Biol. Chem.* **2019**, jbc.RA119.007848. https://doi.org/10.1074/jbc.RA119.007848.
(16) Wild, R.; Gerasimaite, R.; Jung, J. Y.; Truffault, V.; Pavlovic, I.; Schmidt, A.; Saiardi, A.; Jacob Jessen, H.; Poirier, Y.; Hothorn, M.; et al. Control of Eukaryotic Phosphate Homeostasis by Inositol Polyphosphate Sensor Domains. *Science* **2016**, *352* (6288), 986–990. https://doi.org/10.1126/science.aad9858.
(17) Gerasimaite, R.; Pavlovic, I.; Capolicchio, S.; Hofer, A.; Schmidt, A.; Jessen, H. J.; Mayer, A. Inositol Pyrophosphate Specificity of the SPX-Dependent Polyphosphate Polymerase VTC. *ACS Chem. Biol.* **2017**, *12* (3), 648–653. https://doi.org/10.1021/acschembio.7b00026.
(18) Rubio, V.; Linhares, F.; Solano, R.; Martín, A. C.; Iglesias, J.; Leyva, A.; Paz-Ares, J. A Conserved MYB Transcription Factor Involved in Phosphate Starvation Signaling Both in Vascular Plants and in Unicellular Algae. *Genes Dev.* **2001**, *15* (16), 2122–2133. https://doi.org/10.1101/gad.204401.
(19) Puga, M. I.; Mateos, I.; Charukesi, R.; Wang, Z.; Franco-Zorrilla, J. M.; de Lorenzo, L.; Irigoyen, M. L.; Masiero, S.; Bustos, R.; Rodriguez, J.; et al. SPX1 Is a Phosphate-Dependent Inhibitor of PHOSPHATE STARVATION RESPONSE 1 in Arabidopsis. *Proc. Natl. Acad. Sci.* **2014**, *111* (41), 14947–14952. https://doi.org/10.1073/pnas.1404654111.
(20) Wang, Z.; Ruan, W.; Shi, J.; Zhang, L.; Xiang, D.; Yang, C.; Li, C.; Wu, Z.; Liu, Y.; Yu, Y.; et al. Rice SPX1 and SPX2 Inhibit Phosphate Starvation Responses through Interacting with PHR2 in a Phosphate-Dependent Manner. *Proc. Natl. Acad. Sci.* **2014**, *111* (41), 14953–14958. https://doi.org/10.1073/pnas.1404680111.
(21) Qi, W.; Manfield, I. W.; Muench, S. P.; Baker, A. AtSPX1 Affects the AtPHR1–DNA-Binding Equilibrium by Binding Monomeric AtPHR1 in Solution. *Biochem. J.* **2017**, *474* (21), 3675–3687. https://doi.org/10.1042/bcj20170522.
(22) Desai, M.; Rangarajan, P.; Donahue, J. L.; Williams, S. P.; Land, E. S.; Mandal, M. K.; Phillippy, B. Q.; Perera, I. Y.; Raboy, V.; Gillaspy, G. E. Two Inositol Hexakisphosphate Kinases Drive Inositol Pyrophosphate Synthesis in Plants. *Plant J.* **2014**, *80* (4), 642–653. https://doi.org/10.1111/tpj.12669.
(23) Laha, D.; Johnen, P.; Azevedo, C.; Dynowski, M.; Weiß, M.; Capolicchio, S.; Mao, H.; Iven, T.; Steenbergen, M.; Freyer, M.; et al. VIH2 Regulates the Synthesis of Inositol Pyrophosphate InsP 8 and Jasmonate-Dependent Defenses in Arabidopsis. *Plant Cell* **2015**, *27* (4), 1082–1097. https://doi.org/10.1105/tpc.114.135160.
(24) Mulugu, S.; Bai, W.; Fridy, P. C.; Bastidas, R. J.; Otto, J. C.; Dollins, D. E.; Haystead, T. A.; Ribeiro, A. A.; York, J. D. A Conserved Family of Enzymes That Phosphorylate Inositol Hexakisphosphate. *Science* **2007**, *316* (5821), 106–109. https://doi.org/10.1126/science.1139099.
(25) Zhu, J.; Lau, K.; Harmel, R. K.; Puschmann, R.; Broger, L.; Dutta, A. K.; Jessen, H. J.; Hothorn, L. A.; Fiedler, D.; Hothorn, M. Two Bifunctional Inositol Pyrophosphate Kinases/Phosphatases Control Plant Phosphate Homeostasis. *bioRxiv* **2018**, 467076. https://doi.org/10.1101/467076.
(26) Lonetti, A.; Szijgyarto, Z.; Bosch, D.; Loss, O.; Azevedo, C.; Saiardi, A. Identification of an Evolutionarily Conserved Family of Inorganic Polyphosphate Endopolyphosphatases. *J. Biol. Chem.* **2011**, *286* (37), 31966–31974. https://doi.org/10.1074/jbc.M111.266320.
(27) Gu, C.; Nguyen, H. N.; Hofer, A.; Jessen, H. J.; Dai, X.; Wang, H.; Shears, S. B. The Significance of the Bifunctional Kinase/Phosphatase Activities of Diphosphoinositol Pentakisphosphate Kinases (PPIP5Ks) for Coupling Inositol Pyrophosphate Cell Signaling to Cellular Phosphate Homeostasis. *J. Biol. Chem.* **2017**, *292* (11), 4544–4555. https://doi.org/10.1074/jbc.M116.765743.
(28) Albert, C.; Safrany, S. T.; Bembenek, M. E.; Reddy, K. M.; Reddy, K. K.; Falck, J. R.; Bröcker, M.; Shears, S. B.; Mayr, G. W. Biological Variability in the Structures of

Diphosphoinositol Polyphosphates in Dictyostelium Discoideum and Mammalian Cells. *Biochem. J.* **1997**, *327* (2), 553–560. https://doi.org/10.1042/bj3270553.

(29) Barker, C. J.; Wright, J.; Hughes, P. J.; Kirk, C. J.; Michell, R. H. Complex Changes in Cellular Inositol Phosphate Complement Accompany Transit through the Cell Cycle. *Biochem. J.* **2004**, *380* (Pt 2), 465–473. https://doi.org/10.1042/BJ20031872.

(30) Lin, H.; Fridy, P. C.; Ribeiro, A. A.; Choi, J. H.; Barma, D. K.; Vogel, G.; Falck, J. R.; Shears, S. B.; York, J. D.; Mayr, G. W. Structural Analysis and Detection of Biological Inositol Pyrophosphates Reveal That the Family of VIP/Diphosphoinositol Pentakisphosphate Kinases Are1/3-Kinases. *J. Biol. Chem.* **2009**, *284* (3), 1863–1872. https://doi.org/10.1074/jbc.M805686200.

(31) Gu, C.; Nguyen, H.-N.; Ganini, D.; Chen, Z.; Jessen, H. J.; Gu, Z.; Wang, H.; Shears, S. B. KO of 5-InsP 7 Kinase Activity Transforms the HCT116 Colon Cancer Cell Line into a Hypermetabolic, Growth-Inhibited Phenotype. *Proc. Natl. Acad. Sci. U. S. A.* **2017**, *114* (45), 11968–11973. https://doi.org/10.1073/pnas.1702370114.

(32) Wilson, M.; Saiardi, A. Inositol Phosphates Purification Using Titanium Dioxide Beads. *BIO-PROTOCOL* **2018**, *8* (15), e2959. https://doi.org/10.21769/BioProtoc.2959.

(33) Arner, R. J.; Prabhu, K. S.; Thompson, J. T.; Hildenbrandt, G. R.; Liken, A. D.; Reddy, C. C. Myo-Inositol Oxygenase: Molecular Cloning and Expression of a Unique Enzyme That Oxidizes Myo-Inositol and D-Chiro-Inositol. *Biochem. J.* **2001**, *360* (Pt 2), 313–320.

(34) Thomas, M. P.; Mills, S. J.; Potter, B. V. L. The “Other” Inositols and Their Phosphates: Synthesis, Biology, and Medicine (with Recent Advances in Myo-Inositol Chemistry). *Angew. Chemie - Int. Ed.* **2016**, *55* (5), 1614–1650. https://doi.org/10.1002/anie.201502227.

(35) Findeisen, M.; Brand, T.; Berger, S. A 1H-NMR Thermometer Suitable for Cryoprobes. *Magn. Reson. Chem.* **2007**, *45* (2), 175–178. https://doi.org/10.1002/mrc.1941.

(36) Azevedo, C.; Saiardi, A. Extraction and Analysis of Soluble Inositol Polyphosphates from Yeast. *Nat. Protoc.* **2006**, *1* (5), 2416–2422. https://doi.org/10.1038/nprot.2006.337.

(37) Clark, J.; Anderson, K. E.; Juvin, V.; Smith, T. S.; Karpe, F.; Wakelam, M. J. O.; Stephens, L. R.; Hawkins, P. T. Quantification of PtdInsP3 Molecular Species in Cells and Tissues by Mass Spectrometry. *Nat. Methods* **2011**, *8* (3), 267–272. https://doi.org/10.1038/nmeth.1564.

Chapter 4: Towards mass spectrometric analysis of inositol poly- and pyrophosphates

4.1 Introduction

NMR spectroscopy provides information on the structure, chemical environment and concentration of a given analyte. While the information obtained is quite comprehensive, NMR suffers from modest sensitivity, limiting its applicability to analyte concentrations that often far exceed those encountered in a biological or cellular setting. This limitation has been partially overcome by improvements in instrumentation (such as the adoption of CryoProbe^{TM}, where cryogenic cooling of the probe head reduces electronic noise) and methods like hyperpolarization.[1] The most common form of hyperpolarization is dynamic nuclear polarization (DNP) where the spin of unpaired electrons are transferred to nearby nuclei.[2] However, it is still not feasible to routinely detect low concentrations of InsP (in the range < 1 µM) samples by NMR.[3]

The method of choice for dilute samples is, due to its high sensitivity, liquid chromatography-coupled mass spectrometry (LCMS).[4] In conjunction with the elution time provided by the LC, MS characterizes the compounds by their mass. As two compounds can be isobaric (have the exact same weight, e.g. glucose and mannose), standards are necessary to verify the identity of the compound of interest. If this information is not sufficient, fragmentation can provide an additional layer of characterization. The most apparent limitation of MS is the lack of absolute quantification due to varying ionization efficiencies of different compounds. To overcome this limitation, an internal standard is required as a reference intensity.[5]

LC-MS is an integral part in metabolomics studies:[6–8] it can determine the relative concentrations of a given metabolite across different samples and detects compounds at low abundance (e.g. $[dATP]_{cell}$ = 0.97 µM; $[FAD]_{cell}$ = 5.6 µM in immortalized baby mouse kidney cells (iBMK)).[9] Various researchers have successfully applied MS for the quantification of $InsP_6$.[10–17] However, attempts have been limited by the physiochemical properties of $InsP_6$, specifically the inherent high negative charge density. This has resulted in the reliance on anion exchange chromatography during the LC separation step, introducing high

Table 4.1. Comparison of mass spectrometry based methods for the quantification of $InsP_6$.

Publication	Ionization mode [a]	LC method [b]	Salt concentration [c]	LOD [d]
Lee[15]	ESI negative	WAX	110 mM $(NH_4)_2CO_3$	3 pmol
Couso[14]	ESI negative	WAX	150 mM $(NH_4)_2CO_3$	16 pmol
McIntyre[16]	ESI negative	SAX	70 mM KOH	n.d. [e]
Duong[17]	ESI negative	SAX	110 mM $(NH_4)_2CO_3$	25 pmol
Rugova[13]	ICP	SAX	500 mM HNO_3	3 pmol
Sjöberg[10]	ESI negative	WAX	570 mM $(NH_4)_2CO_3$	1 pmol
Ito[11]	ESI negative	HILIC	294 mM $(NH_4)_2CO_3$	5 pmol
Harmel[21]	NMR	n.a. [f]	n.a.	> 60 pmol

[a] ESI negative: electron spray ionization negative ion mode; ICP: inductively coupled plasma
[b] WAX: weak anion exchange; SAX: strong anion exchange; HILIC: hydrophilic interaction.
[c] The highest salt concentration that is injected into the ionization source during the method.
[d] Limit of detection of $InsP_6$
[e] not determined
[f] not applicable

amounts of salt into the ionization source (Table 4.1). All published methods to date are also based on negative ion mode electron spray ionization (ESI negative). This ESI mode is generally considered to produce a less stable spray than its positive counterpart, reducing its applicability.[18,19] Nevertheless, the limit of detection (LOD) achieved by the published methods lies in the range of 1 to 25 pmol, exceeding the sensitivity of NMR spectroscopy

Phosphatidylinositol phosphates also bear multiple phosphoryl groups and have been challenging to detect by LC-MS. Clark and coworkers developed a

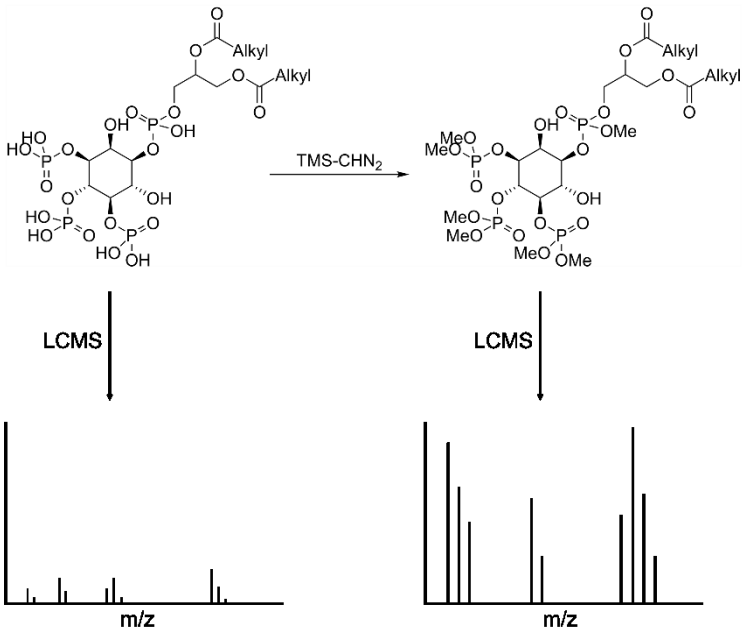

Figure 4.1. Derivatization of Phosphatidylinositol phosphates with TMS-CHN_2 to facilitate MS analysis.

derivatization-based strategy in order to mask the negative charge and improve the ionization efficiency of these species. To do so, trimethylsilyl diazomethane (TMS-CHN_2) was used to methylate phosphatidylinositol phosphates (Figure 4.1).[20] This derivatization improved the sensitivity and allowed for the reproducible quantification of different PtdInsP species in cells.[20]

Here, I aim to develop an InsP and PP-InsP derivatization method that facilitates detection and quantification of biologically relevant sub-picomole amounts of these compounds. This is achieved by elimination of negative charge which impedes efficient ionization. In addition, the derivatization would allow the separation of these less hydrophilic methylated compounds *via* a standard reverse phase method, reducing the burden on the mass spectrometer commonly experienced with the high salt concentrations required for anion exchange LC separation (compare Table 4.1).

4.2 Trimethylsilyldiazomethane methylates inositol hexakisphosphate

Diazomethane (CH_2N_2) is a good methylating agent and has been used extensively for the methylation of carboxylic acids, acidic hydroxyl groups and thiols. The benefits of this reagent are the reaction speed (the reaction occurs within seconds), mild reaction conditions, the absence of non-volatile byproducts, and the ease of the workup.[22] However, major drawbacks of CH_2N_2 are its carcinogenic nature and its propensity of explode unaccountably.[23,24]

Trimethylsilyldiazomethane (TMS-CHN_2) is a stabilized version of diazomethane (CH_2N_2) that must be activated before substrate methylation can occur. Activation proceeds *via* protonation of TMS-CHN_2 followed by TMS deprotection by methanol, generating CH_2N_2 *in situ* (Figure 4.2). The diazomethane is then protonated by the acid, generating an electrophilic center and allowing the formation of the methyl ester.[25,26] Desilylation is critical to ensure high yields with minimal side products.[25] An efficient desilylation step and a protonated substrate are key requirements for the optimization of InsP methylation.

A significant chemical difference between InsPs and PtdInsPs is the large lipophilic tail of PtdInsPs so that the derivatization can be conducted is a mixture of chloroform and methanol, despite the hydrophilic headgroups.[20] InsPs and PP-InsPs, however, are not soluble under these conditions. As a first step, I therefore screened different solvents for the methylation of $InsP_6$ a readily available proxy of PP-InsPs (Figure 4.3a). Both neat MeOH and 4:1 EtOH:MeOH produced the

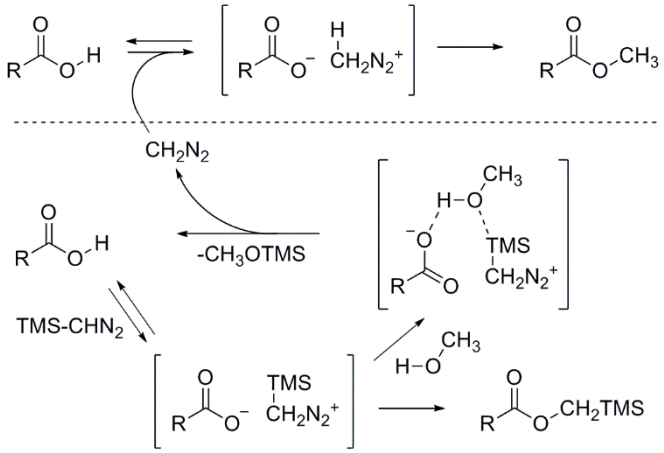

Figure 4.2. Proposed mechanism for the methyl esterification of carboxylic acids. Replicated from Kühnel *et al*.[25]

highest conversion, as measured by an internal standard, and it was decided to continue with MeOH, as it was a less complex system to go forward. The activation of TMS-CHN2 requires a protonated substrate (Figure 4.2).[25] Moreover, the protonation of $InsP_6$ further increases the solubility of InsPs in organic solvents by reducing the ionic character of the compound. Therefore, the acid concentration was optimized and the highest yields were achieved with > 5 mM HCl (Figure 4.3b). After the initial reaction conditions were determined, the limit of detection and linear detection range for the mass spectrometer had to be established. During testing it was found that the signal intensity of dilution series of $InsP_6$ plateaued below a certain concentration. However, this pattern was not detectable if a methylated sample was diluted after derivatization (Figure 4.4a). A possible explanation for this behavior is that free $InsP_6$ undergoes aggregation under these solvent conditions. The aggregates could releases free, methylation-accessible $InsP_6$ in a concentration dependent manner upon dilution. Due to the high propensity of $InsP_6$ to form metal complexes, metal chelators (EDTA and [2.2.2]cryptant) were added to the methylation reaction (Figure 4.4b). Although a small improvement was observed, the problem remained. The addition of the chaotrope urea to the reaction appeared to alleviate the issue to a certain degree but the high concentration of urea rendered this approach impractical (Figure 4.4c). Saiardi and coworkers have established TiO_2-enrichment as a practical method to enrich and purify InsPs from complex mixtures.[27] Indeed, TiO_2-enrichment of the sample before derivatization eliminated the plateau trend and demonstrated that the linear range spans at least five orders of magnitude,

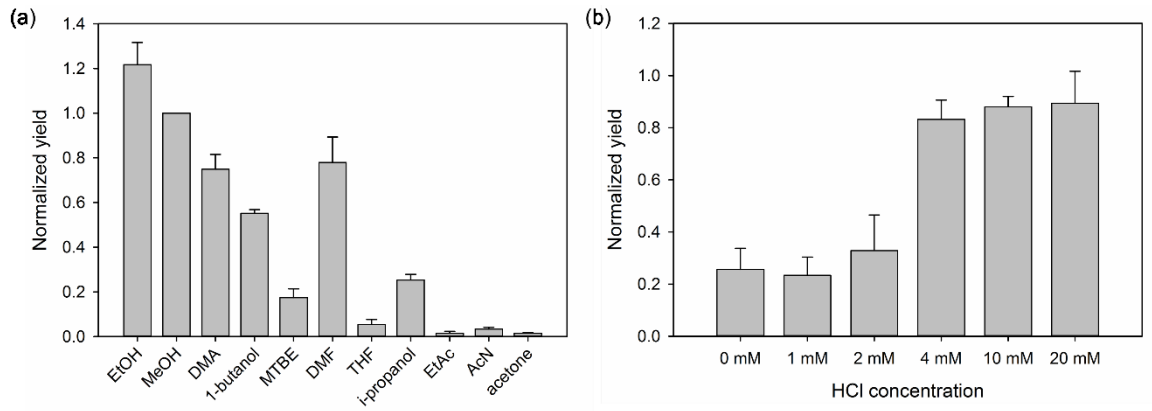

Figure 4.3. Solvent screen for the methylation of $InsP_6$ by TMS-CHN_2. (a) The reactions contained 10 mM HCl, 1 mM EDTA and [$^{13}C_6$]$InsP_6Me_{12}$ as an internal standard in the indicated solvents plus 20 % MeOH. (b) The HCl concentration in the reaction was varied as indicated.

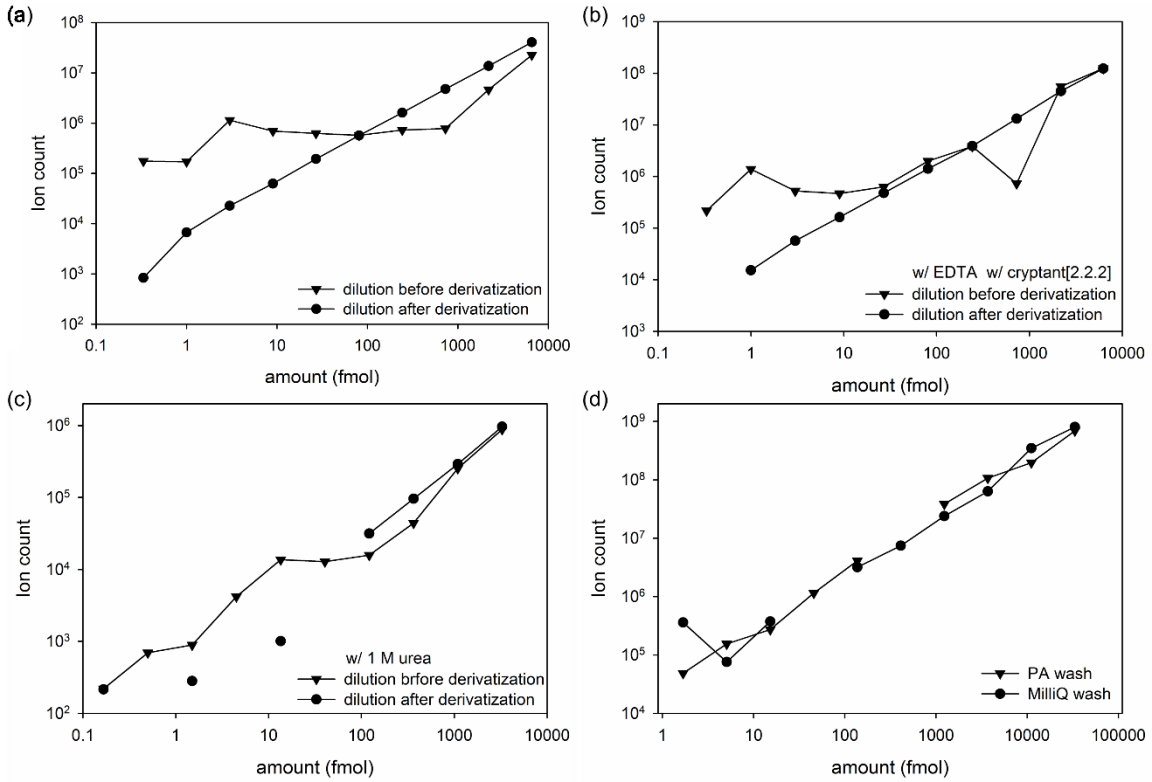

Figure 4.4. Non-linear response during dilution. (a) a sample containing InsP6 and 10 mM HCl in MeOH was diluted either before (triangle) or after (circle) derivatization. (b) The reactions additionally contained 1 mM EDTA and 1 mM [2.2.2]cryptant. (c) The reactions contained additionally 1 M urea. (d) 10 nmol $InsP_6$ was enriched with TiO2 beads and washed either with 1 M perchloric acid (PA) or milli-Q water. The enriched sample was treated as in (a).

providing exceptional sensitivity to levels of <10 fmol (Figure 4.4d). It appears that $InsP_6$ was contaminated with some impurity that promoted aggregation, and this impurity was removed by the TiO_2-enrichment.

To better assess the limit of detection (LOD, signal-to-noise ratio of > 3) and the linear range for the detection of $InsP_6Me_{12}$ (**11**), this species was synthesized in order to determine the LOD independently of the derivatization efficacy. The synthesis of **11** involved phosphitylation-oxidation of *myo*-inositol with *N*,*N*-diethyl-dimethyl phosphoamidite (**S09**). A stock-solution of **11** was then prepared from which a dilution series spanning over six orders of magnitude from 0.1 nM to 554 µM was set up. The samples were run on a LC-MS and the lowest detectable concentration amounted to 8 fmol (Figure 4.5). For quantification purposes, a more stringent signal-to-noise ratio of > 10 is employed. This more stringent data analysis resulted in the same limit of quantification (LOQ) of 8 fmol. The inter-run variability is low (0.5 %), even at the LOQ, and it diminishes at higher concentrations to < 0.05 %. These results highlight the potential of the method for

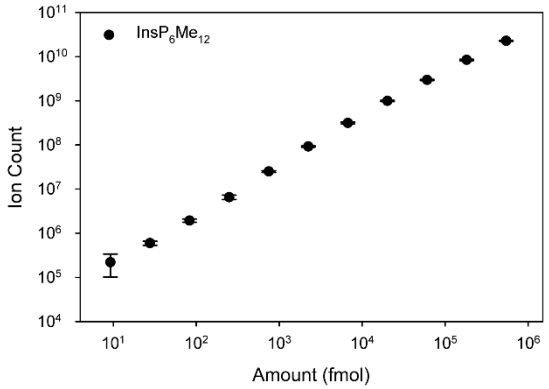

Figure 4.5. Limit of detection for $InsP_6Me_{12}$. The concentration of the $InsP_6Me_{12}$ solution was determined by NMR to be 544.3 µM (against PMe_4Br as internal standard). A triplicates of a dilution series were prepared and each sample was measured three times as technical triplicates. The data is shown as mean ± SD.

the sensitive quantification of $InsP_6$ and InsPs in general. The LOD of the synthetically prepared **11** correspondents well with the lowest detectable signal of derivatized $InsP_6$ (Figure 4.4), indicating that reaction proceeds to full or close to full conversion.

The association of $InsP_6$ and $InsP_6Me_{12}$ with various metals during derivatization, chromatography, and ionization was a concern that was further investigated. Instead of targeted selected ion monitoring (tSIM) of the $[InsP_6Me_{12}+H]^+$ ion, a full range mass spectrum was recorded to quantify different potential adducts that could diminish the signal intensity. The different ion adducts (most prominently $+Na^+$, $+NH_4^+$, and $+1/2\ Ca^{2+}$) together accounted for only 10 % of the signal, making them irrelevant in terms of overall sensitivity (Figure 4.6).

In summary, the derivatization of $InsP_6$ was successfully established as a proof of principle, encouraging its application to PP-InsPs derivatization.

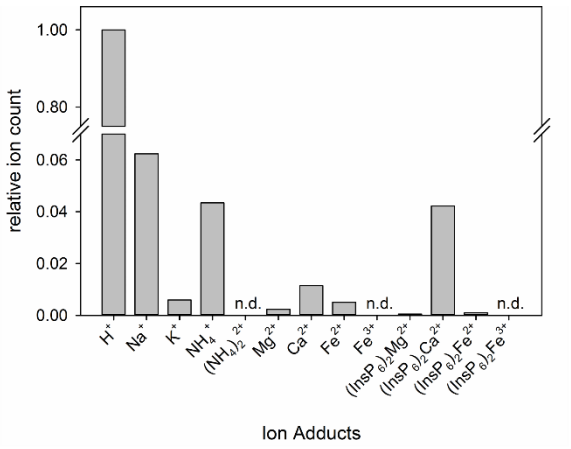

Figure 4.6. Different ion adducts of $InsP_6Me_{12}$. A full-MS measurement was conducted and the peaks corresponding to the different ion adducts were quantified.

4.3 Method optimization for the methylation of $InsP_7$

After the establishment of standard conditions for the derivatization of $InsP_6$, I re-tested these conditions for the derivatization of 5PP-$InsP_5$. This reevaluation was necessary as this species contains a labile phosphoanhydride bond that may be incompatible with the $InsP_6$ conditions. Indeed, upon methylation of 5PP-$InsP_5$, a peak corresponding to $InsP_6Me_{12}$ was observed that showed higher ion counts than the peak corresponding to the fully per-methylated 5PP-$InsP_5Me_{13}$ (**12**). This observation indicated that degradation of 5PP-$InsP_5$ was occurring under these reaction conditions. Variations in reaction time, HCl concentration, solvent, and acid composition did not lead to improvement (Figure 4.7). In order to develop strategies to reduce the degradation, an understanding of the mechanism is required. There are three stages of the workflow during which the degradation could occur: the methylation reaction itself, the acid quench of the remaining diazomethane, and liquid chromatography preceding the MS analysis. During LC, the acidic, aqueous conditions could lead to hydrolysis of the phosphoanhydride bond, generating $InsP_6Me_{11}$ (**13**) and $(MeO)_2OPOH$ (Figure 4.8 green and red arrow). Shortening of the LC gradient led to no change in ion counts, indicating that the LC was not the source of the degradation. During methylation and acidic quench, both hydrolysis and methanolysis could occur. However, quenched samples were stable over several days, suggesting that the methylation reaction itself was problematic.

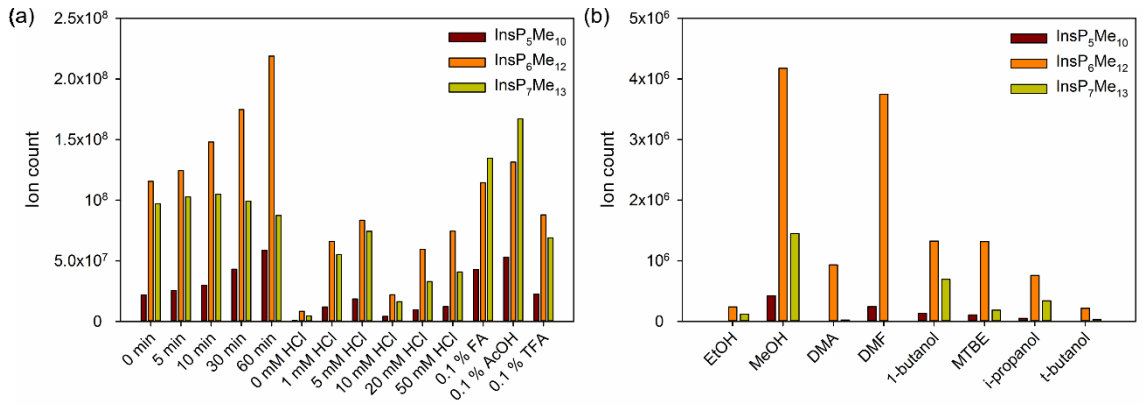

Figure 4.7. 5PP-$InsP_5$ methylation conditions. 1 µM 5PP-$InsP_5$ was methylated under the indicated conditions in MeOH (the reaction was quenched after the indicated time points) and the ion counts of the derivatization products are displayed.

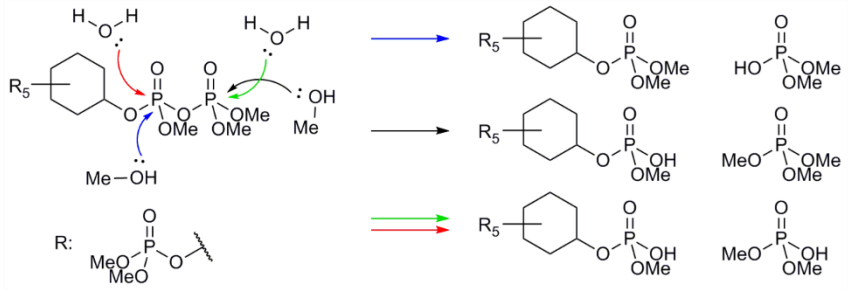

Figure 4.8. Potential mechanisms of hydrolysis of 5PP-InsP$_5$ during methylation with TMS-CHN$_2$.

Table 4.2. Quantification of 5PP-InsP$_5$ methanolysis products.

Solvent	$(MeO)_2OPOH$	$(MeO)_3OP(d_3)$	$(MeO)_3OP$	$InsP_6Me_{12}(d_3)$	$InsP_6Me_{12}$	$InsP_7Me_{13}$
MeOH-d_3	0.86	0.02	0.13	0.14	0.33	0.19
MeOH	0.81	0.00	0.19	0.00	0.45	0.33

In order to quantify the contribution of methanolysis and hydrolysis to the degradation of **7**, I performed the reaction in MeOH-d_3 and regular MeOH, making it possible to track potential methanolysis products by a mass shift of +3 m/z and distinguish these products from a TMS-CHN$_2$ methyl group (Figure 4.8 blue and black arrows, Table 4.2). Based on the relative signal intensities, a third of **11** is the product of methanolysis, while the other two thirds are due to hydrolysis of **7** followed by methylation.

To stabilize the phosphoanhydride bond, I hypothesized that increasing the electron density at the phosphorus would reduce its electrophilicity and therefore increase its stability towards hydrolysis or methanolysis. To this end, diazo ethane (**14**) and diazo propane (**15**) were synthesized and subsequently applied in alkylation reactions of 5PP-InsP$_5$ (Figure 4.9). However, the extent of degradation remained constant in both cases.

An alternative approach was to exploit the methanolysis reaction by using MeOH-d_3 as a solvent thus introducing a mass shift in 5PP-InsP$_5$ derived InsP$_6$Me$_{12}$. For this approach to be useful, the proportion of methanolysis had to be increased and the hydrolysis decreased. Different acids were screened for their ability to promote methanolysis (Figure 4.10). Reactions performed in the presence of toluenesulfonic acid and perchloric acid displayed the highest amount of InsP$_6$Me$_{12}$, but generated significant amounts of InsP$_5$Me$_{10}$ and InsP$_6$Me$_{11}$ as well, thereby invalidating this approach of forced methanolysis.

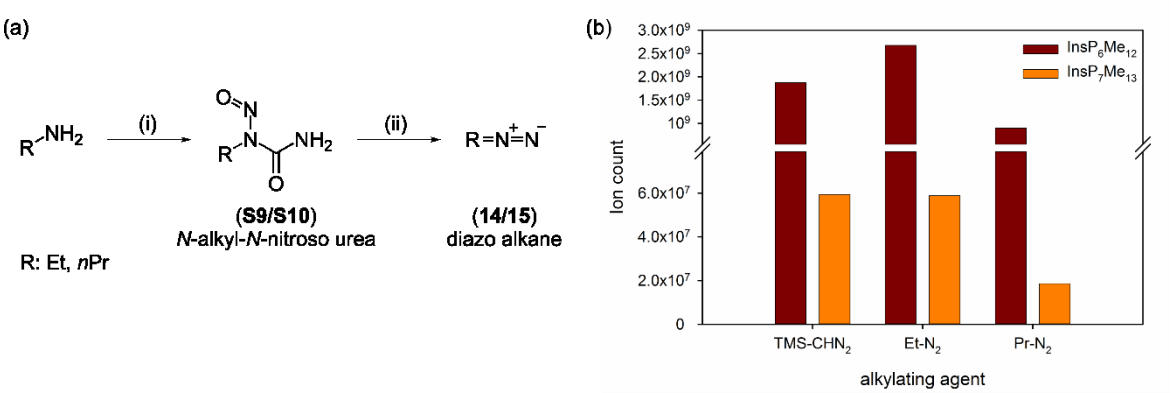

Figure 4.9. Diazoethane and diazopropane do not reduce hydrolysis of 5PP-InsP$_5$. (a) (i) HCl, urea, $NaNO_2$, H_2SO_4, H_2O, 5 h, 0 °C → reflux → 0 °C. (ii) 40 % (w/v) KOH (aq), Et_2O, 30 min, 0 °C. (b) The alkylation was performed with 10 mM HCl in MeOH.

In a complementary strategy, I tried to stabilize the phosphoanhydride bond by buffering the reaction. Use of Bis-(2-hydroxyethyl)-amino-tris(hydroxymethyl)-methane (BisTris) showed promising results and yielded for the first time 5PP-InsP$_5$Me$_{13}$ levels that were higher than InsP$_6$Me$_{12}$ (Figure 4.11). This result was surprising as the methylation mechanism by TMS-CHN$_2$ requires a protonated substrate, which should not be the case in the presence of BisTris. It remains unclear why this condition worked so well.

During the course of the experiments, I noticed varying results based on the production-lot of TMS-CHN$_2$ (purchased as a 2 M solution in diethyl ether from Sigma Aldrich). To systematically test the influence of the reagent on the quality of the methylation reaction, different TMS-CHN$_2$ solutions (in various solvents and

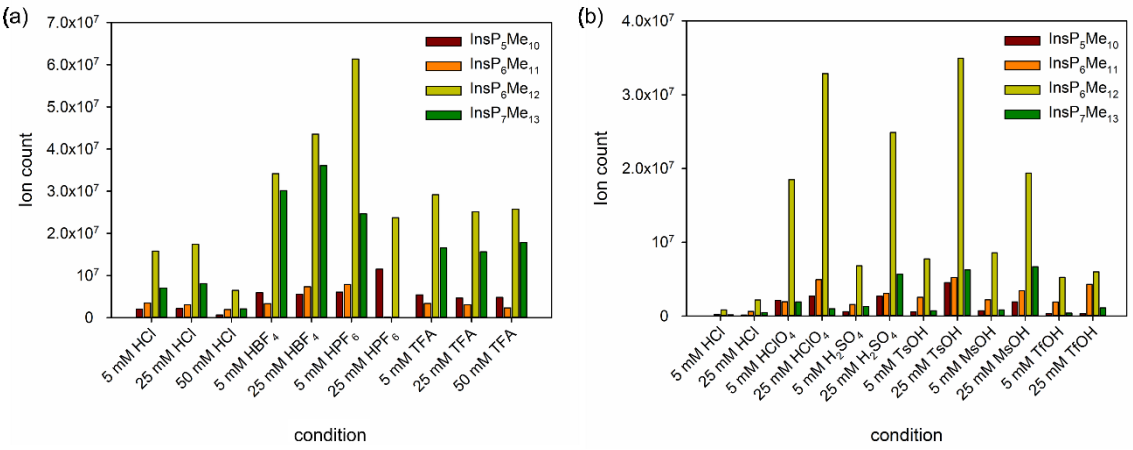

Figure 4.10. Maximizing 5PP-InsP$_5$ methanolysis. 1 µM 5PP-InsP$_5$ was methylated with TMS-CHN$_2$ under the indicated conditions in MeOH and the ion counts of the derivatization products are displayed.

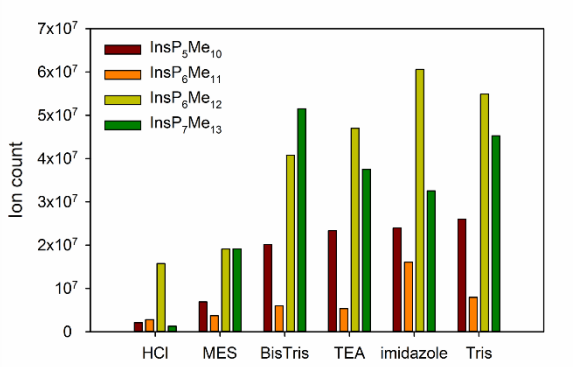

Figure 4.11. Methylation of 5PP-InsP$_5$ under buffered conditions. 2 µM 5PP-InsP$_5$ was methylated with TMS-CHN$_2$ in the presence of 10 mM of the indicated buffers.

from distinct commercial sources) were tested (Figure 4.12). The proportion of **13** remained constant across all reagents but the achievable signal intensity varied greatly, with the TMS-CHN$_2$ in diethyl ether from Sigma Aldrich giving the best result. The large variability of the results indicated to us that contaminants in the reagent might be responsible for the low yielding methylation reactions. The same impurities might play a role in promoting the hydrolysis of **7**, as well.

To test this hypothesis, I prepared diazomethane (**16**) as a solution in diethyl ether from *N*-Methyl-*N*-nitroso-*p*-toluenesulfonamide (**S11**) and purified it by distillation (Figure 4.13a). Compared to TMS-CHN$_2$, methylation of a HCT116 cell extract with **16** displayed a higher overall signal intensity. Furthermore, the standard deviation for the triplicates was constantly smaller for the diazomethane samples (Figure 4.13b), indicating the reaction was more consistent. This result highlights the potential of clean **16** for the derivatization of PP-InsPs.

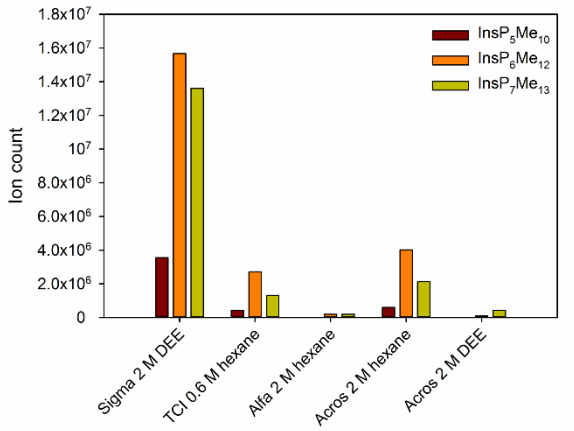

Figure 4.12. Differing quality of TMS-CHN$_2$ sources. TMS-CHN$_2$ from different vendors (Sigma Aldrich, TCI, Alfa Aesar, Acros Organics) in different solvents was tested. 1 µM 5PP-InsP$_5$ was methylated in 10 mM HCl in MeOH.

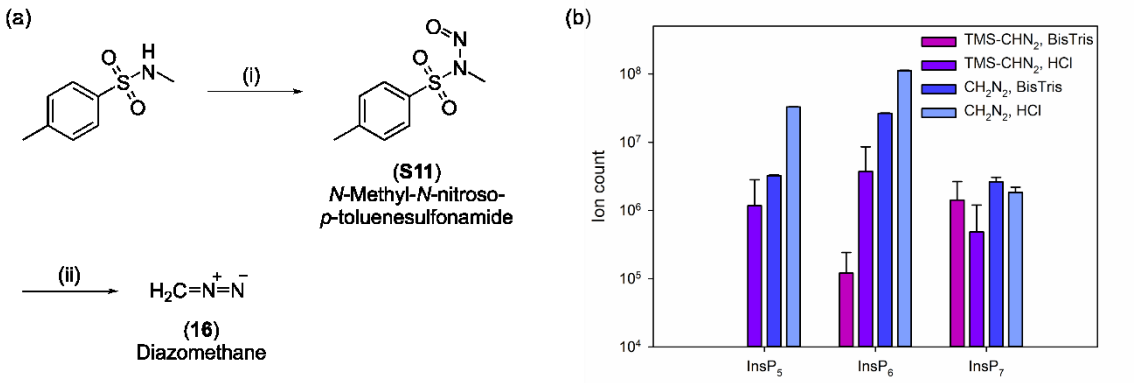

Figure 4.13. Diazomethane methylates inositol pyrophosphates. (a) Synthesis of diazomethane (i) $NaNO_2$, AcOH, H_2O, 20 min, 0 °C. (ii) KOH, EtOH, Et_2O, 20 min, 65 °C. (b) The TiO_2 enriched cell extract of [$^{13}C_6$]*myo*-inositol labeled yeast (25 ODs) was methylated using TMS-CHN_2 or CH_2N_2 in MeOH with either 10 mM BisTris or 10 mM HCl. The samples were measured as technical triplicates.

Another explanation for the relatively high signal intensity of 5PP-InsP_5 degradation products in the MS measurements could be a difference in ionization efficiency between the compounds. Therefore, equal amounts of non-hydrolysable PP-InsP bisphosphonate-analogs (5PCP-InsP_5, and 1,5(PCP)$_2$-InsP_4, a kind gift from Sarah Hostachy and Katy Franke) were derivatized, their detectable ion count quantified, and compared it to InsP_6Me$_{12}$ (Figure 4.14). Surprisingly, the ionization efficiency dropped drastically to 27.9 % and 8.7 %, respectively, adding another level of difficulty in addition to the degradation of PP-InsPs during the methylation.

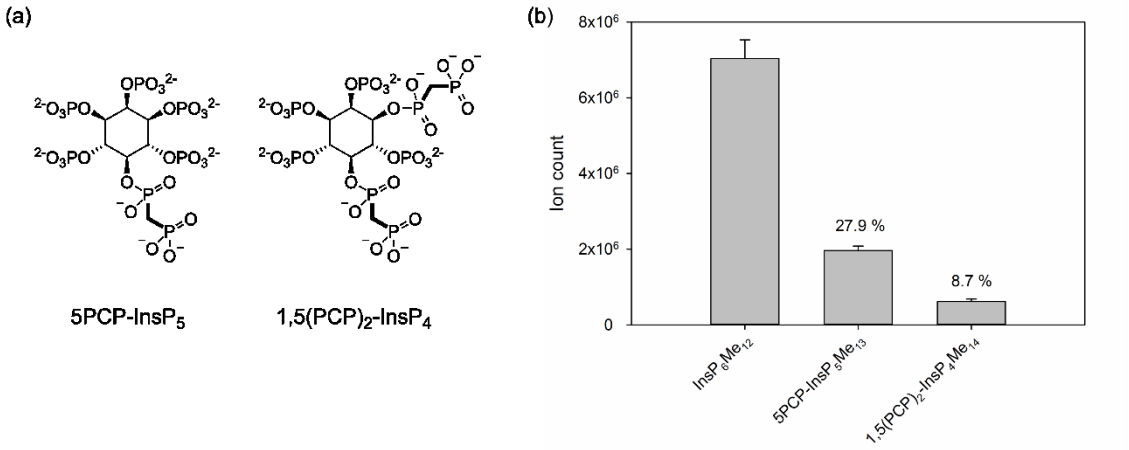

Figure 4.14. Ionization efficiency differs for PP-InsPs. (a) Structures of 5PCP-InsP_5 and 1,5(PCP)$_2$-InsP_4. (b) 1 µM InsP6, 5PCP-InsP_5, and 1,5(PCP)$_2$-InsP_4 were methylated with TMS-CHN_2 and the ion count is displayed.

4.4 Application of the derivatization strategy to biological samples

Although the initial results for the methylation of $InsP_6$ and 5PP-$InsP_5$ did not lead yet to a usable method, they were promising enough motivate me to measure InsP levels in biological samples. As a first approach, several *S. cerevisiae* strains with genetic knock outs of InsP-metabolizing genes were tested (genes listed in Figure 1.1 and Table 4.3). Overnight cultures were extracted using perchloric acid and the PP-InsPs were enriched over TiO_2 beads. The samples were methylated with TMS-CHN_2 and the derivatized samples measured by LCMS.

To our delight, the results mirrored the literature description of the respective knock out strains: Yeast lacking IPK1 (ipk1Δ) and unable to generate $InsP_6$, showed an increase in the precursor $InsP_5$ and a marked decrease in $InsP_6$.[28] A KCS1 (the yeast IP6K homolog) knockout strain (kcs1Δ) retained wildtype-like levels of $InsP_5$ and $InsP_6$ while displaying reduced levels of $InsP_7$.[29] Finally, strains with knockouts of VIP1 (vip1Δ), and SIW14 (vip1Δsiw14Δ) accumulate 5PP-$InsP_5$ due to their inability to further metabolize this compound and, indeed, the strains exhibited increased $InsP_7$ levels compared to wildtype (Figure 4.15a).[30] While the detectable changes were not as drastic as described in the literature, these results nevertheless highlight the potential of a derivatization based LC-MS method to analyze InsP and PP-InsP levels in cellular samples.[28–30] To show the applicability of this method in profiling the InsP content of more complex organisms, whole *C. elegans* and mammalian HEK293T cells were subjected to the same workflow and the samples measured (Figure 4.15b). $InsP_5$, $InsP_6$ and $InsP_7$ could be detected and to our knowledge this is the first demonstration that *C. elegans* contains PP-InsPs.

Table 4.3. Effect of genetic knockouts on cellular PP-InsP levels

Genotype		Effect on		
Yeast	Human	$InsP_6$	$InsP_7$ [a)]	$InsP_8$
ipk1Δ	IPK1	n.d. [b)]	n.d.	n.d.
kcs1Δ	IP6K	Unchanged	n.d. [c)]	n.d.
vip1Δ	PPIP5K	Unchanged	Increased	n.d.
siw14Δ vip1Δ		Unchanged	Increased	n.d.

[a)] combined levels of 1PP-$InsP_5$ and 5PP-$InsP_5$.
[b)] not detectable.
[c)] small amounts of 1PP-$InsP_5$ remain that are usually not detectable.

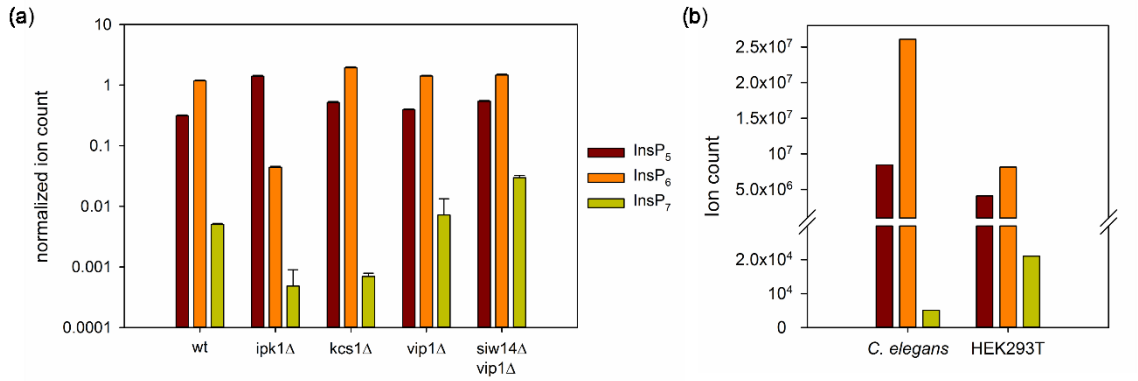

Figure 4.15. Methylation of various cellular extracts. (a) 25 ODs of cells were taken from overnight cultures. The InsPs were extracted and enriched over TiO_2. The enriched samples were methylated with TMS-CHN_2 and measured on a Q-Exactive. (b) C. elegans wt worms (50 µl) were lysed with glass beads in 1 M perchloric acid and the extract was treated as in a. HEK293T cells were trypsinized (PCV: 25 µl) and lysed in 1 M perchloric acid and the extract was treated as in (a).

Although yeast contains similar amounts of $InsP_7$ and $InsP_8$, no $InsP_8$ could be detected in any of the cellular samples. In light of the $InsP_7$ degradation during methylation and the differences in ionization efficacy, this is not surprising, as the $InsP_7$ signals were already only barely above the background (see Chapter 4.3). To establish whether cellular $InsP_8$ was detectable, I methylated a PP-InsP extract from *D. discoideum*, a slime mold with the highest reported PP-InsP concentration in an organism (up to 180 µM).[31] In this extract, both $InsP_7$ and $InsP_8$ were observed, confirming that $InsP_8$ is technically detectable provided the concentration is high enough (Figure 4.16).

After these proof of principle experiments, I measured the incorporation kinetics of [$^{13}C_6$]*myo*-inositol in growing yeast. This knowledge is important in the context

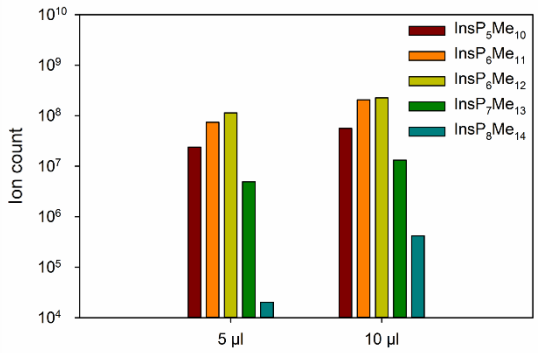

Figure 4.16. Detection of $InsP_8$ in *D. discoideum*. The indicated volume of an extract from *D. discoideum* (a kind gift from Adolfo Saiardi) was methylated with TMS-CHN_2 and analyzed by LC-MS.

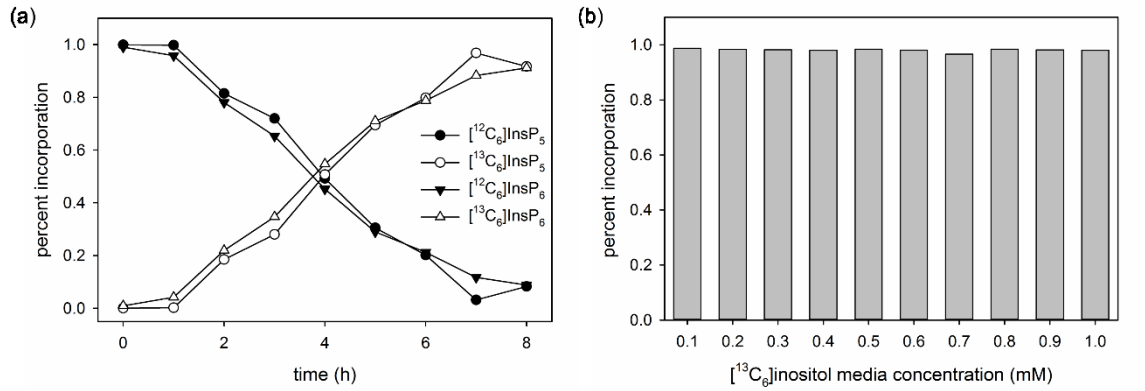

Figure 4.17. [$^{13}C_6$]*myo*-inositol incorporation in yeast. (a) Yeast was inoculated into SD medium supplemented with 475 µM [$^{13}C_6$]*myo*-inositol at OD 0.1 and grown at 30 °C. Every hour the optical density was measured and 5 ODs of cells were collected. The cells were lysed with bead beating in 1 M perchloric acid and the extract was enriched over TiO_2 beads. The samples were methylated with TMS-CHN_2 and measured on a Q-Exactive. (b) Yeast was inoculated at OD 0.1 into SD medium supplemented with varying concentrations of [$^{13}C_6$]*myo*-inositol and grown overnight. The samples were prepared as in (a).

of metabolic labeling of cells with [$^{13}C_6$]*myo*-inositol for NMR measurements (see Chapter three). By directly monitoring the incorporation into $InsP_6$ via LC-MS, we would be able to optimize labeling time and [$^{13}C_6$]*myo*-inositol concentration. For this experiment, wildtype yeast was grown in SD medium, supplemented with 475 µM [$^{13}C_6$]*myo*-inositol, and samples taken every hour. The rate of [$^{13}C_6$]$InsP_5$ and [$^{13}C_6$]$InsP_6$ increase was the same as the rate of [$^{12}C_6$]$InsP_5$ and [$^{12}C_6$]$InsP_6$ decrease and matched the growth rate of yeast, indicating that under these conditions yeast does not synthesize *myo*-inositol *de novo* (Figure 4.17a). In order to establish the required amount of [$^{13}C_6$]myo-inositol in the medium to prevent the *de novo* synthesis, different concentrations were tested (100 µM - 1000 µM). Even at 100 µM [$^{13}C_6$]*myo*-inositol *de novo* synthesis was not observed (Figure 4.17b).

4.5 Outlook

The presented work highlights the potential of a derivatization-based MS approach to measure and quantify InsPs and PP-InsPs at biologically relevant concentrations. The derivatization reaction appears to be high yielding and the mass spectrometry sensitivity is outstanding, especially when compared to existing methods (compare Table 4.1). It is promising that biological samples can be analyzed with this approach.

The envisioned method worked well for $InsP_6$ with minimal methodology refinement. With further optimization, this method holds great potential for the analysis of $InsP_6$ and lower inositol phosphates. Access to ^{13}C-labeled $InsP_5$ and $InsP_6$ would allow the incorporation of these compounds as internal standards in order to measure endogenous InsPs quantitatively.

The method is in principle also suitable for the analysis of metabolic fluxes. Currently, it is poorly understood how the interconversion of InsPs proceeds and the mechanisms by which these processes are regulated. The highly sensitive detection of small amounts of analytes enables the pursuit of pulse-chase-type experiments with ^{13}C-labeled *myo*-inositol or ^{18}O-labeled phosphate to dissect the underlying regulatory mechanisms. The introduction of an internal standard will facilitate the quantitation of endogenous levels of InsPs in different tissues and under various conditions to test the standing paradigms that the InsP pool is rather static. The high sensitivity and the resulting low requirement for sample amounts will allow for the quantification of InsPs and PP-InsPs in various organelles. Especially PP-InsP levels in the nucleus will be informative as GO-term analyses of PP-InsP interacting proteins contained nuclear processes (e.g., nucleolus and RNA pol I/III complex).[32] Efforts towards these aims are ongoing.

While the method optimization for the InsPs appears to be straight-forward, this cannot be said about the PP-InsPs. Detection of these compounds suffers two major drawbacks. On the one hand, the compounds are partially degraded during the methylation, while on the other hand, the ionization efficiency drops drastically with increasing numbers of pyrophosphate groups. Both processes especially hamper the detection of $InsP_8$. At the moment, the avenue to an effective derivatization and detection method remains questionable. Forcing the hydrolysis of the phosphoanhydride bond in order to label the PP-InsPs with Me-d_3 groups is

not promising as there appear to be several competing degradation pathway. A more promising approach might be the use of generator-produced and distilled diazomethane, as this gave the highest levels of 5PP-InsP_5Me_{13} during the screening of conditions. Further reaction optimization might prove this avenue viable.

If the PP-InsP degradation cannot be avoided after all, another possible strategy could be to quantify the amount of degradation in each sample based on an internal ^{13}C-labeled standard in order to back-calculate the original PP-InsP concentrations in the sample.

4.6 Methods

General Information

All chemicals were purchased from Sigma Aldrich, VWR, Carl Roth, Thermo Fisher Scientific, Alfa Aesar, TCI and used without further purification unless stated otherwise. Deuterated solvents were purchased from Euriso-Top. Telos® was ordered from Kinesis. Normal phase flash chromatography was performed using analytical grade solvents and silica gel from VWR (40-63 µm) as stationary phase. Automated flash chromatography was performed using gradient grade solvents on a CombiFlash® Rf from Teledyne Isco using prepacked CombiFlash® columns (40-63 µm). LC-MS analysis was carried out with an Agilent 1260 Infinity Binary LC system connected to an Agilent 6130 Quadrupole LC/MS system with a ZORBAX Rapid Resolution HT Narrow Bore SB-C18 1.8 µm column (2.1 x 50mm) at 30 °C using API-ESI (atmospheric pressure ionization-electrospray) in positive ion mode. The eluent consisted of 10% ACN in water with 0.1% formic acid at 0.7 mL/min flow rate.

NMR spectra were recorded on Bruker spectrometers operating at 300 or 600 MHz for proton nuclei, 75 or 151 MHz for carbon nuclei or 122 and 244 MHz for phosphorous nuclei. NMR data are given as follows: chemical shift δ in ppm (multiplicity, coupling constant(s) J Hz, relative integral) where multiplicity is defined as: s = singlet, d = doublet, t = triplet, q = quartet, m = multiplet, br = broad or combinations of the above. The software used to control the spectrometer was topspin 3.5 pl6. Temperature had been calibrated using d_4-methanol and the formula of Findeisen et al.[33]

High-resolution mass spectrometer was performed by direct inject on an Orbitrap™ Q-Exactive mass spectrometer (Thermo Fisher Scientific). The derivatized samples were analyzed with an Unltimate 3000 UHPLC system connected to an Orbitrap™ Q-Exactive with a Agilent poroshell EC-C18 2.7 µm column (4.6 x 150 mm) in positive ion mode at a resolution of 70,000. The eluent consisted of ACN in water with 0.1 % formic acid at 0.15 ml/min flow rate.

Synthesis

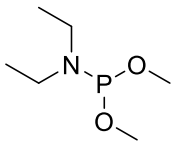

Dimethyl *N,N*-Diethylphosphoramidite (S09)

Dimethyl *N,N*-Diethylphosphoramidite was synthesized according to a procedure from Johns and colleagues.[34]

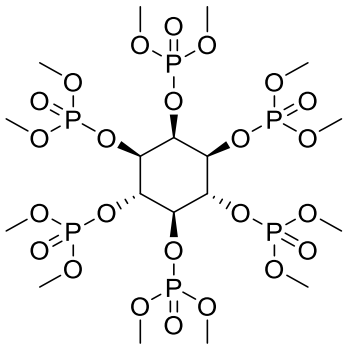

Dodecamethyl inositolhexakisphopshate, $InsP_6Me_{12}$ (11)

The compound was synthesized based on a method by Podeschwa and coworkers.[35] **S09** (962 mg, 5,83 mmol) was added to a suspension of *myo*-inositol (150 mg, 0,83 mmol) and 1H-tetrazole (700 mg, 9,99 mmol) in anhydrous Dichloromethane (60 ml) and the solution was stirred overnight at room temperature. For work up the solution was cooled to -40 °C and an anhydrous solution of *m*CPBA (4307 mg, 17,19 mmol) in DCM (45 ml, dried with Na_2SO_4) was added. The solution was allowed to warm to room temperature, and the stirring was continued for another hour. The reaction mixture was diluted with DCM (150 ml) and washed consecutively with aqueous Sodium bisulfite (20 %, 100 ml, twice) and saturated $NaHCO_3$ (three times, 100 ml). After evaporation the product was purified via flash chromatography with a gradient of 0 to 50 % MeOH in DCM. The yield was 10 %.

^{1}H NMR (600 MHz, D_2O) δ 3.92 (m, 36H), 4.67 (q, *J* = 8.8 Hz, 1H), 5.26 (d, *J* = 8.8 Hz, 1H).

^{13}C NMR (151 MHz, D_2O) δ 55.5 (b), 72.7, 74.98, 75.18, 75.42

^{31}P NMR (243 MHz, D_2O) δ -3.85, -2.73, -2.28, -2.09.

HRMS (ESI/Orbitrap) m/z: $[M + H]^+$ calcd. for $C_{18}H_{43}O_{24}P_6$ 829.0564; Found 829.0554.

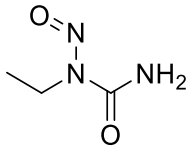

_N_-nitroso-_N_-ethyl urea (S10)

_N_-nitroso-_N_-ethyl urea (**S10**) was synthesized according to a procedure from Dyer and colleagues.[36] A solution of ethyl amine (6000 mg, 93.17 mmol) in water (14.1 ml) was cooled in an ice bath and neutralized by the addition of saturated HCl (8.7 ml). Urea (18.633 g, 310.25 mmol) was added and the solution was refluxed for 3 h. Sodium nitrite (6.85 g, 99.32 mmol) was added and the solution was cooled in a dry ice-acetone bath and during 1 h siphoned under the surface of a stirred mixture of sulfuric acid (6.2 g, 63.3 mmol) and ice (40 g) which was also cooled by a dry ice-acetone bath. The frothy precipitate was collected by filtration and washed 3 times with ice cold water.

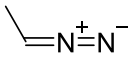

Diazoethane (14)

Diazoethane (**14**) was synthesized according to a procedure from Dyer and colleagues.[36] _N_-nitroso-_N_-ethyl urea (**S9**) (131.14 mg, 1 mmol) was added to a mixture of Et_2O (1.4ml) and 40 % (w/v) KOH (aq) (0.4 ml) at 0 °C. The mixture was allowed to stand for 30 min at 0 °C. The ethereal solution was removed with a glass pipette and directly used.

Due to the volatile nature, no NMR or HRMS was taken.

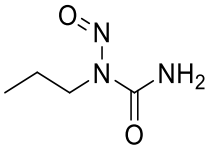

_N_-nitroso-_N_-propyl urea (S11)

_N_-nitroso-_N_-propyl urea **(S11**) was synthesized according to a procedure from Dyer and colleagues.[36] A solution of n-propyl amine (5000 mg, 84.59 mmol) in water (14.1 ml) was cooled in an ice bath and neutralized by the addition of saturated HCl (8.7 ml). Urea (16.917 g, 281.68 mmol) was added and the solution was refluxed for 3 h. Sodium nitrite (6.22 g, 90.17 mmol) was added and the the solution was cooled in a dry ice-acetone bath and during 1 h siphoned under the

surface of a stirred mixture of sulfuric acid (5.6 g, 57.1 mmol) and ice (34 g) which was also cooled by a dry ice-acetone bath. The frothy precipitate was collected by filtration and washed 3 times with ice cold water.

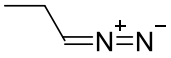

Diazopropane (15)

Diazopropane (**15**) was synthesized according to a procedure from Dyer and colleagues.[36] *N*-nitroso-*N*-propyl urea (**S10**) (131.14 mg, 1 mmol) was added to a mixture of Et2O (1.4ml) and 40 % (w/v) KOH (aq) (0.4 ml) at 0 °C. The mixture was allowed to stand for 30 min at 0 °C. The ethereal solution was removed with a glass pipette and directly used.

Due to the volatile nature, no NMR or HRMS was taken.

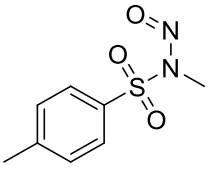

***N*-Methyl-*N*-nitroso-*p*-toluenesulfonamide, Diazald (S12)**

N-Methyl-*N*-nitroso-*p*-toluenesulfonamide (**S11**) was synthesized according to a procedure from Ouwerkerk and colleagues.[37] *N*-Methyl-*p*-toluenesulfonamide (9.26 g, 50 mmol) was dissolved in acetic acid (80 ml) and the solution was cooled on ice. NaNO2 (5.17 g, 75 mmol) was dissolved in water and over the course of 20 min dropped into the reaction. The reaction solution was stirred for 20 min and subsequently diluted with water (200 ml). This solution was extracted three times with ether. The organic layers were combined, washed with saturated bicarbonate and dried over Na2SO4. The ether was evaporated to afford the title compound in 96 % yield.

^{1}H NMR (600 MHz, $CDCl_3$) δ 7.89 (d, *J* = 9 Hz, 2H), 7. 4 (d, *J* = 8 Hz, 2H), 3.15 (s, 1H), 2.48 (s, 1H).

^{13}C NMR (151 MHz, $CDCl_3$) δ 146.13, 134.11, 130.36, 128.01, 28.9, 21.75

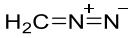

Diazomethane (16)

Diazomethane was synthesized in a Diazald reactor from Sigma-Aldrich according to the manufacturer's instructions. Fill the condenser with dry ice, then add isopropanol slowly until the cold-finger is about one-third full. Add ethanol (95%, 6 mL) to a solution of potassium hydroxide (3 g) in water (4,8 mL) in the reaction vessel. Attach a 100 mL receiving flask (with Clear-Seal joint) to the condenser and cool the receiver in dry ice/isopropanol bath. Provide an ether trap at the side-arm (the glass tube must have firepolished ends). The trap should be cooled in a dry ice/isopropanol bath. Place a separatory funnel (with Clear-Seal joint) over the reaction vessel and charge the funnel with a solution of *N*-Methyl-*N*-nitroso-*p*-toluenesulfonamide (**S12**) (3,0 g, 14 mmol) in ether (27 mL). Warm the reaction vessel to 65 °C with a water bath and add the Diazald solution over a period of 20 minutes. The rate of distillation should be approximately the rate of addition. Replenish the cold-finger with dry ice as necessary. When all the Diazald has been used up, slowly add 10 mL of ether and continue the distillation until the distillate is colorless. If the distillate is still yellow, add another 10 mL of ether and continue the distillation.

4.7 References

(1) Griffin, J. L.; Keun, H.; Richter, C.; Moskau, D.; Rae, C.; Nicholson, J. K. Compartmentation of Metabolism Probed by [2-13C]Alanine: Improved 13C NMR Sensitivity Using a CryoProbe Detects Evidence of a Glial Metabolon. *Neurochem. Int.* **2003**, *42* (1), 93–99.

(2) Ardenkjaer-Larsen, J. H.; Boebinger, G. S.; Comment, A.; Duckett, S.; Edison, A. S.; Engelke, F.; Griesinger, C.; Griffin, R. G.; Hilty, C.; Maeda, H.; et al. Facing and Overcoming Sensitivity Challenges in Biomolecular NMR Spectroscopy. *Angew. Chemie - Int. Ed.* **2015**, *54* (32), 9162–9185.

(3) Marion, D. An Introduction to Biological NMR Spectroscopy. *Mol. Cell. Proteomics* **2013**, *12* (11), 3006–3025.

(4) McLafferty, F. W. A Century of Progress in Molecular Mass Spectrometry. *Annu. Rev. Anal. Chem.* **2011**, *4* (1), 1–22.

(5) Wong, A. L. A.; Xiang, X.; Ong, P. S.; Mitchell, E. Q. Y.; Syn, N.; Wee, I.; Kumar, A. P.; Yong, W. P.; Sethi, G.; Goh, B. C.; et al. A Review on Liquid Chromatography-Tandem Mass Spectrometry Methods for Rapid Quantification of Oncology Drugs. *Pharmaceutics*. November 8, 2018, p 221.

(6) Emwas, A.-H.; Roy, R.; McKay, R. T.; Tenori, L.; Saccenti, E.; Gowda, G. A. N.; Raftery, D.; Alahmari, F.; Jaremko, L.; Jaremko, M.; et al. NMR Spectroscopy for Metabolomics Research. *Metabolites* **2019**, *9* (7), 123.

(7) Gika, H.; Virgiliou, C.; Theodoridis, G.; Plumb, R. S.; Wilson, I. D. Untargeted LC/MS-Based Metabolic Phenotyping (Metabonomics/Metabolomics): The State of the Art. *Journal of Chromatography B: Analytical Technologies in the Biomedical and Life Sciences*. June 1, 2019, pp 136–147.

(8) Jang, C.; Chen, L.; Rabinowitz, J. D. Metabolomics and Isotope Tracing. *Cell*. May 3, 2018, pp 822–837.

(9) Park, J. O.; Rubin, S. A.; Xu, Y. F.; Amador-Noguez, D.; Fan, J.; Shlomi, T.; Rabinowitz, J. D. Metabolite Concentrations, Fluxes and Free Energies Imply Efficient Enzyme Usage. *Nat. Chem. Biol.* **2016**, *12* (7), 482–489.

(10) Sjöberg, P. J. R.; Thelin, P.; Rydin, E. Separation of Inositol Phosphate Isomers in Environmental Samples by Ion-Exchange Chromatography Coupled with Electrospray Ionization Tandem Mass Spectrometry. *Philos. Trans. R. Soc. B Biol. Sci.* **2002**, *357* (1420), 449–469.

(11) Ito, M.; Fujii, N.; Wittwer, C.; Sasaki, A.; Tanaka, M.; Bittner, T.; Jessen, H. J.; Saiardi, A.; Takizawa, S.; Nagata, E. Hydrophilic Interaction Liquid Chromatography–tandem Mass Spectrometry for the Quantitative Analysis of Mammalian-Derived Inositol Poly/Pyrophosphates. *J. Chromatogr. A* **2018**, *1573*, 87–97.

(12) Recknagel, C.; Thelin, P.; Abraham, M.; Schulz-Bull, D.; Sjöberg, P. J. R. Using Standard Additions to Improve Extraction and Quantification of Inositol Hexakisphosphate in Sediment Samples by Ion Chromatography Electrospray Ionization Mass Spectrometry. *Talanta* **2018**, *188*, 192–198.

(13) Rugova, A.; Puschenreiter, M.; Santner, J.; Fischer, L.; Neubauer, S.; Koellensperger, G.; Hann, S. Speciation Analysis of Orthophosphate and Myo-Inositol Hexakisphosphate in Soil- and Plant-Related Samples by High-Performance Ion Chromatography Combined with Inductively Coupled Plasma Mass Spectrometry. *J. Sep. Sci.* **2014**, *37* (14), 1711–1719.

(14) Couso, I.; Evans, B. S.; Li, J.; Liu, Y.; Ma, F.; Diamond, S.; Allen, D. K.; Umen, J. G. Synergism between Inositol Polyphosphates and TOR Kinase Signaling in Nutrient Sensing, Growth Control, and Lipid Metabolism in Chlamydomonas. *Plant Cell* **2016**, *28* (9), 2026–2042.

(15) Lee, L. Y.; Mitchell, A. E. Determination of D-Myo-Inositol Phosphates in 'Activated' Raw Almonds Using Anion-Exchange Chromatography Coupled with Tandem Mass Spectrometry. *J. Sci. Food Agric.* **2019**, *99* (1), 117–123.

(16) McIntyre, C. A.; Arthur, C. J.; Evershed, R. P. High-Resolution Mass Spectrometric Analysis

of Myo-Inositol Hexakisphosphate Using Electrospray Ionisation Orbitrap. *Rapid Commun. Mass Spectrom.* **2017**, *31* (20), 1681–1689.

(17) Duong, Q. H.; Clark, K. D.; Lapsley, K. G.; Pegg, R. B. Quantification of Inositol Phosphates in Almond Meal and Almond Brown Skins by HPLC/ESI/MS. *Food Chem.* **2017**, *229*, 84–92.

(18) Hayati, I.; Bailey, A. I.; Tadros, T. F. Investigations into the Mechanisms of Electrohydrodynamic Spraying of Liquids. I. Effect of Electric Field and the Environment on Pendant Drops and Factors Affecting the Formation of Stable Jets and Atomization. *J. Colloid Interface Sci.* **1987**, *117* (1), 205–221.

(19) Cole, R. B.; Harrata, A. K. Solvent Effect on Analyte Charge State, Signal Intensity, and Stability in Negative Ion Electrospray Mass Spectrometry; Implications for the Mechanism of Negative Ion Formation. *J. Am. Soc. Mass Spectrom.* **1993**, *4* (7), 546–556.

(20) Clark, J.; Anderson, K. E.; Juvin, V.; Smith, T. S.; Karpe, F.; Wakelam, M. J. O.; Stephens, L. R.; Hawkins, P. T. Quantification of PtdInsP3 Molecular Species in Cells and Tissues by Mass Spectrometry. *Nat. Methods* **2011**, *8* (3), 267–272.

(21) Harmel, R. K.; Puschmann, R.; Nguyen Trung, M.; Saiardi, A.; Schmieder, P.; Fiedler, D. Harnessing 13C-Labeled Myo-Inositol to Interrogate Inositol Phosphate Messengers by NMR. *Chem. Sci.* **2019**, *10* (20), 5267–5274.

(22) Black, T. H. The Preparation and Reactions of Diazomethane. *Aldrichimica Acta* **1983**, *16* (1), 3–10.

(23) de Boer, T. J.; H.J., B. Diazomethane. *Org. Synth.* **1963**, *8*, 250.

(24) Schoental, R. Carcinogenic Action of Diazomethane and of Nitroso-N-Methyl Urethane. *Nature* **1960**, *188* (4748), 420–421.

(25) Kühnel, E.; Laffan, D. D. P.; Lloyd-Jones, G. C.; Martínez Del Campo, T.; Shepperson, I. R.; Slaughter, J. L. Mechanism of Methyl Esterification of Carboxylic Acids by Trimethylsilyldiazomethane. *Angew. Chemie - Int. Ed.* **2007**, *46* (37), 7075–7078.

(26) Fei, N.; Sauter, B.; Gillingham, D. The PK a of Brønsted Acids Controls Their Reactivity with Diazo Compounds. *Chem. Commun.* **2016**, *52* (47), 7501–7504.

(27) Wilson, M. S. C.; Bulley, S. J.; Pisani, F.; Irvine, R. F.; Saiardi, A. A Novel Method for the Purification of Inositol Phosphates from Biological Samples Reveals That No Phytate Is Present in Human Plasma or Urine. *Open Biol.* **2015**, *5* (3), 150014.

(28) Ives, E. B.; Nichols, J.; Wente, S. R.; York, J. D. Biochemical and Functional Characterization of Inositol 1,3,4,5,6-Pentakisphosphate 2-Kinases. *J. Biol. Chem.* **2000**, *275* (47), 36575–36583.

(29) Dubois, E.; Scherens, B.; Vierendeels, F.; Ho, M. M. W.; Messenguy, F.; Shears, S. B. In Saccharomyces Cerevisiae, the Inositol Polyphosphate Kinase Activity of Kcs1p Is Required for Resistance to Salt Stress, Cell Wall Integrity, and Vacuolar Morphogenesis. *J. Biol. Chem.* **2002**, *277* (26), 23755–23763.

(30) Steidle, E. A.; Chong, L. S.; Wu, M.; Crooke, E.; Fiedler, D.; Resnick, A. C.; Rolfes, R. J. A Novel Inositol Pyrophosphate Phosphatase in Saccharomyces Cerevisiae: Siw14 Protein Selectively Cleaves the β-Phosphate from 5-Diphosphoinositol Pentakisphosphate (5PP-IP5). *J. Biol. Chem.* **2016**, *291* (13), 6772–6783.

(31) Pisani, F.; Livermore, T.; Rose, G.; Chubb, J. R.; Gaspari, M.; Saiardi, A. Analysis of Dictyostelium Discoideum Inositol Pyrophosphate Metabolism by Gel Electrophoresis. *PLoS One* **2014**, *9* (1), e85533.

(32) Wu, M.; Chong, L. S.; Perlman, D. H.; Resnick, A. C.; Fiedler, D. Inositol Polyphosphates Intersect with Signaling and Metabolic Networks via Two Distinct Mechanisms. *Proc. Natl. Acad. Sci.* **2016**, *113* (44), E6757–E6765.

(33) Findeisen, M.; Brand, T.; Berger, S. A 1H-NMR Thermometer Suitable for Cryoprobes. *Magn. Reson. Chem.* **2007**, *45* (2), 175–178.

(34) Kitas, E. A.; Perich, J. W.; Tregear, G. W.; Johns, R. B. Synthesis of O-Phosphotyrosine-Containing Peptides. 3. Synthesis of H-Pro-Tyr(P)-Val-OH via Dimethyl Phosphate Protection and the Use of Improved Deprotection Procedures. *J. Org. Chem.* **2005**, *55* (13), 4181–4187.

(35) Podeschwa, M.; Plettenburg, O.; Vom Brocke, J.; Block, O.; Adelt, S.; Altenbach, H. J. Stereoselective Synthesis of Myo-, Neo-, L-Chiro, D-Chiro, Allo-, Scyllo-, and Epi-Inositol Systems via Conduritols Prepared from p-Benzoquinone. *European J. Org. Chem.* **2003**, *2003* (10), 1958–1972.

(36) Dyer, J. R.; Randall, R. B.; Deutsch, H. M. A Convenient Preparation of 1-Diazopropane. *Journal of Organic Chemistry*. American Chemical Society November 1964, pp 3423–3424.

(37) Ouwerkerk, N.; Steenweg, M.; De Ruijter, M.; Brouwer, J.; Van Boom, J. H.; Lugtenburg, J.; Raap, J. One-Pot Two-Step Enzymatic Coupling of Pyrimidine Bases to 2-Deoxy-D-Ribose-5-Phosphate. A New Strategy in the Synthesis of Stable Isotope Labeled Deoxynucleosides. *J. Org. Chem.* **2002**, *67* (5), 1480–1489.